From the lab to the real world: the redox reactivity of Fe-bearing clay minerals in complex biogeochemical environments

Katherine A. Rothwell

A thesis submitted to Newcastle University in partial fulfilment of the requirements for the degree of Doctor of Philosophy within the Faculty of Science, Agriculture, and Engineering

School of Engineering, Cassie Building, NE1 7RU

First submission: December 2018
Revisions: April 2019

In loving memory of my Father, Rod Paton
1946 - 2016

for always encouraging me to be a "real" engineer

Acknowledgements

The work described in this thesis has been undertaken during the most difficult four years of my life. As such, it would not have been possible without the dedicated support of several individuals, to whom I am extremely grateful.

Firstly, I would like to thank Dr Anke Neumann and Professor David Graham for being a fantastic supervisory team. Anke has encouraged me to be rigorous, ambitious, and diligent with my research while providing wonderful support and inspiration. It is hard to express how good a project supervisor Anke has been and my research experience has been significantly enriched and broadened through her input. It is also difficult to avoid catching David's infectious enthusiasm for all branches of environmental engineering. My work has been greatly enriched by the input of Professor Joseph Stucki, Dr Martin Pentrak and Dr Linda Pentrakova (University of Illinois at Urbana-Champaign), who kindly and warmly hosted me for a period in 2017.

I am thankful to the rest of the Neumann Group for their assistance in the laboratory and for always being happy to discuss interesting or puzzling results. In particular, I would like to thank Jim Entwistle for a valuable tutorial into Full Static Hamiltonian fitting of Mössbauer spectra and for acting as "lab-guardian" but also for phenanthroline Fridays and sometimes questionable music choices. I am also indebted to MSc students Xiao Wang and Xiaobin Lou for their assistance in preliminary experiments.

I would like to thank Dr Wojciech Mrozik for giving several hours of his time to assist me with HPLC and Dr Angela Sherry for offering *Shewanella oneidensis* MR-1. I am also indebted to David Earley, Phil Green, David Race, Jane Davis, Graham Patterson and the other technicians in the former School of Civil Engineering and Geosciences for their kindness, friendliness and help with several aspects of my project. I am grateful for the help the late Rob Hunter provided in setting up the Mössbauer spectrometer, which he always did with a smile.

I would not have been able to complete the project without financial support from EPSRC, the Clay Minerals Society and the Mineralogical Society of Great Britain and Ireland and I am very grateful for these grants.

Finally, I would like to thank my family and close friends for their practical and emotional support. In particular, Mum, Rose Hawkswood and Laura McGinty have kept me sane for the last few months. I am extremely thankful to Craig Thompson for offering his design skills and time to visualise my conceptual model and for the several occasions where he forced me sit and work when I needed to but felt like I couldn't. He has been the best friend anyone could ask for.

Abstract

Microbial and chemical processes drive reduction of structural iron in clay minerals, which, in turn, can facilitate the reduction of a range of contaminants including nitroaromatic compounds. Fe-bearing clay minerals are largely resistant to reductive dissolution and can thus undergo redox cycling, rendering them an important and renewable source of electron equivalents in natural environments. However, their reactivity outside controlled laboratory environments is currently not well understood.

Here, we used a series of batch experiments of increasing complexity to assess how components representative of natural systems influence the reactivity of Fe-bearing clay minerals. We investigated the degradation of a nitroaromatic compound (NAC, 50 μ 2-acetylnitrobenzene) in suspensions of 2.0 g/L nontronite NAu-1, at a range of Fe(II)/Fe(tot) ratios (pH 7.5) in the presence of various naturally occurring redox active phases in order to develop a mechanistic understanding of how iron-rich clay minerals behave in complex natural environments.

Specifically, we investigated the influence of:

i The naturally ubiquitous reductant aqueous Fe(II) that reduces clay mineral Fe while forming a potentially reactive Fe-oxidation product;

ii Fe(II)-organic ligand complexes, using small acids representative of natural organic matter;

iii Electron transfer mediators (ETMs) representative of microbial exudates.

Our results show that Fe(II)-reduced nontronite, that may occur in natural systems facilitates the degradation of NACs more rapidly than microbially reduced clay minerals of comparable reduction extents. Fe(II)-reduced nontronite exhibits biphasic reduction kinetics, which are unique to abiotically reduced nontronite, due to the presence two distinct reactive Fe(II)-entities. We found that these were both contained within the mineral structure for NAu-1 reduced using dithionite whereas for Fe(II)-reduced NAu-1, although the highly reactive site was likely to comprise the same structural Fe(II) as the dithionite-reduced mineral, the site with lower reactivity likely comprised Fe(II) associated with the secondary Fe-bearing phase that forms as a result of the mineral reduction.

We show that carboxylate Fe(II)-organic ligand complexes may rapidly reduce both clay mineral Fe(II) and NACs. In the presence of the Fe(II)-organic complexes, the nontronite acts as a redox buffer providing a sink of electrons in its native form but regenerating the reactive organic Fe(II) pool in its reduced form. We generally observed more rapid NAC reduction in the presence of quinone and flavin-containing ETMs and the magnitude of this effect depended on both ETM structure and clay mineral Fe reduction extent. Overall, we highlight the importance of considering all phases in complex biogeochemical systems when assessing contaminant fate in natural and engineered systems.

Contents

List of Figures

List of Tables

Chapter 1
Introduction

From the onset of the Industrial Revolution, there has been a legacy of anthropogenic pollution in groundwater, sediments and soils (6). As a result of disasters such as the Love Canal hazardous waste site, which saw over 200 households impacted at a cost of $> \$ 7$ million to the US government (7), the impact of anthropogenic land contamination has become a public health and economic concern (8, 9).

Nitroaromatic compounds (NACs) are a contaminant class of particular relevance due to their high toxicity and include numerous mutagenic or carcinogenic compounds (10). Historically, they have been widely used, primarily as industrial solvents and explosives (11). It is estimated that in the USA alone approximately 1.2 million tonnes of soil are affected by contamination with explosive species (12). Traditionally, pumping and incineration methods have been used to remediate NAC-contaminated environments (10). However, due to the costly nature and inefficacy of these processes there has been a recent drive to find more cost-effective and sustainable remediation solutions, with a particular focus on Monitored Natural Attenuation (MNA) (13).

In-situ reductive transformation of contaminants has been identified as a promising and cost-effective remediation technique for NACs and various other contaminant classes (14, 15). Generally, iron is the most abundant redox-active element in the Earth's crust and various iron species have been proposed to facilitate the reductive degradation of NACs (16). In particular, Fe-bearing clay minerals are ubiquitously present in the environment (17) and structural Fe(II) within these minerals has been documented to act as a renewable source of electron equivalents (18, 19) to facilitate contaminant reduction (20–25). However, the reactivity of Fe-bearing clay minerals outside of controlled laboratory environments is currently not well understood.

To enable effective design of engineered remediation solutions, a mechanistic understanding of the redox processes affecting Fe-bearing clay minerals in complex environments is required. Currently, an understanding of the combined reactivity of co-existing Fe-bearing clay minerals and the influence of complex interactions with other soil components is lacking. Therefore this project aims to systematically evaluate the reactivity of iron-bearing clay minerals in combination with other components characteristic of natural systems, reconciling laboratory studies with field based results.

To achieve this, we have undertaken four chapters of work to bridge the gap between the lab and the real world as follows:

Chapter 2 provides a review of the literature documenting current knowledge of the reactivity of Fe-bearing clay minerals and identifying key gaps in knowledge concerning their behaviour;

Chapter 3 assesses how the reactivity of Fe-bearing clay minerals towards NACs is influenced by the presence of aqueous Fe(II), which is a currently under-studied ubiquitous natural reductant;

Chapter 4 evaluates how the reactivity of Fe-bearing clay minerals towards NACs is influenced by the presence of Fe(II)-organic complexes, using small organic acids as an analogue for functional groups abundantly found in natural organic matter (NOM); and,

Chapter 5 investigates how the reactivity of Fe-bearing clay minerals towards NACs is influenced by the presence of quinone- and flavin-containing electron transfer mediators (ETMs) as an analogue for electron shuttling compounds produced by microorganisms.

We then summarise our findings and provide a conceptual model highlighting the novel interactions between Fe-bearing clay minerals and other components characteristic of natural systems our work has identified.

Chapter 2
Redox reactivity of iron-bearing clay minerals: implications for reductive contaminant transformation

2.1 Introduction

The Fe(III)/Fe(II) redox cycle is fundamentally important within the Earth's critical zone, as it has a controlling influence on the global biogeochemical cycles of nutrients and mineral weathering rates (26–31). In anaerobic environments, Fe phases act as donors and acceptors of electron equivalents for the transformation of a number of environmental pollutants and the Fe(III)/Fe(II) redox cycle therefore governs their mobility, bioavailability and toxicity (32–35). The reduction of a contaminant is often desirable as it results in the formation of reduction products that are less mobile and toxic in the environment, such as the transformation of Cr(VI) to Cr(III) and chlorinated ethylenes to acetylene/ethene. However, products with greater toxicity may also be produced (14).

Iron is the fourth most abundant element in the lithosphere and a large proportion is held in the structure of phyllosilicate minerals (17, 36). The majority of clay minerals contain iron, which is found in both the octahedral and tetrahedral sheets within 1:1 and 2:1 layered clay minerals (see example structure in Figure 2.1) and also within the gibbsite/brucite sheet of 2:1:1 minerals, as a pillar between 2:1 sheets or as a charge-balancing cation in the interlayer (37, 38). Due to their swelling nature, large reactive surface area and ubiquitous presence in nature, smectites are of particular interest for contaminant transformation and nontronites are particularly iron rich containing around 20 % or more (24, 27, 38).

A number of Fe(II)-containing and surface-bound Fe(II) species are capable of reducing contaminants including iron sulfides (40, 41) siderite (42), green rusts (35, 41), magnetite (43, 44), and iron (oxyhydr)oxides (42, 45, 46). Similarly, structural Fe(II) in clay minerals is known to facilitate the reductive transformation of a range of contaminants (20, 21, 23, 24, 45, 47–53). As clay minerals are both ubiquitously present and less sensitive to reductive dissolution they are likely to be of importance in natural systems where Fe-reducing bacteria and periodically anaerobic conditions are present, as illustrated in Figure 2.2 (38, 54).

However, it is only since the late 1980s that work has focussed on redox reactions of Fe-bearing clay minerals, as historically clay minerals have been considered as a sorbent phase only (56–58) and the redox properties of clay minerals and their resulting reactivity towards contaminant species are not yet well understood (55). This review summarises work to date concerned with redox reractions of clay minerals, including the following:

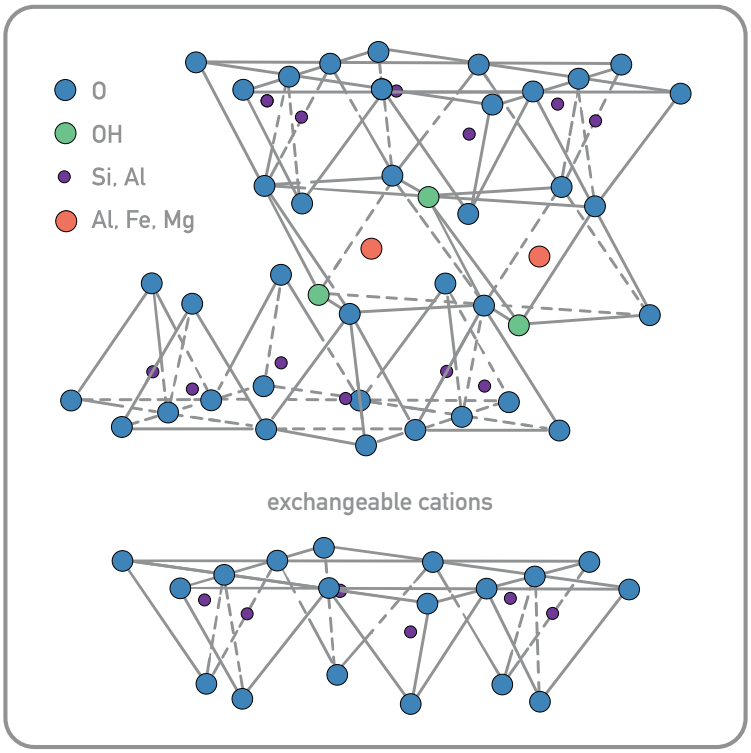

Figure 2.1: Typical structure of a 2:1 montmorillonite, adapted from (39).

i An outline of the redox properties of clay minerals;
ii The methods applied to elucidate the reactivity and structural environment of Fe in clay minerals;
iii Which contaminants undergo reductive/oxidative transformation;
iv The thermodynamics of the processes; and,
v Factors controlling the reactivity of clay minerals in complex biogeochemical environments, including interactions with organic soil components.

This knowledge is key to allow representative modelling of redox processes in the environment to be undertaken, which will in turn contribute to a better understanding of contaminant behaviour and nutrient cycling in complex biogeochemical environments and will enable effective design of remediation solutions and earth systems engineering.

2.2 Structural Fe in clay minerals: a renewable source of electron equivalents in the environment

Fe(II) may be natively present in the structure of trioctahedral clay minerals such as chlorites (59) and micas or octahedrally coordinated Fe(III) may be microbially or abiotically reduced under anaerobic conditions (37, 38). The structural coordination of Fe(II) and the mechanism of its formation is known to drastically affect its reactivity (20, 22). Therefore, an understand-

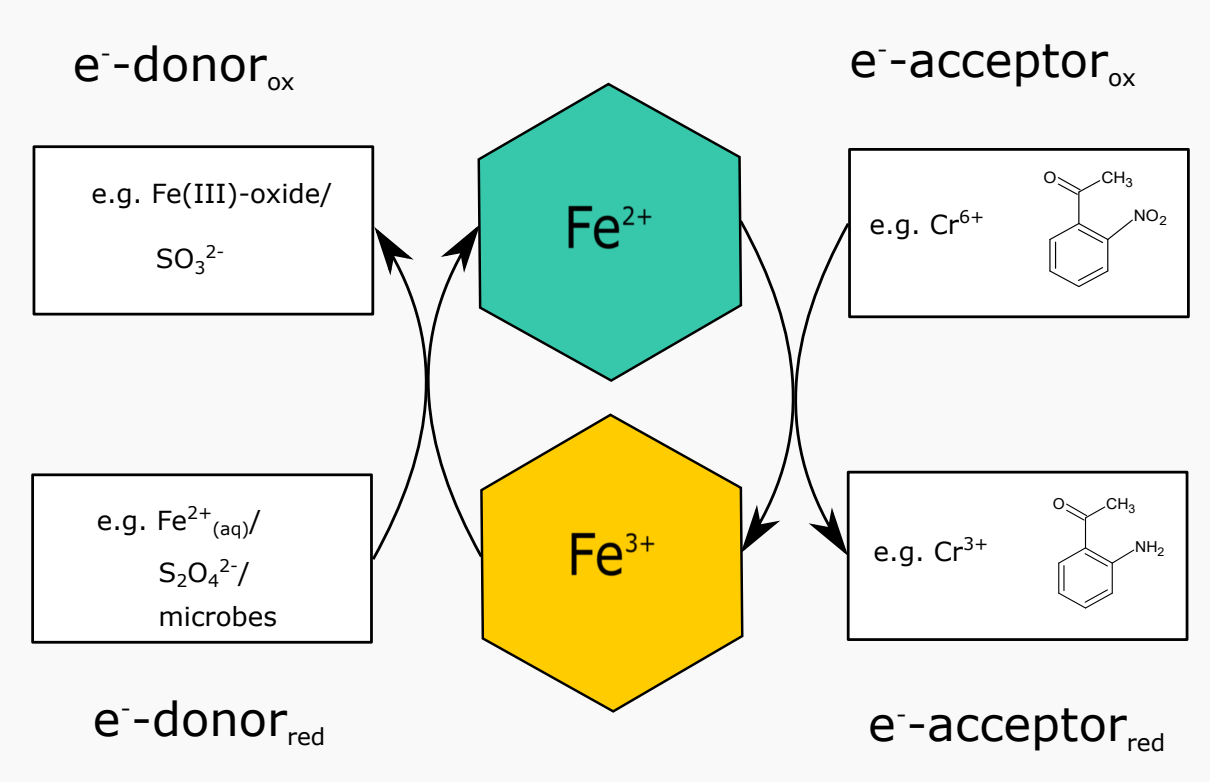

Figure 2.2: Illustration of the redox cycling behaviour of octahedral iron in clay minerals. Structural Fe(III) (yellow hexagon) may be reduced chemically/biologically to form structural Fe(II) (green hexagon). This Fe(II) is retained in the mineral structure and may donate electrons to various contaminants, concomitantly reforming the structural Fe(III) that may then be reduced again. Adapted from (55).

ing of the Fe reduction mechanisms is key to understanding the reactivity of clay minerals in natural environments.

Changes in the oxidation state of Fe in clay minerals were initially documented using a range of inorganic reducing agents including sulfide (60), tetraphenylboron (61), hydrazine (62) and most frequently dithionite (63). The reduction potential of dithionite is low enough (E_H = -0.66V vs SHE at pH 7 (64)) that generally $>$ 90 % of clay mineral structural Fe can be reduced (65, 66). Reduction of octahedral Fe(III) by dithionite is thought to occur as a semi-random process with electron transfer occurring through either basal plane or edge sites with the resulting Fe(II) randomly distributed in the octahedral sheet, initially creating preferentially mixed valence Fe(II)Fe(III) sites (67, 68). At higher reduction extents, dioctahedral Fe(II)Fe(II) sites are formed and structural rearrangements occur, including dehydroxylation and formation of trioctahedral Fe(II) domains to balance the increased negative charge (67, 69). Although tetrahedrally coordinated iron may be found within clay minerals, the reduction of iron in the tetrahedral sheet of clay minerals remains the subject of considerable debate (55, 70, 71).

Microbial reduction of structural Fe(III) in clay minerals has also been widely documented, initially by Stucki and Getty in 1986 (72) and has since been extensively studied with four review papers published on the subject (17, 73–75). Within natural systems, microbial oxidation and reduction is thought to be a predominant mechanism of Fe cycling (75) and due to the ubiquitous nature of clay minerals in natural sedimentary environments it is likely that

the microbial reduction of clay minerals is an important process for global nutrient cycling. However, the extent of Fe reduction is generally less for bacterially reduced than for dithionite reduced clay minerals; typically $<$ 45 % Fe(II) dependent on microbial strain and clay mineral type (76) relative to $>$ 90 % for dithionite reduction (65). Microbial reduction may be enhanced in the presence of an electron shuttling compound (commonly anthraquinone-2,6-disulfonate (AQDS)), which may yield more rapid or higher Fe reduction extents (21, 24, 75).

Recent work has also indicated different mechanisms for microbial and chemical reduction of Fe-bearing clay minerals. Early infra-red spectroscopic studies indicated few structural differences resulting from dithionite and biotic clay Fe mineral reduction (69). More recently, work using Mössbauer spectroscopy revealed that microbial reduction resulted in the production of discrete Fe(II) and Fe(III) domains contrasting the mixed valence Fe(II)Fe(III) pairs created by dithionite-reduction. Therefore, it is likely that microbial reduction occurs as a moving front originating from edge-surfaces of clay minerals whereas dithionite-reduction is pseudo-random and occurs from clay mineral basal planes (68).

The difference in Fe reduction mechanism and resulting mineral structures also leads to differences in mineral reactivity. Iron-rich smectites containing clustered di/trioctahedral Fe(II) transform organic contaminants rapidly with characteristic biphasic reduction kinetics that were attributed to the presence of two types of, potentially regenerable, reactive Fe(II) sites in the mineral structure (20, 48). The structural nature of these Fe(II) sites of higher and lower reactivity is the subject of some debate. However, spectroscopic studies have suggested that they comprise various di/trioctahedral Fe(II) coordinations (63, 65, 69, 77, 78) that may form in iron-rich clay minerals where octahedral clustering of iron can occur due to its high site occupancy, confirming the influence of structural Fe content on the reaction mechanisms of clay minerals towards NACs and other contaminants. In contrast, microbially reduced and iron-poor ($\leq$ 10 %wt Fe) clay minerals react more slowly and appear to contain one reactive site (20).

Naturally occurring abiotic reductants, such as aqueous Fe(II) and sulfide species, may also be of importance for the formation of reactive Fe(II) species within clay minerals (60, 79). Recently, it has been shown that the reaction of structural Fe(III) in smectites with aqueous Fe(II) results in interfacial electron transfer between the two species, resulting in the reduction of structural Fe(III) and the formation of a solid Fe(III)-containing product (47, 53, 80, 81). A mechanistic understanding of clay mineral reduction by aqueous Fe(II) is currently lacking. However, it is likely to be of importance for contaminant degradation in the environment (25, 47, 53).

In addition to transferring electrons to reducible contaminants, Fe(II) in clay minerals may also be (re)oxidised both abiotically by O_2/air or microbially, for example, by nitrate-dependent iron oxidising bacteria such as *Pseudogulbenkiania spp.* (82, 83). As a result, structural Fe in clay minerals may go through reduction-reoxidation cycling and this process has been documented within the critical zone, for example in periodically flooded paddy fields (54, 84). Abiotic oxygenation of clay mineral Fe(II) has been shown to produce hydroxyl

radicals that may facilitate the oxidative transformation of contaminants (85–87), although that is outside the scope of this review.

Redox cycling of Fe in clay minerals is thought to be generally reversible, implying that Fe-bearing clay minerals can act as a renewable source of electron equivalents for contaminant reduction (84, 88, 89). However, the reversibility of this process is governed by the mechanism and extent of reduction (55, 68, 84, 90). (19) observed limited dissolution from the structure of nontronite NAu-2 that had undergone biological redox cycling, leading to the formation of secondary minerals such as illite. However, after the removal of poorly crystalline/fine NAu-2 particles in the first reduction/oxidation cycle, no further dissolution was measured. They also did not measure a redox cycling to have had a significant impact on the rate and extent of nitrate reduction by biologically-reduced NAu-2 although another study found that the rate of reduction of technetium by biologically-reduced NAu-2 increased in the first two cycles before reaching a plateau (18).

2.3 Field Studies

Due to their ability to undergo redox cycling, Fe-bearing clay minerals are likely to have an important influence on contaminant fate in the environment. Although the importance of Fe(II) as a reductant has been highlighted in the field (33, 91, 92), only a limited number of field-based studies have investigated the redox reactivity of phyllosilicates.

Several studies have been undertaken to enhance the development of engineered remediation techniques involving the *in-situ* reduction of contaminants with the aim to remove them from soils and/or groundwater (14, 93). The reduction of chlorinated solvents, hexavalent chromium and radionuclides has been successfully demonstrated and may be enhanced, although with potentially problematic side effects, by the addition of dithionite or aqueous Fe(II) as in-situ reducing agents (14, 93–102). Other studies on natural sediments have indicated that rates of contaminant reduction in natural sediments can be generally predicted as a function of Fe(II) concentrations (101) or dissolved organic carbon (DOC) levels in organic rich environments (90).

Although it has been demonstrated that *in-situ* reductive transformation is a viable method of contaminant degradation, specific mechanisms and reactive phases controlling the rate of contaminant reduction have not yet been identified beyond general trends. The available literature suggests a complex system where some contaminants may be reduced either directly by Fe-bearing mineral phases or microbially with simultaneous redox cycling of Fe in phyllosilicate minerals (100, 103). The extent to which each process contributes to the overall reaction rate is currently unknown, preventing reliable predictions and and the development of accurate models.

However, further work has specifically highlighted the importance of Fe-bearing clay minerals for redox-active contaminant transformation in natural systems. Lee and Batchelor (2003) investigated the reduction of hexavalent chromium and tetrachloroethylene (PCE) by a number of Fe(II)-bearing minerals including pyrite, iron-oxides magnetite and green rust, biotite,

montmorillonite and vermiculite in comparison to a natural soil. Although pyrite and iron oxide species had reductive capacities approximately 1-3 times greater than the phyllosilicate species, the reactivity of the phyllosilicates resembled that of natural soil suggesting that Fe(II) in clay minerals may control contaminant reduction in soil. Similarly, (104) investigating abiotic Tc(VII) reduction in heterogeneous sediments spanning a large redox transition zone found that the most reactive section of the core contained a diverse range of Fe-bearing species, predominantly Fe-bearing phyllosilicates and siderite. Furthermore, Fe-bearing clay minerals have also been suggested to be the predominant reductive species for nitrate in aquifers (45, 56).

2.4 Laboratory Studies

2.4.1 Methods of assessing contaminant transformation by Fe-bearing clay minerals

Despite the evidence for the important role that Fe-bearing clay minerals play in natural sediments, there is currently a lack of field based knowledge concerning the influence of individual mineral phases and soil components on the redox activity of Fe-bearing clay minerals in environmental systems. Laboratory studies have come some way towards overcoming this hurdle. However, quantifying the redox reactivity of mineral associated Fe(II) has been historically problematic due to the difficulty of measuring the *in-situ* redox potentials of surface-bound and structural Fe(II) species (42).

To solve this problem, reactive probe compounds have often been used and the reductive capacity of a specific Fe(II)-phase in different environments can be measured according to the rate of reduction of a specific probe molecule. However, it should be noted that reduction rates for different classes of compounds will follow different trends (42). Problems with this method may also arise as significant differences in reduction rate may occur as a result of small changes in experimental conditions and solution chemistry (105) therefore making application to complex real-world systems difficult.

The next section of this review will summarise current knowledge concerning the redox reactivity of Fe-bearing clay minerals towards select organic and inorganic contaminants that have been widely used as reactive probe compounds.

2.4.2 Nitroaromatic Compouds

Nitroaromatic compounds (NACs) include classes of explosives, pesticides, polymers and dyes and have been widely used to probe the reactivity and reaction mechanisms of Fe-bearing clay minerals (11, 20, 106), including in this current study.

The complete reduction mechanism for nitrobenzene(s) to aniline(s), derived through measuring the isotopic fractionation of nitrogen, is shown in Figure 2.3 and proceeds through a series of electron transfer and protonation steps (107, 108). The rate limiting step is thought to be the formation of nitrosobenzene (6 in Figure 2.3). Substitued nitrobenzenes containing chloro-, methyl-, acetyl-, and other functional groups have commonly been used to probe the

reaction mechanisms of Fe-bearing reductants. There are two advantages of using substituted NACs: firstly, the addition of different functional groups changes the reduction potentials of the NACs allowing for thermodynamic dependencies to be explored (20–22). Secondly, depending on the location of the functional group (i.e. ortho/meta/para) the distribution of charge will vary therefore changing the affinity of the NAC to sorb to mineral surfaces (50, 79). This allows a useful distinction between the reactivity of surface-bound and structural Fe(II) to be made.

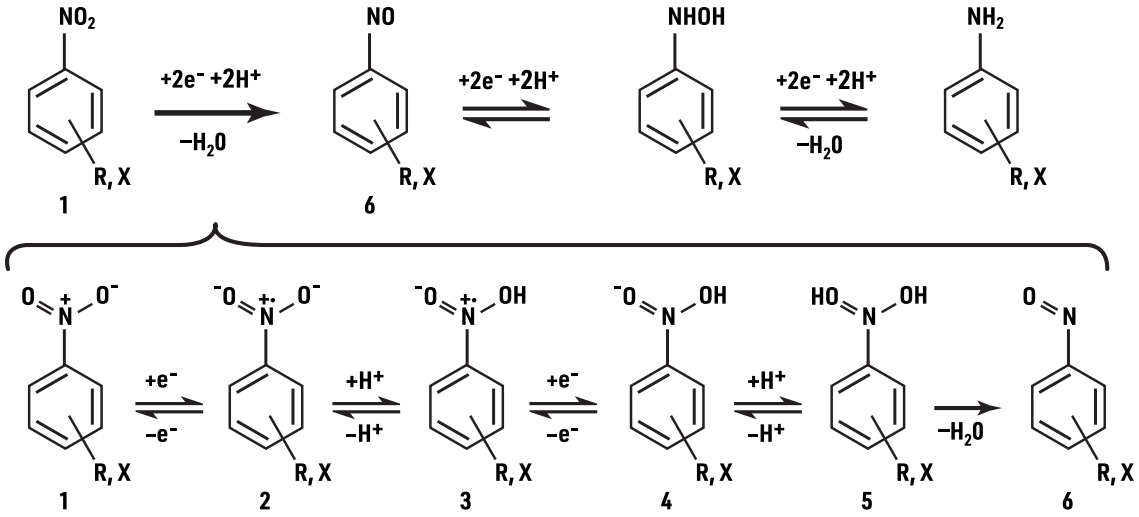

Figure 2.3: Series of electron transfer and protonation reactions that occur during the reduction of nitrobenzenes to anilines. The bottom detail highlights the mechanism for the first electron transfer step and the formation of nitrosobenzene, which is thought to be rate limiting. Adapted from (107, 108).

Hofstetter *et al.,* (2003) (79) proposed three potential reactive Fe(II) sites in clay minerals:

1. Octahedral Fe(II);
2. Fe(II) complexed by edge hydroxyl groups; and
3. Fe(II) at basal siloxane surfaces bound by ion exchange.

They used NACs with different structural properties to identify reactive Fe(II) sites in dithionite-reduced ferruginous smectite (SWa-1), Arizona montmorillonite (SAz-1) and iron-free hectorite (SHCa-1) (79). Around 13 % of the total Fe in nontronite was found to be reactive and octahedral Fe(II) was later identified as the predominant reactive site (50) with electron transfer likely occurring through the basal planes. Subsequently, (20) observed biphasic reduction kinetics of NACs by iron-rich clay minerals, suggesting the presence of two

types of reactive Fe(II) site in the clay mineral structure, not present in iron-poor clay minerals, as discussed in detail in Section 2.2.

Recent work has also used NACs to identify differences in the reactivity of biologically- and dithionite-reduced clay minerals (22) and also the influence the presence of Fe-bearing clay minerals has on the biologically-driven reduction of NACs (21). Despite containing a comparable structural Fe(II) content, the dithionite-reduced minerals (nontronite NAu-2 and montmorillonite SWy-2) were able to reduce the NAC probe more rapidly than NAu-2 and SWy-2 reduced by *Shewanella putrefaciens* strain CN32 (22). The differences are likely due to the differing structures of microbially- and chemically-reduced clay minerals where Fe(II) is limited to mineral edges for microbially-reduced minerals but chemical reduction causes the Fe(II) to be distributed through the octahedral sheet (68) (Section 2.2). The presence of NAu-2 and SWy-2 was found to enhance the rate of NAC reduction by strain CN32, which respired concurrently on both clay mineral Fe(III) and nitrobenzene and over long time scales ($>$ 500 hours) structural Fe(II) was identified as the predominant reducing agent (21).

NACs with different functional groups have been used to gain thermodynamic insights into the reduction of contaminants by clay minerals. Specifically, Linear Free Energy Relationships (LFERs), relating the one-electron reduction potential (E^1_H) of the NAC species to the reduction rate constants for specific clay minerals have been produced. Both (20) and (22) have published LFERs for NAC reduction and both observed a linear correlation between log k (second-order) and (E^1_H) with a slope of < 1, indicating that although the transfer of the first electron correlates with the reduction rate constants, it does not exclusively control the reduction kinetics (20). Discrepancies also exist between the two studies, and different slopes for the LFERs were observed with (20)'s study suggesting a greater dependence on NAC E^1_H (slope = -0.67 for SWy-2, pH 7.5) than (22)'s study (slope = -0.48 for SWy-2, pH 6.8). It is unclear where this discrepancy arises from although it is possible that small changes in reaction conditions (e.g. buffer, pH) are responsible.

2.4.3 Chlorinated compounds

In contrast to the wide attention given to NAC reduction by Fe-bearing minerals, abiotic reductive degradation of chlorinated hydrocarbons has historically been overlooked with research focussing on microbial degradation pathways. However, abiotic degradation pathways of these widespread pollutants are thought to produce less harmful reduction products than microbial degradation, that can lead to the accumulation of highly toxic vinyl chloride (40, 109, 110).

Diverging results exist for chlorinated ethanes relative to the more persistent and toxic chlorinated ethylenes. Chlorinated ethanes are more easily degraded and have been more widely investigated. Cervini-Silva *et al.,* (2001) investigated the ability of SWa-1 to reduced a range of chlorinated ethanes. The study had variable results suggesting that although a high concentration of Fe(II) created favourable conditions for reduction, degradation via dehydrochlorination facilitated by the clay mineral acting as a Lewis base predominated (52). (48) also investigated the degradation of chlorinated ethanes and concluded that the degradation

mechanism is dependent on the structure of the chlorinated aliphatic where hexachloroethane was degraded by dehydrochlorination and carbon tetrachloride was reductively dechlorinated. This study also observed biphasic kinetics for CCl_4 reduction in the presence of iron-rich clay minerals indicating that the biphasic behaviour is a characteristic of the clay mineral reactivity rather than contaminant structure.

Chlorinated ethylenes are more resistant to degradation under environmental conditions with some studies indicating that fully-dithionite reduced iron-rich nontronites are not able to facilitate their reduction (111). However, Lee and Bachelor (2004) found that biotite, vermiculite and montmorillonite minerals were capable of reducing chlorinated compounds with a reduction capacity similar to that of a natural soil (112) and a study investigating chlorinated ethylene degradation by natural sediments has suggested that oxidative transformation facilitated by Fe-bearing minerals including illite, kaolinite and biotite (102).

To date most work has focussed on the use of NACs and chlorinated compounds as reactive probe molecules. However, reactive Fe(II)-bearing minerals are known to be able to reduce other classes of compounds including pesticides, disinfectants and other industrial chemicals (113, 114). Therefore, it is likely that Fe-bearing clay minerals are also important for the reductive transformation for these groups of compounds although this is yet to be investigated.

2.4.4 Inorganic contaminants

Inorganic contaminants have also been used to elucidate reaction mechanisms of Fe-bearing clay minerals, particularly for non-smectitic Fe-rich clay minerals. The reduction of Cr(VI) to the less toxic and mobile Cr(III) by Fe(II)-bearing clay minerals has been well documented in field and laboratory studies and redox manipulation is often employed as a remedial technique at sites contaminated with Cr(VI) (93, 98, 99).

Biotite, vermiculite and montmorillonite clay minerals pretreated with dithionite had a reductive capacity towards Cr(VI) comparable with that of a natural soil (95) and the reactivity of dithionite-reduced smectite, montmorillonite, illite, vermiculite and kaolinte towards Cr (VI) correlates with their Fe(II) content (115). However, although these studies prove that Fe-bearing clay minerals are capable of facilitating the reduction of Cr(VI) they do not focus on reaction mechanisms. However, microbially reduced clay minerals have also been shown to reduce Cr(VI) and smectites (NAu-2, SWy-2) have been found to be more reactive than chlorite (CCa-2) and biotite (23, 116). Significantly, the reduction product was identified as Cr_2O_3 and was retained within the clay matrix following reduction, preventing the reoxidation and subsequent remobilisation of the chromium.

The redox reactivity of clay minerals is particularly relevant for the transformation of radionuclides as smectites are commonly used as backfill materials for nuclear waste repositories (117).

The reduction of pertechnate (TcO_4^-) to less mobile Tc(IV) species by structural iron in clay minerals has been well documented (18, 118). Although Fe(II) at iron (oxyhydr)oxide surfaces was found to result in a more rapid reduction process, phyllosilicate species were

found to be prolific in natural sediments (104). The importance of clay minerals are again highlighted as they were able to both reduce Tc(VII) and hold the resulting Tc(IV) within the solid matrix therefore preventing reoxidation (24). Bishop *et al.*, (2011) compared the reactivity of bioreduced- (strain CN32) chlorite, palygorskite and five members of the smectite-illite series towards pertechnate. Again, smectites were found to be most reactive and three factors were suggested to contribute to their enhanced reactivity; smectites generally have a larger reactive surface area, a less negative surface charge and a higher layer expandability than other clay minerals (24).

The importance of structural and surface-associated Fe(II) in a variety of minerals has also been documented as important for the reduction of a variety of other radionuclides including Pu(V) and Np(V) although to our knowledge, studies linking their reduction specifically to clay minerals are currently lacking (119, 120).

2.4.5 Electrochemical analyses of Fe-bearing clay minerals

Recently, electrochemical methods for measuring the reduction potential (E_H) of clay minerals have been developed (121–124) using electron transfer mediating compounds to allow indirect measurement of electron accepting/donating capacity. Figure 2.4 displays the redox profiles of four smectites, based on work by (123), indicating the range of conditions that the minerals are redox active across and a comparison to the one-electron reduction potentials of various nitroaromatic compounds (NACs) as an example contaminant class (106). The redox profiles vary for different smectites, which are redox active across different E_H ranges.

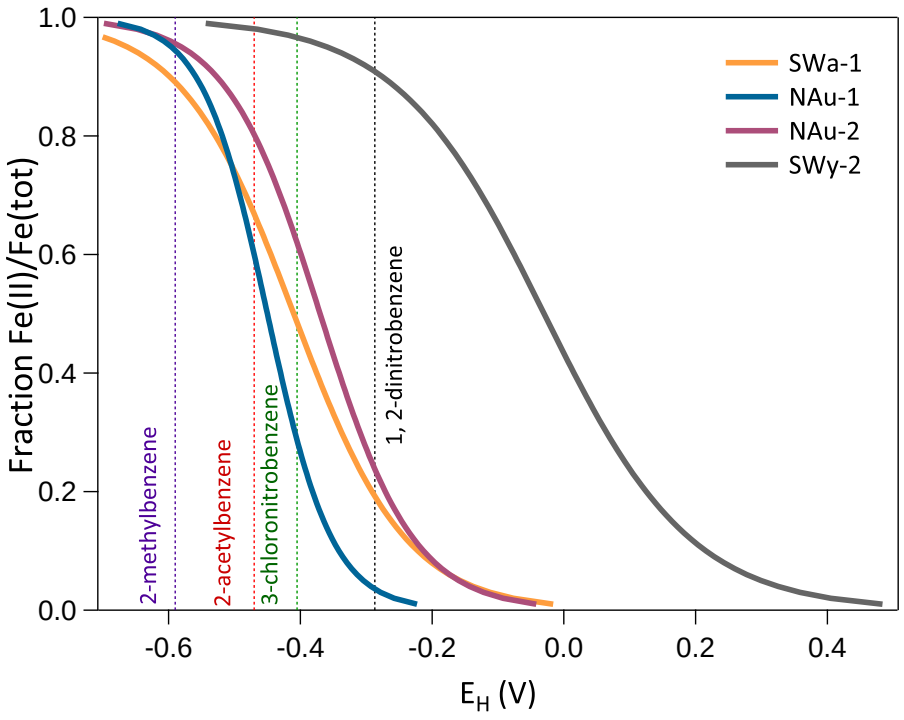

Figure 2.4: Redox profiles of smectites NAu-1, NAu-2, SWa-1 and SWy-2 derived by Gorski *et al.*, (2013) (123) compared to the E_H^1 values of various nitroaromatic compounds (106).

The redox profiles were also measured for smectites that had undergone cycles of reduction and oxidation. Consistent with previous work, they identified permanent structural changes to occur in the minerals after the first reduction step (84) that was reflected as a hysteresis in the redox profiles of the smectites. For nontronite NAu-1, this meant that after the first redox cycle, a more negative reduction potential was measured at lower reduction (% Fe(II)/Fe(tot)) extents (123).

Electrochemical methods are an exciting and promising technology for assessing the reduction capacity of Fe-bearing minerals. However, due to their novelty attempts to use this method to connect measured clay mineral E_H values with contaminant transformation remain in the early stages (25, 53, 124, 125). Although they have been utilised develop thermodynamic frameworks reactivity of single, well-characterised, mineral phases (46, 125), systems containing more than one redox-active phase, such as a Fe(II)-reduced clay mineral and associated Fe(III)-containing product becomes more difficult (25, 124) highlighting the difficulty of assessing the reactivity of Fe-bearing minerals in complex biogeochemical environments.

2.5 Approaches to assessing the reactivity of Fe-bearing clay minerals in complex natural systems

Laboratory studies have demonstrated the range of contaminants that Fe-bearing clay minerals may reduce in the environment and possible reduction mechanisms have been proposed. However, discrepancies are evident in published reduction rate constants between studies investigating the same clay minerals, possibly as a result of small changes in reaction conditions and solution chemistry. It is therefore difficult to identify trends that can be applied generally rather than for specific contaminants under specific conditions.

A lack of translation from laboratory studies to real world applications remains as many of the trends identified in laboratory studies have not been tested in real world environments and as such several open questions remain unanswered including:

i How do naturally occurring abiotic reductants (e.g. aqueous Fe(II)) and the presence of other redox-active mineral phases influence Fe-bearing clay mineral reactivity?

ii How do redox-active organic components (e.g. natural organic matter, microbes/microbial exudates) influence Fe-bearing clay mineral reactivity?

iii What are the implications of coexisting systems of redox-active components for Fe-bearing clay mineral reactivity in complex biogeochemical environments?

2.5.1 Interactions between Fe-bearing clay minerals, aqueous Fe(II) and other minerals

Recently, Fe(II)-reduced clay minerals have been demonstrated to be capable of facilitating the reduction of NACs, Cr(VI) and U(VI) (25, 47, 53). However, the mechanisms of this process are not yet clearly understood. The reduction of structural Fe(III) by aqueous Fe(II) results in the formation of a solid Fe(III)-containing product. Different Fe phases have been proposed

depending on solution conditions and Fe concentrations, including green-rust (25), ferrihydrite, magnetite (47) and lepidocrocite (80) using various spectroscopic techniques including Mössbauer (80), Extended X-ray Absorption Fine Structure (EXAFS), X-ray Diffraction (XRD) and Scanning Transmission Electron Microscopy-Energy Dispersive X-ray (STEM EDX) (25, 47).

As previously discussed, Fe(II) associated with mineral surfaces, in particular iron oxides, has been documented as a key reductant within natural systems affecting both contaminant degradation and mineral reduction and recrystallisation (34, 80, 81, 101, 126–128). Although their reactivity has been documented, it is currently unclear which Fe(II) pool (clay mineral or oxidation product) is predominantly reactive and the next chapter of this thesis aims to elucidate this using NACs.

2.5.2 Interactions of Fe-bearing clay minerals and Natural Organic Matter (NOM)

Natural Organic Matter (NOM) comprises complex, naturally occurring, heterogeneous organic molecules with various structural and functional properties (129, 130). NOM has a fundamental role in many naturally occurring redox processes (90, 131) and is ubiquitously present alongside reactive mineral-bound/aqueous Fe(II) (132–134). NOM has the capacity to directly reduce various elements in soil including Fe(III) (135, 136) and contains electron shuttling quinone moieties that are well known to enhance the rate of contaminant reduction (136–139). It is therefore likely to have a significant influence on the reactivity of Fe-bearing clay minerals.

NOM also contains ligand functional groups such as carboxylic and salicylic acids that can strongly complex Fe (130, 140). This action may inhibit reactivity through the removal of Fe(II) from the aqueous phase. However, Fe(II)-NOM complexes generally have lower reduction potentials than aqueous Fe(II) (140) and can directly reduce contaminants (132, 136).

Despite a recent renewed interest concerning the combined influence of organic matter and Fe-bearing minerals on contaminant transformation (141), to our knowledge, little work has investigated the influence of NOM on the reactivity of Fe-bearing clay minerals and we aim to address this gap in understanding in Chapter 4 of this thesis.

2.5.3 The influence of microbes and microbially-produced compounds on the redox reactivity of clay minerals

Iron is an essential, often limiting nutrient in many natural systems and in anaerobic environments, microorganisms are known to use Fe(III) in clay mineral structures as a terminal electron acceptor (17, 75). However, iron exists primarily in the solid phase and is not readily bioavailable without direct cell contact (32). As a result, microorganisms may produce exudates with a range of redox active groups to act as electron transfer mediators or chelating ligands in order to increase the accessibility of solid-bound (142, 143) and these compounds are widely present in soils (144–147).

Several classes of exudate compound exist that may influence the reactivity of Fe-bearing clay minerals. Firstly, several bacterial species are capable of producing electron shuttling

moieties, such as menaquinone and various flavin compounds to enhance dissimilatory iron reduction (143, 148, 149). Secondly, the production of siderophores (low molecular weight compounds with a high affinity for complex formation with Fe(III)) is a common strategy used by microbes to access solid-phase Fe(III) (150). Although siderophores have a high affinity for Fe(III), Fe(II)-siderophore complexes are capable of forming within temporarily anoxic environments, and have been shown to facilitate NAC reduction (1, 151). Other redox-active compounds associated with microbes include membrane proteins, particularly cytochromes. Cytochromes are membrane-bound hemeproteins and cytochrome c has previously been linked to enhanced bioreduction of contaminants (152, 153).

However, despite recent research highlighting the importance of microbial exudates for contaminant transformation in natural environments (154–156), little is currently known about their redox interactions with Fe-bearing clay minerals. We address this in Chapter 5 of this thesis.

2.6 Implications for the reactivity of Fe-bearing clay minerals in complex natural environments

Our review has highlighted the importance of Fe-bearing clay minerals for contaminant transformation in natural systems and we have identified the following broadly accepted views on the reactivity of Fe-bearing clay minerals:

i Clay minerals are ubiquitous within natural environments and contain varying amounts of structural iron (27, 38);

ii Clay mineral Fe may act as a renewable source of electron equivalents within natural environments capable of transforming a wide range of inorganic and organic contaminants (18–20, 24, 84);

iii Structural Fe(III) within clay minerals may be reduced across an astonishingly wide range of environmental conditions ($\Delta \mathrm{E_H} \sim 900$ mV) (123) and the mechanism of reduction governs the extent and type of potentially reactive Fe(II) sites that are formed (17, 63, 157);

iv Generally, smectites with a high structural iron content are the most redox-active type of iron-bearing clay mineral (20, 24, 116).

However, discrepancies exist in the literature and a number of open questions remain unanswered, which are summarised as follows:

i A general understanding of electron transfer mechanism and cycling is well established for single iron-bearing mineral species under controlled conditions (20, 46, 50, 125, 158). However, in the environment, redox conditions are dynamic and can lead to the coexistence of several redox active mineral phases. An understanding of the combined reactivity and interactions between these coexisting phases, particularly Fe(II)-reduced clay minerals and Fe(III)-containing oxidation products, is currently lacking;

ii NOM has a controlling influence on the redox properties of natural systems and may interact with, and influence the reactivity of iron-bearing clay minerals (139, 141). However, the impact of NOM on the reactivity of Fe-bearing clay minerals is yet to be quantified;

iii Abundant microbial exudates such as siderophores and quinone moieties in the environment may also influence the reactivity and stability of Fe-bearing clay minerals (1, 149, 153). Currently, there is little consensus concerning the likely influence of these microbially-produced compounds on the reactivity of Fe-bearing clay minerals within complex systems containing a variety of coexisting Fe-species and NOM.

Therefore, there is a need to make a jump between lab-based results concerning reduction rates and electron transfer mechanisms based on single reactive phases to complex real world systems. Such a new framework will create a detailed understanding of driving redox reactions allowing efficient interventions in earth systems such as the remediation of contaminated sites to be undertaken and enhance models to predict the fate of contaminants and nutrients in complex biogeochemical environments. We aim to take initial steps towards addressing this in this thesis.

Chapter 3
Assessing the redox reactivity of Fe(II)-reduced clay minerals

3.1 Introduction

Iron-bearing clay minerals are ubiquitously present in natural environments (38, 59) and both chemical (65, 66, 69) and microbial (76, 159, 160) reduction of structural Fe(III) in clay minerals has been documented. The resulting Fe(II) remains in the clay mineral structure and has been shown to be capable of reducing a range of environmentally relevant contaminants including nitroaromatic compounds (20, 21, 50), halogenated hydrocarbons (48), pesticides (49, 161), nitrate (45), radionuclides (24) and hexavalent chromium (23, 53). Due to their silicate framework, Fe-bearing clay minerals are largely resistant to reductive dissolution and can thus undergo redox cycling (84), rendering Fe-bearing clay minerals an important and potentially renewable source of electron equivalents in natural environments.

The reaction between Fe(II)-bearing clay minerals and contaminants has been studied using mostly clay minerals that were treated with strong reducing chemicals such as dithionite and thus contained almost exclusively Fe(II) in their structure (38, 55, 59). Iron-rich smectites with high reduction extents, i.e., with high Fe(II)/Fe(total) ratios, transformed organic contaminants quickly and exhibited characteristic biphasic reaction kinetics that were attributed to the presence of two types of reactive Fe(II) sites within the clay mineral structure (20, 48). In groundwater, however, where relevant redox potentials range between -0.2 mV and +0.1 mV (162), much lower Fe reduction extents of $\leq$11% are expected for Fe-rich clay minerals, based on electrochemically characterised clay mineral redox profiles (122). It is currently unknown whether Fe-rich clay minerals with low(er), and thus environmentally more relevant, Fe reduction extents will exhibit the same biphasic kinetics as documented for completely reduced clay minerals in laboratory studies.

Interestingly, much lower clay mineral Fe reduction extents of up to 40% Fe(II)/Fe(total) (21, 65, 84) have been reported to arise from microbial reduction. In contrast to chemically reduced clay minerals, microbially reduced clay minerals transformed organic contaminants following simple, non-biphasic second order kinetics (21, 22), similar to what has been observed for clay minerals with low Fe content (20). These observations are consistent with the presence of only one reactive Fe(II) site in both microbially reduced Fe-rich and chemically reduced Fe-poor clay minerals (20), suggesting that in addition to clay mineral total Fe content also the pathway and/or extent of clay mineral Fe reduction may determine the resulting clay mineral Fe redox reactivity.

Spectroscopic studies have indeed proposed that microbial and chemical reduction of clay mineral Fe occurs via different mechanisms and results in different structural Fe(II) entities. Microbial Fe reduction leads to discrete domains of Fe(II) and Fe(III) in Fe-rich clay minerals, and thus only one type of Fe(II) entity, and has been rationalised by a reduction front proceeding from the clay mineral edges inward through the octahedral sheet (68, 163). In contrast, clay mineral reduction by dithionite is thought to occur through the clay mineral basal siloxane surfaces in a pseudo-random fashion (69), creating preferentially mixed-valence dioctahedral Fe(II)Fe(III) species (61, 65). At high Fe reduction extent, upon further reduction of mixed valence Fe(II)Fe(III) sites to Fe(II)Fe(II) entities, structural rearrangements occur in Fe-rich clay minerals to accommodate the increased negative charge and lead to Fe(II) clustering into trioctahedral domains within the octahedral sheet (68, 164, 165). While trioctahedral domains have been identified as one of the reactive Fe(II) species in dithionite-reduced Fe-rich smectites during contaminant reduction, mixed-valent Fe(II)Fe(III) entities could not be detected in the same study using infrared (IR) spectroscopy but rather a variety of octahedral Fe(II)-metal cation pairs (157). It is possible that these two distinct mechanisms of clay mineral Fe reduction, which lead to different reactive Fe(II) species within the clay mineral structure, will thus result in different bulk redox reactivities towards contaminants, even at similar clay mineral Fe reduction extents.

In addition to chemical and microbial Fe reduction, recent work has demonstrated that aqueous Fe(II), an abundant microbially produced reductant in anoxic environments (47), is also capable of transferring electrons to structural Fe in clay minerals. This results in the formation of clay mineral Fe(II) and, interestingly, one or more Fe(III) oxidation products, which differ with clay mineral identity and experimental conditions (25, 47, 80, 81, 128, 166, 167). At circumneutral pH values, Fe(II) sorption and structural Fe reduction at Fe-rich clay minerals occurs predominantly via edge OH groups (166), similar to what has been proposed for microbial reduction. It is thus conceivable, albeit currently untested, that Fe(II)-reduced clay minerals might resemble microbially reduced clay minerals in both structure and reactivity. Furthermore, the presence of an *in-situ* solid Fe(III) oxidation product might additionally affect the overall observed rate of organic contaminant transformation, because the formed iron oxide/hydroxide phase may be reactive itself in the presence of aqueous Fe(II), as previously reported (42).

Here, we used a nitroaromatic compound (2-acetylnitrobenzene) as a reactive probe to assess the reactivity of reduced Fe-rich nontronite NAu-1. We evaluated the reactivity of dithionite-reduced NAu-1 and systematically varied its reduction extent from 3.5% to 91% Fe(II)/Fe(total), to determine whether biphasic reduction kinetics occur at all reduction extents. We then compared the reactivity of dithionite- and Fe(II)-reacted NAu-1 reduced to the same Fe(II)/Fe(total) ratios, to establish whether Fe(II)-reduced NAu-1 reacts similar as chemically reduced or microbially reduced clay mineral. We complemented our kinetic assessment with spectroscopic analyses (UV-vis and Mössbauer spectroscopy) to identify the reactive Fe(II) species in dithionite- and Fe(II)-reduced NAu-1 as well as at different reduction extents.

3.2 Materials and methods

3.2.1 Mineral preparation

A complete list of chemicals used is provided in the Supporting Information (S3.1). Nontronite NAu-1 ($M^{+}_{1.05}[Si_{6.98}Al_{1.02}][Al_{0.29}Fe_{3.68}Mg_{0.04}]O_{20}OH_4$, 21.5 wt% Fe) was purchased from the Source Clays Repository (http://www.clays.org) and size fractionated and Na^+-homoionized to obtain the 0.1-0.5 μm fraction (168) (details in S3.2). The absence of admixtures was confirmed using Fourier transform infrared (FT-IR) spectroscopy and the purified mineral was freeze dried, ground and passed through a 150 μm sieve prior to use.

3.2.2 Reduction of iron-bearing clay minerals using dithionite

All mineral reduction was undertaken in an anaerobic chamber (Glovebox Systemtechnik GS040113) under an N_2 atmosphere ($\leq$1 ppm O_2). A modified citrate-bicarbonate-dithionite method was used to reduce Fe in the clay minerals (63, 79). To achieve the desired Fe(II)/Fe(total) ratio, the amount of sodium dithionite salt added was varied according to the stoichiometry required or, for the case of complete reduction, an excess of three times the mass of the clay mineral was used. Subsequently, the suspensions were homoionised with Na^+ and washed with deoxygenated deionised water (18 MΩ cm). The final concentration of clay mineral within the stock suspensions (target: 15 g L^{-1}) as well as the reduction extent was checked by determining the Fe(II) and Fe(total) concentrations in a defined volume of suspension, following digestion with hydrofluoric acid (HF), based on a modified 1,10-phenanthroline method (169, 170).

3.2.3 Reduction using aqueous Fe(II)

Stock solutions of Fe(II) (100 mM) were prepared inside the glovebox by dissolving metallic Fe (Fe(0)) in 1M HCl for 3 hours at 60°C followed by dilution with deoxygenated deionised water and filtration through a 0.2 μm nylon filter. In addition to Fe(0) in its natural isotopic composition, Fe(II) solutions were also prepared from metallic Fe enriched in the ^{56}Fe or the ^{57}Fe isotope (Isoflex, San Francisco. Purity = 99.92 % ^{56}Fe, 95.02 % ^{57}Fe), for preparing samples for Mössbauer spectroscopy.

Batch reactors were prepared in glass vials (20 mL) and contained 15 mL 0.5 mM - 3.5 mM Fe(II) solution, depending on the desired reduction extent; 10 mM MOPS (3-(N-morpholino)propanesulfonic acid) buffer adjusted to pH 7.5 $\pm$ 0.1 using 1 M NaOH or 1 M HCl; and 50 mM NaCl as ionic strength buffer. The initial aqueous Fe(II) and Fe(total) concentrations were determined by subjecting a 30 μL sample from each reactor to the colourimetric 1,10-phenanthroline assay(170).

Clay mineral NAu-1 samples of 30.0 $\pm$ 0.5 mg were stored in the anaerobic chamber overnight to ensure the absence of oxygen at the mineral surface and were then added to the batch reactors to initiate smectite Fe reduction by aqueous Fe(II). Equilibration was carried out on an end-over-end rotator in the dark to prevent photooxidation and for exactly 24 hours

to allow the same, maximum reduction extent to be reached before the initiation of kinetic experiments and to prevent ageing effects as observed previously (25, 50).

To quantify the reduction extent of the nontronite and to trace the formation of the solid iron oxidation product, reactors of the same composition were prepared but using ^{56}Fe(II) and ^{57}Fe(II) solution, respectively. As demonstrated previously, using Mössbauer-invisible ^{56}Fe(II) allows to monitor changes in clay mineral Fe speciation (80, 81, 127, 166), whereas using Mössbauer-visible ^{57}Fe(II) allows to selectively assess the fate of the added aqueous Fe(II) (80, 81, 127, 166), as the ^{57}Fe in the clay mineral only contributes $\leq$0.1% of the spectral area in the resulting Mössbauer spectra.

3.2.4 Kinetic batch experiments

Kinetic batch reactors were either identical with the reactors resulting from reduction using aqueous Fe(II) or were prepared from the stock suspensions of dithionite-reduced NAu-1. The latter contained a total volume of 15 mL NAu-1 suspension (final concentration: 2.0 g L^{-1}) and 10 mM anoxic MOPS adjusted to pH 7.5 $\pm$ 0.1. Reactors were prepared containing reduced clay suspensions with reduction extents of 3.5%, 5%, 10%, 15% 30%, 50%, 75% and 100% Fe(II)/Fe(total) for dithionite-reduced NAu-1 and 3.5%, 5% and 8% Fe(II)/Fe(total) for Fe(II)-reduced NAu-1. All experiments were undertaken in triplicate and the extent of reduction was checked using both Mössbauer spectroscopy and HF digestion with the 1,10-phenanthroline assay (169, 170).

Kinetic experiments were initiated by spiking the batch reactors with 30 μL methanolic stock of 2-acetylnitrobenzene (2AcNB) to give an initial concentration of $\sim$50 μM. 2AcNB was chosen as a representative nitroaromatic compound as it is non-planar and will therefore not be affected by sorption to the mineral surface (50) and has been widely used in other studies. Samples of 500 μL were periodically withdrawn and passed through a 0.22 μm nylon filter to remove the mineral and thus stop the reaction, and were stored in the fridge at 4 °C prior to HPLC analysis.

3.2.5 Analytical methods

Quantification of 2AcNB and the reduction product 2-acetylaniline (2AcAn) was carried out by HPLC equipped with a DAD dector (Agilent 1260 Infinity II or Thermo Fisher Dionex UtiMate 3000), using an LC-18 column (XBridge C18 3.5 μm) and MeOH/H_2O (40/60), as previously described (20).

3.2.6 Mössbauer spectroscopy

The structural coordination and reduction extent of Fe in the smectites was analysed using cryogenic (4 - 77 K) ^{57}Fe-Mössbauer spectroscopy. Sample preparation and details of instrument set up and measurements are described in S3.3.

Fitting of the spectra was undertaken using Recoil software (Ottawa, Canada) using a Voigt based fitting approach (171) for samples that did not exhibit any magnetic ordering, or using Full Static Hamiltonian site analysis for samples containing ordered phases.

UV-vis spectroscopy

Quantification of the abundance of Fe(II)-O-Fe(III) species in dithionite-reduced NAu-1 was undertaken using UV-vis spectroscopy (Varian Cary 5) at a wavelength of 730 nm. The spectrometer utilised a flow through cell, in which anaerobic conditions were maintained by constant flushing with N_2 and contained accessories to counteract specular and diffuse reflection from the clay mineral particles.

3.2.7 Kinetic modelling

Kinetics of 2AcNB reduction in smectite suspensions were modelled applying a second order kinetic rate law. As previously suggested for iron-rich clay minerals, the kinetic rate law included the presence of two reactive Fe(II) sites with distinct reactivities (equation 3.1)(20):

$$\frac{\partial[\mathrm{NAC}]}{\partial \mathrm{t}} = -\mathrm{k_A} \cdot [\mathrm{Fe(II)_A}] \cdot [\mathrm{NAC}] - \mathrm{k_B} \cdot [\mathrm{Fe(II)_B}] \cdot [\mathrm{NAC}] \tag{3.1}$$

The second order rate constants $\mathrm{k_A}$ and $\mathrm{k_B}$ describe the intrinsic reactivities of the Fe(II) sites of high and low reactivity, respectively; [NAC] the aqueous concentration of 2AcNB; and $[\mathrm{Fe(II)_A}]$ and $[\mathrm{Fe(II)_B}]$ the concentration of the two reactive Fe(II) sites. A mass balance equation for the total Fe(II) concentration, $[\mathrm{Fe(II)_{total}}]$, in the system was included as a boundary condition in the mathematical model as:

$$[\mathrm{Fe(II)_{total}}] = [\mathrm{Fe(II)_A}] + [\mathrm{Fe(II)_B}] \tag{3.2}$$

For comparison, the kinetic data were also fit with a kinetic rate law including only one reactive Fe(II) site, which results in a simplified version of equation 3.1 with $\mathrm{k_B}$ set to 0 and the value of $[\mathrm{Fe(II)_A}]$ equal to $[\mathrm{Fe(II)_{total}}]$:

$$\frac{\partial[\mathrm{NAC}]}{\partial \mathrm{t}} = -\mathrm{k} \cdot [\mathrm{Fe(II)_{total}}] \cdot [\mathrm{NAC}] \tag{3.3}$$

Using a least squares method implemented in Matlab, the appropriate differential equation was used to fit the measured data based on the Nelder-Mead simplex method and resulted in estimated values for parameters $\mathrm{k_A}$, $\mathrm{k_B}$ and the initial concentration of $\mathrm{Fe(II)_A}$ (equation 3.1), or k (equation 3.3). Standard deviations of the estimated log parameters were calculated using linear error propagation. The previously suggested model (20) additionally incorporated the interconversion of the two reactive Fe(II) sites to correctly describe the kinetics of respike experiments. Similar to a previous study with no respike experiments (48), we omitted this step from our model.

3.3 Results and Discussion

3.3.1 Nitroaromatic compound reduction with dithionite-reduced NAu-1

To assess how organic contaminant reduction in the environment may be affected by abiotically reduced Fe-bearing clay minerals, we used 2-acetylnitrobenzene (2AcNB) as a reactive probe (106) and monitored its reductive transformation to the corresponding aniline in suspensions of NAu-1 reduced with dithionite to structural Fe(II)/Fe(total) ratios between 3.5% and 91%. The reactors thus contained 0.32-8.2 mM clay mineral Fe(II), which provide more than the 300 μM electrons required for the stoichiometric transformation of the initially added 50 μM 2AcNB to the corresponding aniline (106).

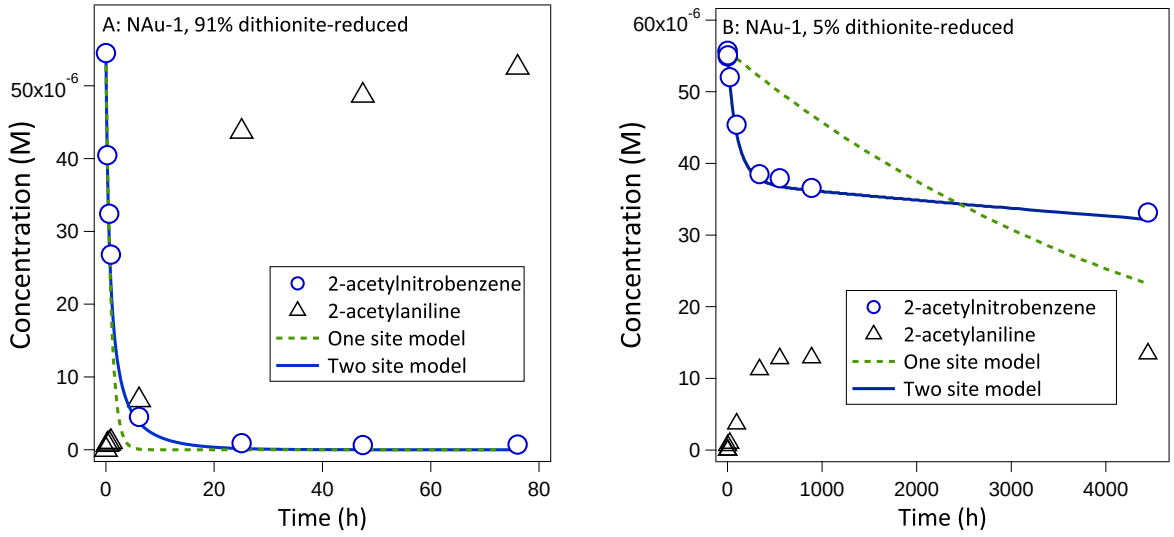

Figure 3.1: Typical reduction kinetics of 2-acetylnitrobenzene (blue circles) to 2-acetylaniline (black triangles) in suspensions of dithionite-reduced NAu-1, with initial clay mineral Fe reduction extents of (a) 91% Fe(II)/Fe(total) and (b) 5% Fe(II)/Fe(total). The data were fit with a second order kinetic model representative of one reactive Fe(II) site (green dashed line, equation 3.3) and a biphasic, two site kinetic model (blue solid line, equation 3.1).

Typical concentration time courses for the transformation of 2AcNB to 2-acetylaniline (2AcAn) in suspensions of dithionite-reduced NAu-1 are shown in Figure 3.1. For NAu-1 with a reduction extent (i.e., Fe(II)/Fe(total) ratio) of 91%, an initially rapid decrease in 2AcNB concentration was followed by a slower reaction after 1-5 hours and transformation to 2AcAn was complete after 72 hours (Figure 3.1A). Transformation of 2AcNB was considerably slower for NAu-1 dithionite-reduced to 5% Fe(II)/Fe(total) (Figure 3.1B) and complete transformation was not reached after 4500 hours ($>$ 6 months). Despite the slow transformation, the reduction kinetics followed the same biphasic behaviour as observed for NAu-1 reduced to 91% Fe(II)/Fe(total) (Figure 3.1A) and could not be fit with the one-site model (green dashed line in Figure 3.1, equation 3.3). We obtained analogous results for the transformation of 2AcNB for all suspensions containing dithionite-reduced NAu-1 (Figures S3.1a-e). Similar biphasic transformation kinetics have also been documented previously for dithionite-reduced, Fe-rich smectites during their reaction with nitroaromatic compounds and halogenated hydrocarbons

(20, 48, 50). We thus suggest that biphasic reaction kinetics are an intrinsic property of dithionite-reduced Fe-rich clay minerals and are independent of the clay mineral's reduction extent.

Interestingly, recent work found that Cr(VI) reduction with dithionite-reduced NAu-1 rather followed a one-site, second-order kinetic rate law similar to equation 3.3.(53) Because Cr(VI) transformation was complete within only 12 minutes and over 50% of the initially present Cr(VI) were transformed before the first sample could be taken, we suspect that the biphasic reduction kinetics were not captured in these rapid transformation experiments. This hypothesis is further supported by our observation that increasingly rapid transformation at higher clay mineral Fe reduction extent, and thus higher Fe(II) concentration, resulted in increasingly smaller differences in goodness-of-fit between one-site and two-site kinetic models (Figures 3.1, S3.1a-e).

Our observation of biphasic reduction kinetics for dithionite-reduced NAu-1 across the entire range of Fe(II)/Fe(total) ratios from 5% to 91% points to the presence of two reactive clay mineral Fe(II) species with different intrinsic reactivities (20, 48) even at very low reduction extents. In contrast, reduction of a range of nitroaromatic compounds with microbially reduced NAu-2, an Fe-rich clay mineral with similar structure and Fe content as NAu-1, followed a one-site second-order kinetic rate law similar to equation 3.3 for all Fe(II)/Fe(total) ratios between 8% and 34% (22). This marked difference in reaction kinetics of dithionite and bio-reduced clay minerals at similar, low Fe(II)/Fe(total) ratios suggests that not the clay mineral Fe reduction extent but rather the pathway of clay mineral Fe reduction is critical for the resulting observable contaminant reduction (or Fe(II) oxidation) kinetics.

3.3.2 Nitroaromatic compound reduction with Fe(II)-reduced NAu-1

The strong dependence of clay mineral reductive reactivity on the pathway of clay mineral Fe reduction raises the fascinating question of how the reactivity of clay minerals reduced with aqueous Fe(II) will compare to that of bio-reduced and dithionite-reduced clay minerals. To answer this question, kinetics of 2AcNB reduction were investigated in suspensions of NAu-1 reduced with aqueous Fe(II) to 3.5-8% Fe(II)/Fe(total) ratios (166, 167). Although the maximum reduction extent is much lower than after dithionite reduction, it is comparable to that observed for bio-reduced NAu-1 (75, 172) and the resulting structural Fe(II) concentrations of 0.32-0.72 mM (Table 3.1) are again in excess of the reduction equivalents required for the stoichiometric transformation of 2AcNB in our experiments.

Reduction of 2AcNB with Fe(II)-reduced NAu-1 at reduction extents at or above 5% was, again, characterised by biphasic kinetics (Figures 3.2A, S3.2), similar to what we observed for dithionite-reduced NAu-1. The similarity in transformation kinetics of dithionite- and Fe(II)-reduced Fe-rich clay mineral could imply that similar reactive Fe(II) species were formed and/or that the clay mineral Fe reduction pathway is similar for these two abiotic reductants. In addition, biphasic Fe(II) oxidation kinetics could be a unique characteristic of abiotically reduced Fe-rich clay minerals and could potentially be used to distinguish the pathway of clay

mineral Fe reduction in environmental settings. However, unlike dithionite-reduced NAu-1 of comparable reduction extents, Fe(II)-reduced NAu-1 with 8% and 5.5% Fe(II)/Fe(total) ratios completely transformed 2AcNB to 2AcAn within 1000 and 1400 hours, respectively (compare Figures 3.1B and 3.2A). The higher extent of 2AcNB reduction suggests that the overall reductive reactivity and/or reductive capacity of Fe(II)-reduced NAu-1 was significantly higher compared to the dithionite-reduced equivalent.

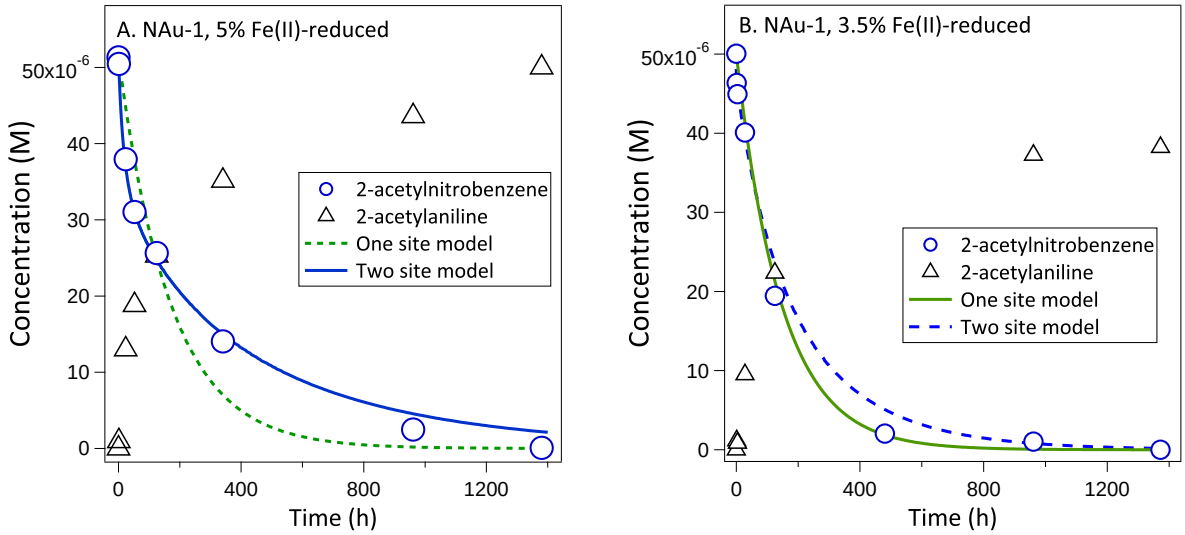

Figure 3.2: Reduction kinetics of 2-acetylnitrobenzene (blue circles) to 2-acetylaniline (black triangles) in suspensions of Fe(II)-reduced NAu-1. (a) For NAu-1 with an initial clay mineral Fe reduction extent of 5% Fe(II)/Fe(total) typical biphasic transformation kinetics were observed (two-site model: blue solid line, equation 3.1; for comparison, the fit to the one-site model (equation 3.3) is shown as green dashed line). Similar reduction kinetics were also found for Fe(II)-reduced NAu-1 with 8% reduction extent (Figure S4). (b) In contrast, 2-acetylnitrobenzene transformation with NAu-1 with an initial clay mineral Fe reduction extent of 3.5% Fe(II)/Fe(total) followed one-site second-order kinetics (green solid line, equation 3.3; for comparison, the fit to the two-site model (equation 3.1) is shown as blue dashed line).

Although the same clay mineral Fe(II) concentrations were present in our experiments with Fe(II)- and dithionite-reduced NAu-1, residual aqueous Fe(II) remained in the reactors after reduction of NAu-1 with Fe(II). This residual aqueous Fe(II) could have interacted with the clay mineral also after the initial electron transfer reaction, potentially adding to the reductive capacity of Fe(II)-reduced NAu-1 and/or re-generating the reactive clay mineral Fe(II) via continuous interfacial electron transfer (166, 167). Because we, and others, found that aqueous Fe(II) alone cannot transform 2AcNB (51, 173) (Figure S3.3) and only limited transformation occurs in the presence of Fe(II) sorbed to Fe-free hectorite, silica or alumina surfaces (51, 79) electron transfer from aqueous Fe(II) to the solid phase(s) is required. To explore whether the reduction equivalents stored in the residual aqueous Fe(II) could account for the observed differences in reduction capacities of Fe(II)- and dithionite reduced NAu-1, we calculated the electron balance for the reaction by taking into account the amount of 2AcNB transformed, changes in the clay mineral Fe(II)/Fe(III) ratio as well as the aqueous Fe(II) concentration before and after reaction with 2AcNB (Table 3.1).

Table 3.1: Electron balance for NAC reduction by Fe(II)-reduced NAu-1. Concentrations are shown in mM.

Before 2AcNB addition							**After complete reaction with 2AcNB.**		
Reactor		**Initial aqueous Fe(II)**	**Aqueous Fe(II) after NAu-1 addition**	**Fe(II) sorbed**	**NAu-1 Fe(II) formed**	**Oxidation product/sorbed Fe(II)**	**Aqueous Fe(II)**	**Further Fe(II) removal**	**NAu-1 Fe(II) remaining**
3.5% reduced	Fe(II)-	1.2	0.67	0.53	0.32	0.21	0.23	0.24	0.02 (0%)
5.5% reduced	Fe(II)-	2	1.14	0.86	0.41	0.45	0.73	0.41	0.15 (2%)
8% reduced	Fe(II)-	3.5	2.03	1.47	0.72	0.75	1.25	0.78	0.42 (5%)

Following the initial addition of NAu-1 to solution containing aqueous Fe(II), 0.53-1.47 mM Fe(II) was removed from the aqueous phase. Mössbauer analysis of NAu-1 reacted with aqueous ^{56}Fe(II) revealed that 0.32-0.72 mM of this solid-associated Fe(II) each transferred one electron to clay mineral Fe(III) and were thus oxidised to Fe(III). Each of the resulting Fe(II) pools, i.e. structural Fe(II) in NAu-1 and solid-associated Fe(II), could account for a high proportion of, if not for all, 2AcNB reduction (53-120 μM and 37-125 μM, respectively, accounting for the 1:6 stoichiometry). After complete transformation of 2AcNB, clay mineral Fe(II) had significantly decreased to 0-2.5% of the total Fe and a further 0.24-0.78 mM Fe(II) had been removed from the aqueous phase, which could each, again, account for 2AcNB reduction (53-83 μM and 40-195 μM, respectively; making it impossible to unambiguously assign the source of reduction equivalents for 2AcNB from electron balances alone. However, our calculation clearly demonstrate that structural Fe(II) in Fe(II)-reduced NAu-1 was contributing to the observed redox reactivity and that the residual aqueous Fe(II) redistributed over the time of our experiments.

Interestingly, at the very low reduction extent of 3.5% Fe(II)/Fe(total), 2AcNB transformation with Fe(II)-reduced NAu-1 deviated from the biphasic, two-site behaviour and was best described using one reactive Fe(II) site (Figure 3.2B). The observed reaction kinetics resembles what has been reported for bio-reduced NAu-2 (21), suggesting that in both cases a similar reactive Fe(II) species was present and/or clay mineral Fe reduction occurred via a similar pathway. Although the same clay mineral loading (2 gL^{-1}) and reactive probe compounds of similar intrinsic reactivity were used (20), nitroaromatic compound transformation with Fe(II)-reacted NAu-1 with a reduction extent of 3.5% was complete after 1400 hours (Figure 3.2B), whereas negligible transformation was found with bio-reduced NAu-2 containing 8% Fe(II)/Fe(total) (21), as well as dithionite-reduced NAu-1 containing 3.5% Fe(II)/Fe(total) (Figure S3.1a). Our results suggest that structural Fe(II) in the clay mineral alone was not responsible for 2AcNB transformation in the presence of Fe(II)-reacted NAu-1 with 3.5% Fe(II)/Fe(total). In this case, 2AcNB transformation was rather driven by the solid-associated Fe(II) formed from the interaction of aqueous Fe(II) with NAu-1, possibly in combination with the formed Fe(III) and/or the residual aqueous Fe(II).

3.3.3 Analysis of kinetic parameters for the contaminant transformation by Fe(II)-reduced and dithionite-reduced NAu-1

To further explore the similarities and differences in the reactivity of dithionite-reduced and Fe(II)-reduced clay minerals, including the role of the solid-associated Fe(II) at very low Fe reduction extents, we analysed the kinetic parameters obtained from the mathematical models for describing the 2AcNB transformation kinetics. The parameters fit with the models include the rate constants of the reactive Fe(II) site(s), which describe their intrinsic reactivities(20) and are presumed to be linked to their identity (157), and, in case of the two-site kinetic model (equation 3.1), also the concentration of the highly reactive Fe(II) species.

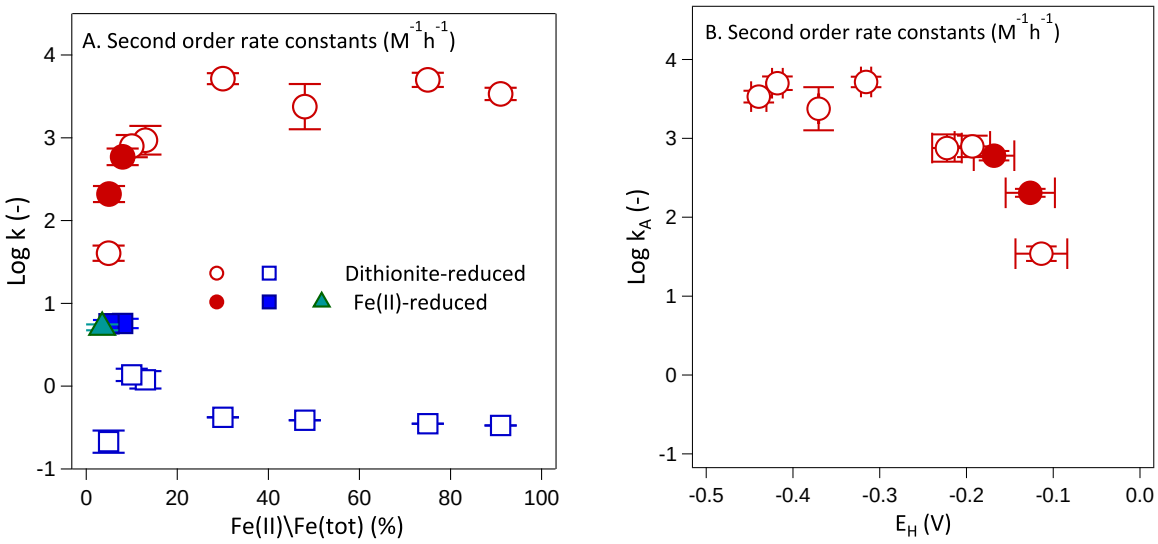

Figure 3.3: (A) Logarithms of second order rate constants of 2AcNB reduction with dithionite- and Fe(II)-reduced NAu-1 as a function of clay mineral structural Fe(II)/Fe(total) ratios. Parameters were evaluated using the two-site kinetic model (equation 3.1) for all data sets, except for 2AcNB reduction with Fe(II)-reacted NAu-1 with 3.5% Fe(II)/Fe(total), for which the one-site model (equation 3.3) was used. Rate constants of the highly reactive Fe(II) site (k_A) are shown as red circles, of the low reactive site (k_B) as blue squares and of one reactive site (k) as green triangle. (B) Second order rate constants of the highly reactive Fe(II) site (k_A) as function of the clay mineral Fe redox potential, E_H, over the range of NAu-1 reduction extents. E_H values were calculated using the electrochemically determined Nernstian profile of NAu-1 (123). Error bars represent standard deviations of the parameters.

For dithionite-reduced NAu-1, the value of the highly reactive Fe(II) site's rate constant (k_A, red open circles in Figure S3.9A) increased two orders of magnitude between 5% and 30% Fe(II)/Fe(total) ratios and then plateaued. Because the kinetic rate constants describe the intrinsic reactivity of the reactive Fe(II) sites, the observed increase in rate constant suggests that either different reactive Fe(II) sites were formed and/or involved in probe compound transformation, or that the intrinsic reactivity of the same Fe(II) species changed with increasing reduction extent. Interestingly, an identical trend was observed for the rate constants k_A of Fe(II)-reduced NAu-1 (red filled circles in Figure S3.9A), albeit over a smaller range of reduction extents and below the threshold at which the rate constant plateaued for dithionite-reduced NAu-1. Our observation of the identical trend for dithionite- and Fe(II)-reduced NAu-1 suggests that the same reactive Fe(II) species was responsible for the initial fast phase of the reaction or, alternatively, that the same changes in Fe(II) site reactivity occurred, regardless of the reduction method applied.

To explore whether the systematic changes in rate constant values were connected to changes in the system's overall free energy, we investigated the relationship between rate constant k_A and the clay mineral reduction potential E_H, which we calculated using the electrochemically determined Nernstian profile for NAu-1 (123) and our measured NAu-1 reduction extents (Table S3.1). We found a steep, non-linear increase in rate constant values with decreasing reduction potential between -0.11 and -0.32 V (Figure S3.9B). Further decrease in reduction potential, corresponding to an increase in clay mineral Fe reduction beyond 30% (Table S3.1), did not lead to higher rate constants, indicating that the intrinsic reactivity and/or

type of highly reactive Fe(II) sites became independent of the clay mineral's free energy. We thus conclude that for both dithionite- and Fe(II)-reduced NAu-1, a simple (linear) free-energy relationship cannot be derived for the entire range of reduction extents and that at a reduction extent of around 30% Fe(II)/Fe(total), a significant change in reaction mechanism and/or relative contributions of additional processes such as sorption or mass-transfer to the overall transformation occurred. Although our findings challenge the linear free energy relationship proposed for Cr(VI) reduction with a clay mineral of similar Fe content and structure (NAu-2) and covering Fe reduction extents between 26% and 98% Fe(II)/Fe(total) (53), we suggest that structural differences between Cr(VI) and 2AcNB might have led to the deviating trends observed, similar to their different reactivity trends with the same range of Fe(II)-bearing minerals (42).

Compared to the highly reactive Fe(II) sites, the rate constants of the second, less reactive Fe(II) sites ($\mathrm{k_B}$) of dithionite-reduced NAu-1 were 2-4 orders of magnitude lower (open blue squares in Figure S3.9A, Table S3.1), in agreement with previously observed differences between $\mathrm{k_A}$ and $\mathrm{k_B}$ values determined for dithionite-reduced Fe-rich smectites (20, 157). Although the values of $\mathrm{k_B}$ increased slightly with clay mineral Fe reduction extent, $\mathrm{k_B}$ values (log) remained at the same intermediate level of around -0.5 (Table S3.1) at reduction extents of $\geq$30% Fe(II)/Fe(total) and overall varied less than 1 order of magnitude. The different trends of $\mathrm{k_A}$ and $\mathrm{k_B}$ values resulted in an increasing gap from 2 to 4 orders of magnitude between the two rate constants with increasing clay mineral Fe reduction extent. We also note that the uncertainty of log $\mathrm{k_B}$ values increased significantly at Fe(II)/Fe(total) ratios exceeding 30%, which we attribute to the kinetics being dominated by the highly reactive Fe(II) sites at higher reduction extents (compare Figures 3.1A and B). Regardless of the uncertainty associated with the absolute value of log $\mathrm{k_B}$, low reactivity Fe(II) sites need to be invoked to correctly describe the observed 2AcNB reduction kinetics and contribute more to the overall clay mineral Fe(II) reactivity at lower reduction extents.

In contrast to similar trends in $\mathrm{k_A}$ values observed for dithionite- and Fe(II)-reduced NAu-1, the values of $\mathrm{k_B}$ determined for Fe(II)-reduced NAu-1 are notably and statistically significantly higher by 0.5-1.5 orders of magnitude than those of dithionite-reduced NAu-1 (compare filled and open blue squares in Figure S3.9A, Table S3.1). Our finding suggests that in Fe(II)- and dithionite-reduced NAu-1, different low-reactivity Fe(II) species were present and/or contributed to 2AcNB transformation, or that the same Fe(II) species were present but had different reactivities. Interestingly, the value of the rate constant determined for Fe(II)-reduced NAu-1 with the very low Fe(II)/Fe(total) ratio of 3.5% (triangle in Figure S3.9A, Table S3.1) and where only one reactive site controlled the reaction, coincided with the $\mathrm{k_B}$ values obtained for Fe(II)-reduced NAu-1 with 5.5% and 8% Fe(II)/Fe(total) ratios. Because the same rate constant value (log k or log $\mathrm{k_B}$ of 0.71-0.76, Table S3.4) was consistently found for all Fe(II)-reduced NAu-1 in our study, we hypothesise that k and $\mathrm{k_B}$ indeed represent the reactivity of the same Fe(II) species in Fe(II)-reduced NAu-1 and that this species is distinct from the low reactivity Fe(II) site in dithionite-reduced NAu-1. Because we ruled out clay mineral struc-

tural Fe(II) as the reactive species in Fe(II)-reacted NAu-1 with 3.5% Fe(II)/Fe(total), it is plausible that the low/only reactive in Fe(II)-reduced NAu-1 could be Fe(II) bound to/in the oxidation product resulting from electron transfer between aqueous and clay mineral Fe. Published rate constants for nitroaromatic compound transformation with Fe(II)-reacted Fe oxides under similar reaction conditions (42, 51, 173, 174) are of the same order of magnitude as our log k and log $\mathrm{k_B}$ values (Table S3.5) and seem to support this hypothesis, yet unambiguous assignment of the Fe(II) sites in the kinetic model to physical Fe(II) species requires further direct evidence.

In addition to rate constants, the kinetic model also provides the initial concentration of the highly reactive Fe(II) sites ($[\mathrm{Fe(II)_A}]$ (Table S3.4) in equation 3.1) and, per difference, also of the low reactivity Fe(II) sites ($\mathrm{Fe(II)_B}$). The calculated concentrations of $\mathrm{Fe(II)_A}$ were also almost identical for dithionite- and Fe(II)-reduced NAu-1 (Figure 3.4A), further corroborating our conclusion that the same highly reactive Fe(II) species was present, irrespective of the reductant used. Interestingly, the initial concentration of highly reactive Fe(II) sites strongly correlated with the clay mineral reduction extent and showed a very distinctive pattern. With increasing structural Fe(II)/Fe(total) ratio, the highly reactive Fe(II) sites became more abundant up to a maximum at a reduction extent of 48% (note the split y axis), before decreasing again as the reduction extent continued to increase (Figure 3.4A). The observed trend is similar to that reported for the abundance of octahedral mixed valence Fe(II)–Fe(III) pairs in dithionite-reduced Fe-rich smectites, (67) suggesting that the highly reactive Fe(II) site might correspond to Fe(II)–Fe(III) entities. However, based on kinetic analysis alone, we cannot identify the structural identity of the clay mineral Fe(II) species, nor the contribution of the oxidation product to the reactivity in Fe(II)-reacted clay mineral suspensions.

3.3.4 Linking reactivity and structure of abiotically reduced nontronite

3.3.4.1 What is the nature of the highly reactive Fe(II) sites?

To link the reactive Fe(II) sites used in the kinetic model to specific Fe entities within the clay mineral structure, we complemented our kinetic analysis with UV-vis and Mössbauer spectroscopy, which have both been used to study clay mineral Fe reduction mechanisms and to identify the resulting Fe(II) entities (65, 67, 68) Structural Fe(II) species that have been suggested to contribute to the redox reactivity of dithionite-reduced clay minerals include dioctahedral Fe(II)–Fe(III) pairs, trioctahedral Fe(II) entities, and Fe(II) bound to other octahedral cations such as Al or Mg (65, 157).

To test for the presence and relative abundance of Fe(II)-O-Fe(III) species (or, octahedral Fe(II)–Fe(III) pairs) at the beginning of our experiments, we quantified the UV-vis absorbance of the corresponding intervalence charge transfer (IVCT) band at 730 nm (65, 67) for dithionite-reduced NAu-1 over the same range of Fe(II)/Fe(total) ratios as in the kinetic experiments (3.5%-91%). As expected, the absorbance, and thus the number of Fe(II)-O-Fe(III) entities, increased with increasing Fe reduction extent but then reached a plateau at an Fe(II)/Fe(total) ratio of 30% (Figure 3.4B). The absorbance pattern clearly contrasts previous observations,

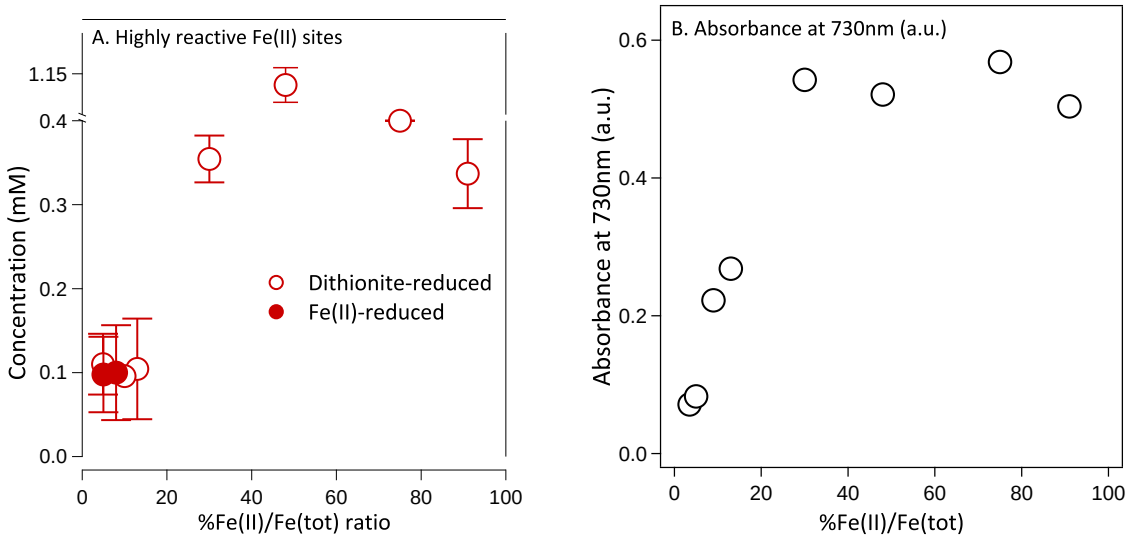

Figure 3.4: (A) Concentration of highly reactive Fe(II) sites resulting from fitting the kinetic data to the two-site model (equation 3.1) and (B) UV-vis absorbance at 730nm (175) as a function of NAu-1 reduction extent. Error bars represent standard deviations of the parameters.

where a distinct maximum was reached at reduction extents around 40-50%, (65, 67) and also differs from the trend observed for the concentration of highly reactive Fe(II) sites (compare Figures 3.4A and B). It is thus unlikely that Fe(II)-O-Fe(III) groups are the clay mineral entities corresponding to the highly reactive Fe(II) sites in the kinetic model. However, both absorbance at 730 nm and the kinetic rate constant of the highly reactive Fe(II) sites exhibit remarkably similar dependences on the clay mineral Fe reduction extent (compare Figures S3.9A and 3.4B), which could suggest a link between the two properties. The full optical absorption spectra for NAu-1 at reduction extents of 3.5 % - 91 % is provided in Figure S3.5.

An alternative interpretation of the absorbance band at 730 nm can be developed when taking into account that electron hopping between neighbouring Fe atoms in the octahedral sheet of nontronites is fast at room temperature, (158) at which the UV-vis measurements were carried out. Due to the high electron mobility within the nontronite lattice, (65) electrons added to the clay mineral during the reduction process would, at least partially, be delocalised, which, in turn, would prevent the formation of distinct and localised Fe(II)–Fe(III) pairs. This hypothesis is further supported by the lack of a distinct absorption band in the infrared (IR) spectra of partly reduced Fe-rich clay minerals that would correspond to bending vibrations of clay mineral hydroxyl groups attached to mixed-valent Fe(II)–Fe(III) pairs.(157) Furthermore, charge balance at low reduction extents is maintained by the absorption of cations from solution (165) and we calculated that cation sorption dominates up to an Fe reduction extent of around 16% in NAu-1, as detailed in SI S8. The clay mineral dioctahedral structure is therefore preserved, at a minimum, up to this reduction extent, which also coincides with the Fe(II)/Fe(total) ratio at which the absorbance at 730 nm started to plateau (Figure 3.4B). The absorbance band at 730 nm could thus be an indicator of electron doping of the bulk structure comprising connected dioctahedral Fe atoms, (176) which might affect the electronic structure of the semiconductor-like octahedral sheet of the nontronite. Due to the delocalised nature

of the electrons, increasing electron doping would thus increase the intrinsic reactivity of clay mineral Fe(II), i.e. rate constants (Figures S3.9A), rather than the number of reactive sites, which remained constant at reduction extents below 20% (Figure 3.4A). At reduction extents higher than ∼16%, uptake of protons dominates over cation sorption to balance the additional charge created in the octahedral sheets. Increasing protonation of structural hydroxyl groups leads to their subsequent dehydroxylation and to clay mineral structural rearrangements, including trioctahedral domain formation (164, 165). Unless the trioctahedral entities comprise almost exclusively Fe(II) atoms and contain appreciable amounts of Fe(III) above the threshold of 1:10 Fe(III)/Fe(II), further Fe reduction and structural rearrangements will not result in increasing absorbance at 730 nm, (177) suggesting that our observations (Figure 3.4B) are consistent with the formation of Fe(II) trioctahedral entities at reduction extents exceeding 30%. In ferruginous smectite, a clay mineral with a similar structure as NAu-1 (Mg-poor, 12.6 wt% Fe, tetrahedral excess charge), trioctahedral Fe(II) entities have been linked to highly reactive Fe(II) sites in the kinetic model, whereas dioctahedral Fe(II) coordinated to octahedral cations, including Al and Fe(II), was related to sites with a lower reactivity (157).

To further explore the extent of Fe(II) clustering in our dithionite-reduced NAu-1, we used cryogenic Mössbauer spectroscopy at temperatures between 77 K and 4 K. We initially analysed all dithionite-reduced NAu-1 samples at 13 K to detect clay mineral Fe(II) and Fe(III) as distinct species by slowing electron hopping to below the Mössbauer characteristic time (10^{-8} s) (80). As expected, the Mössbauer spectra showed clearly defined Fe(III) and Fe(II) doublets for NAu-1 reduced to Fe(II)/Fe(total) ratios between 3.5% and 13% (Figure S3.6a). At Fe(II)/Fe(total) ratios of 30% and higher, we additionally observed a poorly resolved spectral feature due to partial magnetic ordering, which was absent at higher temperatures (Figures S3.6 b,c, S3.7), and thus Mössbauer spectra of these samples were collected at 77 K (Figure S3.6 c,d) to determine their Fe reduction extent. Although the reduction extent for the onset of partial magnetic ordering coincides with that at which the UV-vis absorbance at 730 nm plateaued, an increase in magnetic ordering temperature with increasing Fe(II) content has been observed for a range of clay minerals and has been assigned to an increased Fe(II) ferromagnetic component and increased charge transfer between neighbouring Fe(II) and Fe(III), (67, 178) rather than Fe clustering.

When the samples were cooled to 4 K, however, magnetic ordering was visible at all reduction extents (Figure S3.8) and increased ordering was observed at higher reduction extents, consistent with an increased Fe(II) ferromagnetic component in the mineral (178). Magnetic ordering was not well developed and evident only as broadening in the spectra of NAu-1 with Fe(II)/Fe(total) ratios lower than 20 %. The lack of distinct hyperfine interactions in spectra collected at 4 K has been previously interpreted as a lack of spatially segregated Fe(II) and Fe(III) domains, which would allow magnetic exchange to occur (68). Our observations thus suggest the presence of mixed valent Fe(II)-Fe(III) domains in dithionite-reduced NAu-1 with Fe(II)/Fe(total) ratios below 20 % and corroborate our conclusions that at these reduction extents, NAu-1 contains mostly dioctahedral Fe(II) species for redox reaction with reactive

probes. In contrast, spectra of NAu-1 dithionite-reduced to extents ≥20 % contained distinct magnetically ordered features, similar to those observed for fully dithionite-reduced Garfield nontronite (68) and indicative for the presence of spatially segregated Fe(II) and Fe(III) domains. In the spectrum of NAu-1 reduced to an Fe(II)/Fe(total) ratio of 20% (Figure S3.8b, Table S3.4), a broad poorly resolved phase, similar to that seen in the 13% reduced-sample comprises 26% of the spectral area. However, additionally two clearly resolved sextets are visible (47% of total area) and exhibit hyperfine parameters consistent with octahedral Fe(III) (**?**). The rest of the spectrum is dominated by an Fe(II) octet (18% of total area) that is not well resolved but can be fit using parameters previously reported for Fe(II) in dioctahedral glauconite (178) and trioctahedral annite and ferrous biotite (178, 179) (Table S3.5). Two doublets occupy the remaining 2% of the spectral area and comprise Fe(II) and Fe(III) species that have not magnetically ordered, as indicated by their presence as doublets. At higher Fe reduction extent, the poorly resolved, broad component is no long present and identical components as found at 20% Fe(II)/Fe(total) were present in the Mössbauer spectra, with the dominance of the collapsed Fe(II) octet increased with increasing reduction extent, occupying 87% of the spectral area in the most reduced sample (Figure S3.8c, Table S3.4).

Our combined spectroscopic and kinetic analyses thus suggest that at reduction extents below 30%, the highly reactive Fe(II) site in the kinetic model corresponds to dioctahedrally bound Fe(II), which is mostly likely connected to Fe(III) and exhibits an increasing reactivity rather than an increase in abundance with increasing reduction extent. For dithionite- and Fe(II)-reduced NAu-1, both kinetic parameters of the highly reactive Fe(II) site (Figure S3.9) and Mössbauer spectra are almost identical, indicating that the same reactive species was present regardless of the reductant used, even though our data set for Fe(II)-reduced NAu-1 is limited. Only at reduction extents exceeding 20%, proton sorption dominates over cation uptake, which leads to dehydroxylation and the onset of the formation of trioctahedral Fe(II) domains (Figure S3.8), which then comprise the highly reactive Fe(II) site. We hypothesise that these trioctahedral entities are initially small, minimising the energy required for concomitant structural rearrangements to take place (165). As reduction increases further, growing the number of small trioctahedral groups becomes energetically less favourable and instead the size of the trioctahedral domains increases, lowering their abundance. This hypothesis is consistent with a maximum of highly reactive site abundance around 50 % Fe(II)/Fe(total) in NAu-1 and its subsequent decrease at higher reduction extents (Figure 3.4A).

3.3.4.2 Low-reactivity sites in Fe(II)- and dithionite-reduced NAu-1

In contrast to the compelling similarities of the highly reactive Fe(II) sites in Fe(II)- and dithionite-reduced NAu-1, the significant differences in the kinetic rate constant of the low reactivity sites (Figure S3.9) suggest the presence and/or involvement of different Fe(II) groups. We therefore used the isotope-specificity of Mössbauer spectroscopy in combination with aqueous Fe(II) enriched in either the ^{56}Fe or ^{57}Fe isotope to study the fate of the aqueous Fe(II) used to reduce NAu-1 (80, 81). Using Mössbauer-invisible ^{56}Fe(II) allowed us to assess the

relationship between Fe(II) removal from solution and clay mineral Fe reduction (80, 167), and we found a linear relationship across the range of reduction extents investigated here (Figure S3.4). In contrast to the 1:1 relationship that has been found for electron transfer from aqueous Fe(II) to both Fe-rich and Fe-poor clay minerals (NAu-2, SWy-2), (80, 167) only 0.55 moles of clay mineral Fe(III) in NAu-1 was reduced for every mole of aqueous Fe(II) removed from solution (Figure S3.4). Although this finding is intriguing in itself and warrants further investigation, in the context of this study, its main significance relates to the result that for all reduction extents, 40-51% (0.22-0.75mM, Table 3.1) of the Fe removed from solution remained Fe(II) and was either sorbed to or part of a mineral phase.

To assess whether the resulting non-structural, solid-bound Fe(II) could have provided reactive Fe(II) species for 2AcNB reduction, we investigated the nature of the Fe(II) removed from solution by using Mössbauer-visible ^{57}Fe(II) in our experiments, which greatly enhanced the signal of the added Fe(II) such that ^{57}Fe present in the clay mineral structure occupied $\leq$0.1% of the spectral area in the Mössbauer spectra. The spectra collected at 4 K of NAu-1 with the same Fe(II)/Fe(total) ratios as used in the 2AcNB transformation experiments (i.e., 3.5%, 5% and 8%) all exhibit magnetically ordered components (Figure S3.9) indicative of Fe atoms bound within mineral phases rather than sorbed to mineral phases. Most strikingly, we found a large Fe(II) octet component, which makes up 31 - 52 % of the spectral area, in addition to the expected Fe(III), as described in previous reports (80, 81, 167). Because unambiguous phase identification is not possible using Mössbauer spectroscopy alone, the hyperfine parameters of these ordered components are consistent with the presence of a range of Fe(II) and Fe(III)-bearing phases, including, but not limited to, ferrihydrite (Fe(III) sextet 1), lepidocrocite (Fe(III) sextet 2), goethite, and green rust (Fe(II) octet plus Fe(III) sextet 2) (180). Depending on the clay mineral used and the reaction conditions applied (pH value, clay mineral to Fe(II) ratio), different minerals have been found to form and for the most similar reaction conditions as applied here, the formation of ferrihydrite (47) and/or green rust (25) was suggested. Irrespective of the specific mineral phase corresponding to the Fe(II) octet in the Mössbauer spectra, it is very likely that this Fe(II) species represent the low-reactivity Fe(II) sites.

An alternative candidate is the second Fe(II) component in the Mössbauer spectra, an Fe(II) doublet constituting 18-20% of the spectral area and sorbed to a mineral phase. Because Fe(II) sorbed to Fe oxides, hydroxides, silica, alumina and Fe-free clay minerals can also transform nitroaromatic compounds, (42, 51, 174) the sorbed Fe(II) in our system could also correspond to the low-reactivity Fe(II) site in Fe(II)-reduced NAu-1. If sorbed Fe(II) was indeed contributing to 2AcNB reduction, sorption to an Fe(III) oxide like lepidocrocite is more likely to result in similar rate constants (log $\mathrm{k_B}$) as observed here rather than sorption to silica or alumina surfaces as found in clay minerals (Table S3.5). Because the *in-situ* formed Fe(II) species cannot be investigated separately, we cannot unambiguously conclude which of the Mössbauer Fe(II) components corresponds to the low-reactivity site in Fe(II)-reduced NAu-1. We can, however, conclude that one, or both, solid-bound Fe(II) components formed

during the interaction with NAu-1 determine the low-reactivity site, as these components are present in the spectra of all Fe(II)-reacted NAu-1 samples, most importantly in the spectrum of Fe(II)-reacted NAu-1 reduced to only 3.5% Fe(II)/Fe(total), where only one reactive site was required for the kinetic fit of the 2AcNB transformation data.

While reduction with aqueous Fe(II) enables specific labelling to monitor the fate of the added Fe, and thus of one of the potential reactive Fe(II) species in the system, this is not possible with dithionite-reduced NAu-1, in which all of the Mössbauer-active Fe resides in the structure. It is therefore not possible, based on spectroscopic analysis, to unambiguously identify the Fe(II) entities corresponding to the low reactivity sites in the kinetic model, which are defined as the remainder of the clay mineral Fe(II) not residing in the highly reactive sites (equation 3.2). Because of this approach and based on previous work suggesting that a diverse range of Fe(II) species could comprise the low reactivity sites in Fe-rich smectites, (157) we refrain from assigning specific Fe(II) entities in dithionite-reduced NAu-1 to its low reactivity sites.

3.4 Summary

To conclude, our results show that Fe(II)-reduced nontronite facilitates the transformation of NACs more rapidly than dithionite- or bio-reduced clay minerals at similar reduction extents. We propose that this is due to different reactive Fe(II) entities. We suggest that Fe(II)- and dithionite-reduced NAu-1 contain the same highly reactive species comprising dioctahedral Fe(II) at reduction extents between 5 % and 30 %. However, at higher reduction extents we observed significant changes in the mineral structure indicating that the highly reactive sites change from dioctahedral to trioctahedral Fe(II).

However, our data suggests that the second, less reactive species is different in Fe(II)- and dithionite-reduced NAu-1. For Fe(II)-reduced NAu-1, we propose that this comprises Fe(II) associated with the Fe-containing phases formed during the electron transfer reaction whereas for dithionite-reduced NAu-1 it is likely to comprise dioctahedral Fe(II)-other cation pairs.

Chapter S3
Assessing the redox reactivity of Fe(II)-reduced clay minerals: Supporting Information

S3.1 Chemicals and Reagents

All chemicals and reagents used in this study were of analytical grade and purchased from either Fisher Scientific/ACROS Organics (sodium chloride, sodium citrate, sodium bicarbonate, sodium dithionite, 1,10-phenanthroline, hydrofluoric acid, hydrochloric acid) or Sigma Aldrich (sodium hydroxide, 2-acetylnitrobenzene, 2-acetylaniline, HPLC grade methanol).

All stock solutions were purged with N_2 for at least an hour before introduction to the anaerobic chamber.

S3.2 Mineral preparation

The 0.1-0.5 μm fraction of the mineral was obtained through repeated centrifugation according to Stoke's law. The fractionated mineral was then washed three times in 1M NaCl solution, in order to achieve Na^+ homoionization and then washed twice with DI water. Finally, mineral impurities were removed by repeated centrifugation for 5 minutes at 8000 rpm, which preferentially leaves the impure fraction in the pellet and the clean fracion in the supernatant. FT-IR was then used to confirm removal of any Fe-oxide, carbonate and kaolin phases.

S3.3 Mössbauer spectroscopy

Samples were prepared for Mössbauer analyses in the anaerobic chamber by extracting the clay mineral solids from the reactors by centrifugation and then placing a small amount between two pieces of Kapton tape, to prevent exposure to oxygen. The aqueous Fe(II)\Fe(tot) was quantified from the supernatant using the 1,10-phenanthroline method (170) and the amount of Fe(II) sorbed to the smectite was calculated as the difference from the initial aqueous Fe(II) concentration (i.e. the amount removed from solution).

The spectra were collected in transmission mode by attaching the sample to a rod using Kapton tape and inserted into a closed cycle helium cryostat. Data was calibrated against an α-Fe foil.

S3.4 Reduction kinetics, dithionite-reduced NAu-1

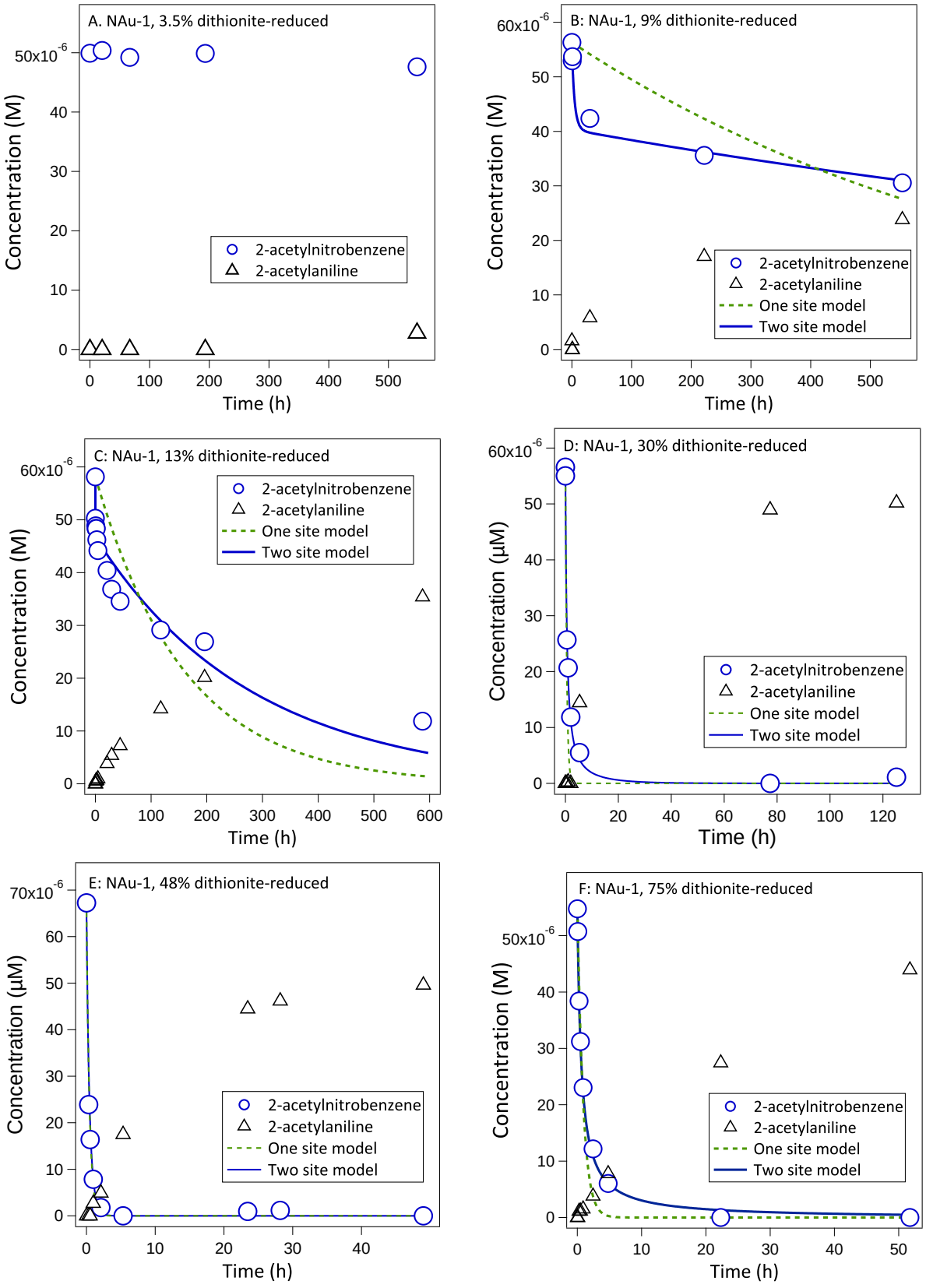

Figure S3.1: Typical reduction kinetics of 2-acetylnitrobenzene (blue circles) to 2-acetylaniline (black triangles) in suspensions of dithionite-reduced NAu-1, with initial clay mineral Fe reduction extents of (a)3.5% Fe(II)/Fe(total) (b) 9% Fe(II)/Fe(total), (c) 13% Fe(II)/Fe(total), (d) 30% Fe(II)/Fe(total), (e) 48% Fe(II)/Fe(total) and (f) 75% Fe(II)/Fe(total). The green dashed line represents a second order kinetic model representative of one reactive Fe(II) site and the blue solid line represents a biphasic, two site kinetic model.

S3.5 Reduction kinetics, Fe(II)-reduced NAu-1

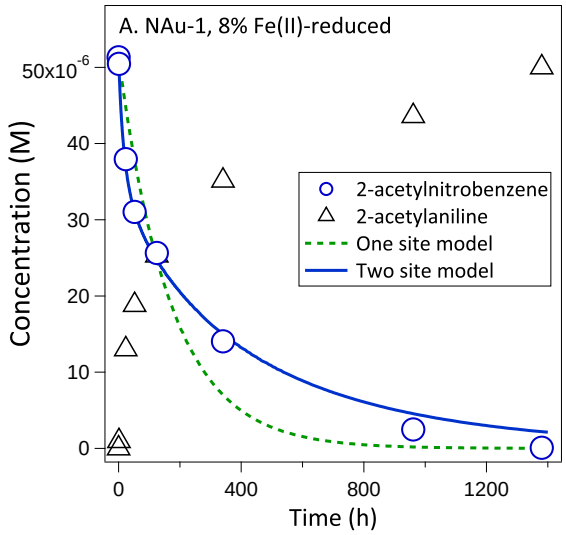

Figure S3.2: Reduction kinetics of 2-acetylnitrobenzene (blue circles) to 2-acetylaniline (black triangles) in a suspension of 8%-reduced NAu-1

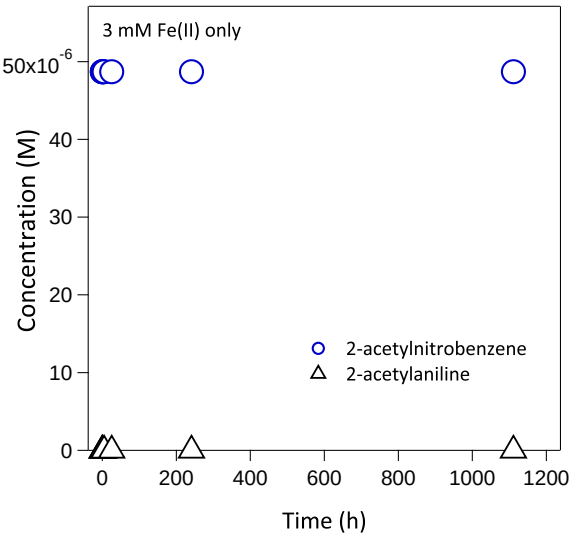

Figure S3.3: 2-acetylnitrobenzene (blue circles) to 2-acetylaniline (black triangles) in a suspension of 3.0 mM Fe(II) alone.

S3.6 Modelled kinetic parameters

Table S3.1: Modelled kinetic parameters for the reduction of 2AcNB by dithionite- and Fe(II)-reduced NAu-1. E_H calculated based on ref (123).
[a] Modelled concentration of highly reactive Fe(II) sites

NAu-1 % Fe(II)/Fe(tot)	NAu-1 Fe(II) (mM)	E_H (V)	log k_A $M^{-1}h^{-1}$	log k_B $M^{-1}h^{-1}$	log k $M^{-1}h^{-1}$	C_A_0[a] (mM)
Dithionite-reduced NAu-1						
3.5	0.32	-	-	-	-	-
5	0.45	-0.11±0.03	1.54±0.09	-1.11±0.13	-	0.11±0.04
10	0.81	-0.19±0.02	2.89±0.14	-0.26±0.07	-	0.10±0.03
13	1.17	-0.22±0.02	2.88±0.17	0.07±0.1	-	0.12±0.06
30	2.70	-0.32±0.01	3.72±0.07	-0.38	-	0.35±0.03
48	4.41	-0.37±0.01	3.38±0.27	-0.4	-	1.11±0.07
75	6.75	-0.42±0.01	3.70±0.09	-0.45	-	0.34±0.06
91	8.19	-0.44±0.01	3.53±0.07	-0.47	-	0.40±0.04
Fe(II)-reduced NAu-1						
3.5	0.32	-0.08±0.03	-	-	0.71±0.04	-
5	0.50	-0.13±0.03	2.31±0.11	0.75±0.04	-	0.10±0.06
8	0.72	-0.17±0.02	2.78±0.21	0.76±0.06	-	0.10±0.09

S3.7 Reduction of NAu-1 by aqueous Fe(II)

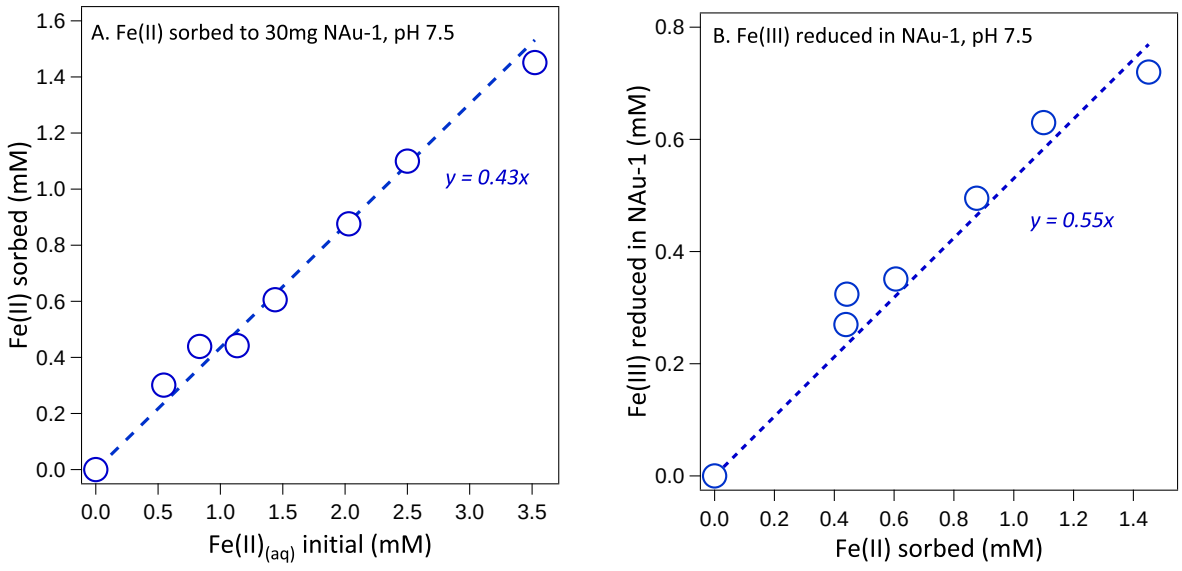

Figure S3.4: Stoichiometry of the reaction between sorbed Fe(II) and structural Fe(III) reduced in NAu-1.

A maximum reduction extent of 8% Fe(II)\Fe(tot) was achieved, which is comparable to that observed by (172) for microbially reduced NAu-1 following the addition of electron shuttle AQDS. For particle size 0.1-0.5μm, which we have selected for in our reactors, we calculated that approximately 0.2% - 1.3% of the structural Fe in NAu-1 is located at the edges and

therefore the 8% reduction corresponds to internal as well as edge-bound Fe(II), contrary to the suggestion made by (172) that only edge-bound Fe was reduced in NAu-1. Other possibilities that may limit further reduction include charge balance limitations (175), the presence of a solid oxidation product at the mineral surface preventing further sorption and therefore electron transfer from Fe(II) or thermodynamic limitations.

It is unclear why the relationship does not show a 1:1 relationship similar to that observed by (80) for the structurally similar NAu-2: in NAu-1 only approximately 50% of the sorbed Fe(II) is able to reduce structural Fe. However, Fe in NAu-2 has also been shown to be more microbially available with up to 32% structural Fe reduction observed by (21) using *Shewanella putrefaciens* strain CN32 with AQDS compared to the 8% observed for NAu-1 by (172) with *Shewanella oneidensis* strain MR-1 and AQDS.

S3.8 Calculation of reduction extent at which proton uptake dominates over cation sorption

Drits and Manceau (2000) (165) proposed a model relating nontronite reduction extent ($\frac{\mathrm{m}}{\mathrm{m_0}}$), cation sorption ($\mathrm{p}$), proton uptake ($\mathrm{n_i}$) and a constant derived from the nontronite structure ($\mathrm{K_0}$) as shown in Equation S1. Proton uptake dominates over cation sorption if $\frac{\mathrm{n_i}}{\mathrm{p}} < 1$.

$$\frac{\mathrm{n_i}}{\mathrm{p}} = \mathrm{K_0}\frac{\mathrm{m}}{\mathrm{m_0}} \tag{S1}$$

The value of $\mathrm{K_0}$ is dependent on the structural Fe content of the nontronite and may be calculated as shown in Equations S2 and S3, where $\mathrm{m_tot}$ = the amount of Fe in the nontronite structure (mmol/g).

$$\mathrm{K_r} = 9.32 - 1.06\mathrm{m_{tot}} + 0.02\mathrm{m_{tot}}^{\,2} \tag{S2}$$

$$\mathrm{K_0} = \mathrm{K_r CEC} \tag{S3}$$

S3.9 Full UV-vis spectra of NAu-1

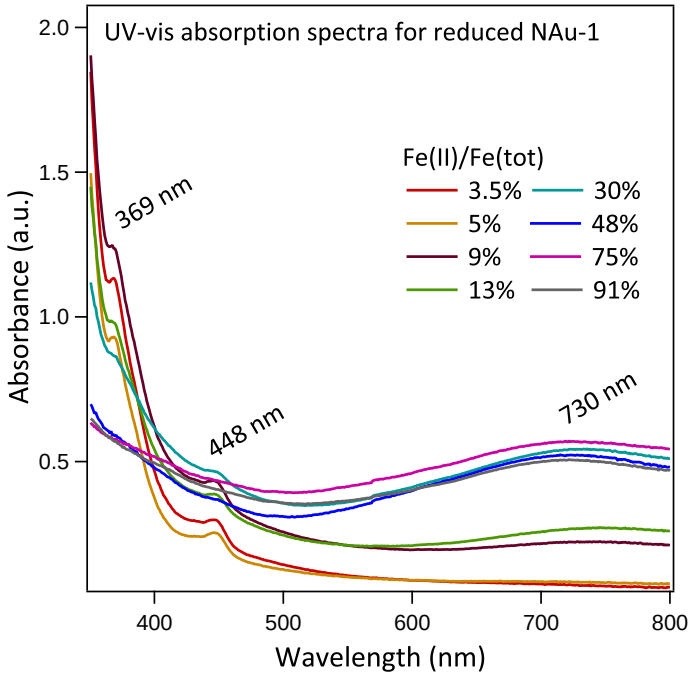

Figure S3.5: Full optical absorption spectra of NAu-1 reduced between 3.5 % and 91 % Fe(II)/Fe(tot). Peaks at 369 nm and 448 nm are attributed to octahedral Fe(III) and the peak at 730 nm is the Fe(II)Fe(III)-OH intervalence charge transfer band (176**?**).

S3.10 Mössbauer spectra of dithionite-reduced NAu-1

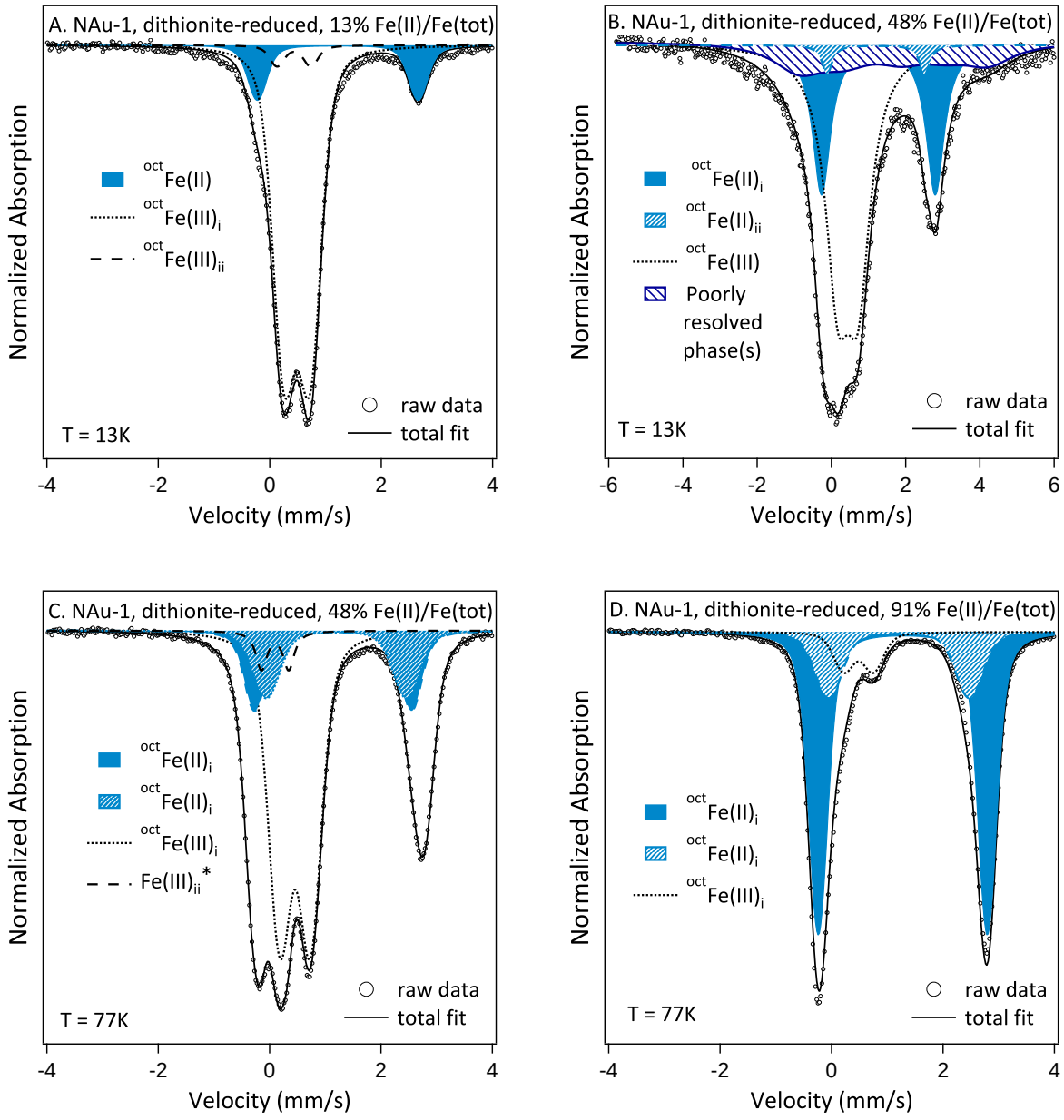

Figure S3.6: Mössbauer spectra of (a) 13% dithionite-reduced NAu-1 measured at 13 K, (b) 48% dithionite-reduced NAu-1 measured at 13 K. Magnetic ordering is evident as broadening, comprising a poorly resolved Fe(II) ordered phase, (c) 48% dithionite-reduced NAu-1 measured at 77 K, and (d) 91% dithionite-reduced NAu-1 measured at 77 K
*Previously attributed to tetrahedral Fe(III) (123).

Table S3.2: Mössbauer parameters for dithionite-reduced NAu-1, measured at 13 K or 77 K and fitted using a voigt based, fixed line width method.
[a] no error data are provided for the poorly resolved phase, due to the associated uncertainty.
[b] Previously tentatively assigned to tetrahedral Fe(III) (123).

Sample	χ^2	Site	CS (mm/s)	QS (mm/s)	H (T)	Area (%)
13% dithionite	1.75	oct Fe(III)i	0.49	0.458 ± 0.004	-	80.19 ±0.02
-reduced NAu-1		oct Fe(III)ii	0.43	0.62 ± 0.02	-	6.8 ± 0.2
13 K		oct Fe(II)	1.23	2.89 ± 0.01	-	12.99 ± 0.03
48% dithionite	0.77	oct Fe(III)i	0.45	0.55 ± 0.01	-	50.18 ±0.04
-reduced NAu-1		oct Fe(II)i	1.27	3.06 ± 0.09	-	26.12 ± 0.04
13 K		oct Fe(II)ii	1.20	2.63 ± 0.05	-	2.77 ± 0.05
		Poorly resolved phase(s)[a]	1.4	-3	10	21
48% dithionite	1.17	oct Fe(III)i	0.46	0.55 ± 0.02	-	47.6 ±0.7
-reduced NAu-1		Fe(III)ii[b]	0.1	0.49 ± 0.02	-	3.96 ± 0.06
77 K		oct Fe(II)i	1.26	3.05 ± 0.01	-	36.0 ± 0.7
		oct Fe(II)ii	1.14	2.81 ± 0.02	-	12.4 ± 0.8
91% dithionite	1.67	oct Fe(III)	0.48	0.55 ± 0.07	-	8.7 ±0.1
-reduced NAu-1		oct Fe(II)i	1.29	3.02 ± 0.01	-	63.2 ± 0.6
77 K		oct Fe(II)ii	1.21	2.74 ± 0.05	-	28.1 ± 0.1

S3.11 Mössbauer spectra of ^{56}Fe(II)-reduced NAu-1

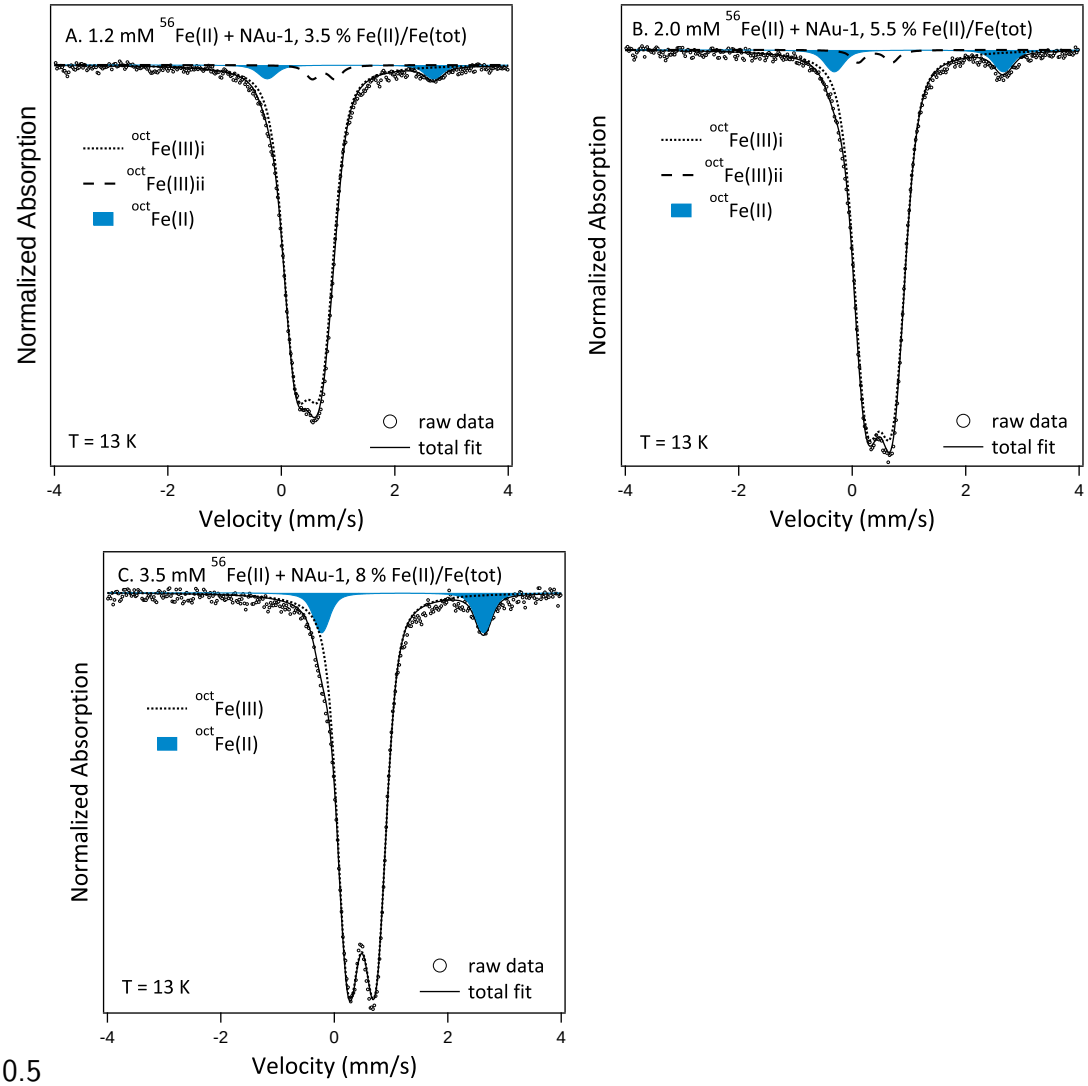

0.5

Figure S3.7: Mössbauer spectra of (a) 1.2 mM ^{56}Fe(II) + NAu-1, (b) 2.0 mM ^{56}Fe(II) + NAu-1, and (c) 3.5 mM ^{56}Fe(II) + NAu-1.

Table S3.3: Mössbauer parameters for ^{56}Fe(II)-reduced NAu-1, measured at 13 K and fitted using a voigt based, fixed line width method.

Sample	χ^2	**Site**	**CS (mm/s)**	**QS (mm/s)**	**Area (%)**
1.2 mM ^{56}Fe(II)	0.76	oct Fe(III)i	0.48	0.45 ± 0.04	93.69 ±0.03
+ NAu-1, 13 K		oct Fe(III)ii	0.75	0.40 ± 0.02	2.81 ± 0.01
		oct Fe(II)	1.22	2.92 ± 0.06	3.51 ± 0.01
2.0 mM ^{56}Fe(II)	0.93	oct Fe(III)i	0.48	0.50 ± 0.03	88.94 ±0.03
+ NAu-1, 13 K		oct Fe(III)ii	0.72	0.13 ± 0.08	5.62 ± 0.05
		oct Fe(II)	1.22	2.8 ± 0.07	5.58 ± 0.01
3.5 mM ^{56}Fe(II)	0.82	oct Fe(III)i	0.48	0.47 ± 0.03	92.00 ±0.06
+ NAu-1, 13 K		oct Fe(II)	1.20	2.85± 0.03	8.00 ± 0.06

S3.12 Mössbauer spectra of dithionite-reduced NAu-1 at 4K

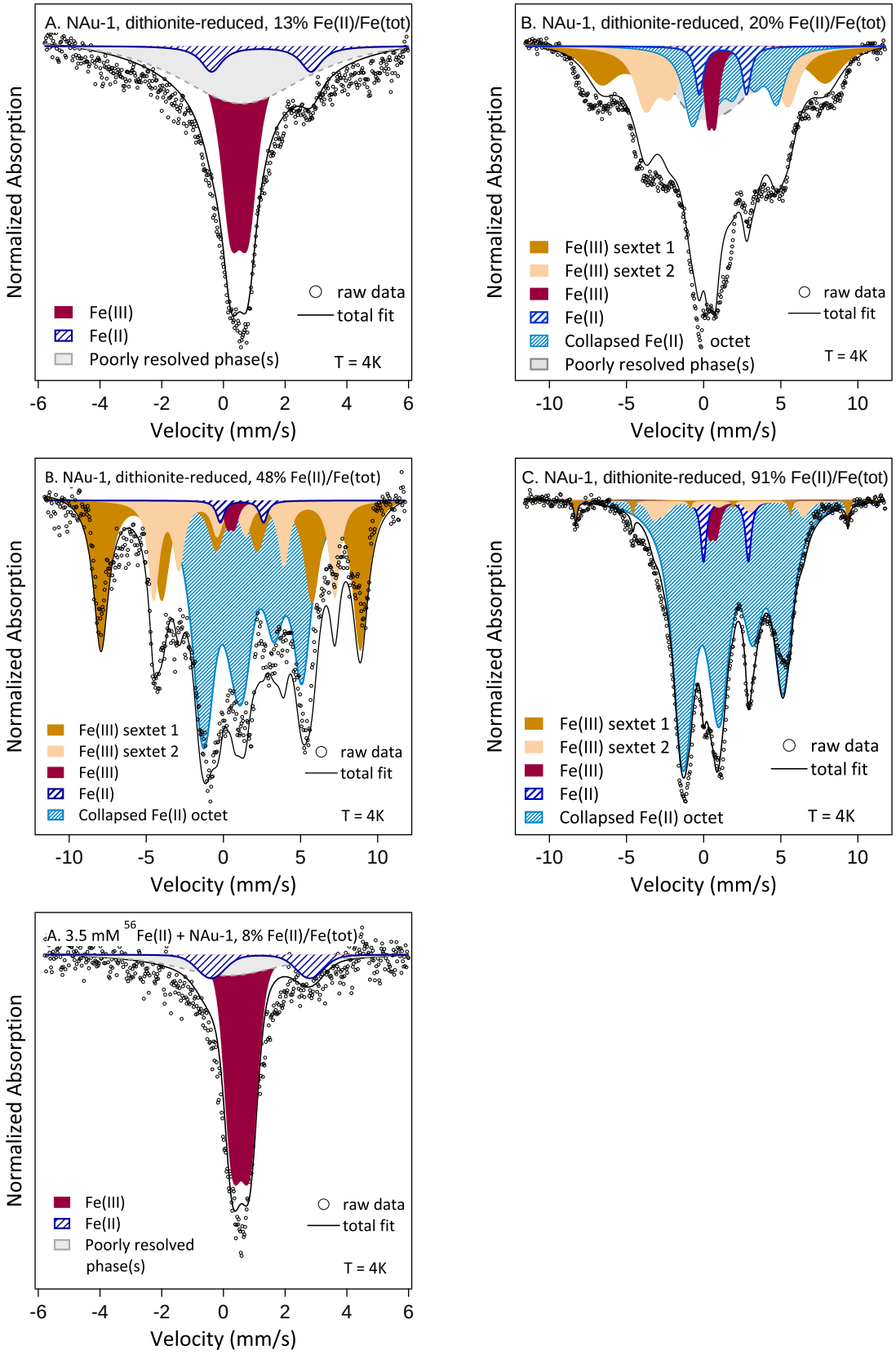

Figure S3.8: Mössbauer spectra collected at 4 K of (a) 13% dithionite-reduced NAu-1, (b) 20% dithionite-reduced NAu-1, (c) 91% dithionite-reduced NAu-1, (d) 8% ^{56}Fe(II)-reduced NAu-1, and (e) 48% dithionite-reduced NAu-1.

Table S3.4: Mössbauer parameters for reduced NAu-1, measured at 4 K, measured at 4 K using a variable line width fitting method (Full Static Hamitonian).

	CS (mm/s)	**H (T)**	$\mathbf{e^2qQ/2}$ **(mm/s)**	η **(-)**	θ **(-)**	**Area(%)**
13% dithionite-reduced NAu-1						
Fe(III) doublet	0.52	-	0.54	0	0	36.8
Fe(II) doublet	1.23	-	3.22	0	0	6.6
Partially resolved phase(s)	0.6	2.2	0.5	0	0	56.6
20% dithionite-reduced NAu-1						
Fe(III) sextet$_1$	0.45	45.1	0.38	0	0	24.4
Fe(III) sextet$_2$	0.64	28.6	0.44	0	0	22.7
Fe(III) doublet	0.52	-	0.45	0	0	4.7
Fe(II) doublet	1.25	-	3.05	0	0	3.9
Collapsed Fe(II) octet	1.66	12.2	-2.9	0.2	90	18.4
Partially resolved phase(s)	0.5	10	0.45	0	0	25.8
91% dithionite-reduced NAu-1						
Fe(III) sextet$_1$	0.52	54.7	0.01	0	0	1.6
Fe(III) sextet$_2$	0.91	30.1	1.4	0	0	4.1
Fe(III) doublet	0.6	-	0.45	0	0	2.9
Fe(II) doublet	1.45	-	2.91	0	0	4.3
Collapsed Fe(II) octet	1.44	17.3	-2.6	0.2	90	87.1
8% ^{56}Fe(II)-reduced NAu-1						
Fe(III) doublet	0.52	-	0.40	0	0	62.7
Fe(II) doublet	1.20	-	3.22	0	0	5.3
Partially resolved phase(s)	0.6	2.2	0.5	0	0	32.0
48% dithionite-reduced NAu-1						
Fe(III) sextet$_1$	0.67	52.2	-0.4	0	0	34.1
Fe(III) sextet$_2$	0.93	36.3	0.84	0	0	14.4
Fe(III) doublet	0.5	-	0.45	0	0	1.2
Fe(II) doublet	1.2	-	2.8	0	0	1.3
Collapsed Fe(II) octet	1.47	16.4	-2.77	0.22	90	49.0

S3.13 Mössbauer parameters for Fe-bearing phyllosilicates from literature

Table S3.5: Mössbauer parameters gathered from literature for trioctahedral and dioctahedral phyllosilicates. All samples were measured at 4 K with the exception of glauconite, which was measured at 1.5 K.

Mineral	Component	IS (mm/s)	QS (mm/s)	H (T)	η (-)	Reference
Synthetic	Fe(III) sextet 1	*	*	49	*	(179)
annite	Fe(III) sextet 2	*	*	40.6	*	
(trioctahedral)	Fe(II) octet	*	*	7.5 - 15	0.2	
Ferrous	Fe(III) sextet 1	*	*	54	*	(178)
biotite	Fe(III) sextet 2	*	*	48	*	
(trioctahedral)	Fe(II) octet	*	-2.75	15	*	
Nontronite	Fe(III) sextet	*	*	49	*	(178)
Nontronite	Fe(III) sextet	*	*	34 - 48	*	(**?**)
Glauconite	Fe(III) sextet	*	*	51	*	(178)

S3.14 Mössbauer spectra of ^{57}Fe(II)-reduced NAu-1

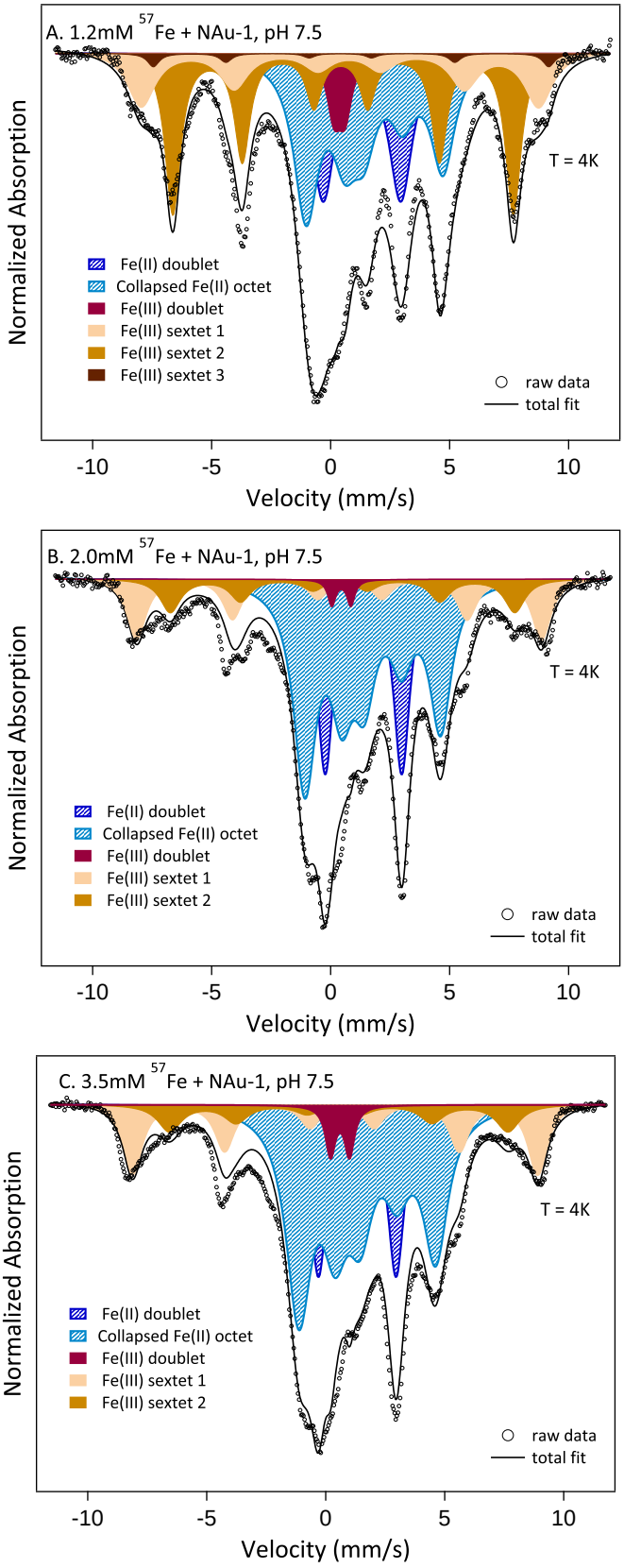

Figure S3.9: Mössbauer spectra of (a) 1.2mM, (b) 2.0mM and (c) 3.5mM ^{57}Fe(II) + NAu-1, at pH 7.5, measured at 4K.

Table S3.6: Mössbauer parameters for ^{57}Fe(II) + NAu-1, measured at 4 K using a variable line width fitting method (Full Static Hamitonian).

	CS (mm/s)	**H (T)**	$\mathbf{e^2qQ/2}$ **(mm/s)**	η (-)	θ (-)	**Area(%)**
1.2 mM ^{57}Fe(II) + NAu-1						
Fe(III) sextet$_1$	0.59	51.8	-0.39	0	0	17.0
Fe(III) sextet$_2$	0.48	44.3	0.10	0	0	27.6
Fe(III) sextet$_3$	0.63	51.5	0.45	0.5	0	1.7
Fe(III) doublet	0.37	-	0.46	0	0	4.1
Fe(II) doublet	1.31	-	3.26	0	0	18.4
Collapsed Fe(II) octet	1.42	13.5	-2.83	0	90	31.3
2.0 mM ^{57}Fe(II) + NAu-1						
Fe(III) sextet$_1$	0.58	52.8	-0.45	0	0	17.3
Fe(III) sextet$_2$	0.45	44.9	0.10	0	0	9.8
Fe(III) doublet	0.45	-	0.80	0	0	1.5
Fe(II) doublet	1.38	-	3.22	0	0	22.3
Collapsed Fe(II) octet	1.36	13.0	-2.83	0	90	49.1
3.5 mM ^{57}Fe(II) + NAu-1						
Fe(III) sextet$_1$	0.54	52.8	-0.29	0	0	18.0
Fe(III) sextet$_2$	0.45	44.1	0.20	0	0	8.4
Fe(III) doublet	0.60	-	0.80	0	0	3.2
Fe(II) doublet	1.32	-	3.26	0	0	18.9
Collapsed Fe(II) octet	1.33	12.8	-3.03	0	90	51.5

S3.15 Reactivity of sorbed Fe(II)

Table S3.7: Rate constants for NAC reduction by Fe(II)-silica, alumina and lepidocrocite from previous studies

Phase	Mineral load (g/l)	Fe(II) conc (mM)	pH	log $\mathbf{k_{obs}}$	log $\mathbf{k_{adj}}$	ref
Silica	10	0.31 sorbed 0.81 total	7.5	1.1E-04	-1.3	(51)
Alumina	10	0.69 sorbed 1.19 total	7.5	3.35E-05	-0.45	(51)
Lepidocrocite$_1$	2.7	0.5$_{(\mathrm{aq})}$	7.2	0.49	0.06	(174)
Lepidocrocite$_2$	2.7	1.0$_{(\mathrm{aq})}$	7.2	0.92	0.49	(174)
Lepidocrocite$_3$	10	1.0$_{(\mathrm{aq})}$	7.2	1.03	0.03	(174)
Lepidocrocite$_4$	1.42	1.0$_{(\mathrm{aq})}$	7.2	0.12	1.35	(42)

For the Fe(II) associated with silica or alumina the logarithm of reduction rate constants (log $\mathrm{k_{adj}}$), adjusted for concentration and mass loadings to be comparable to our data, range from -1.3 to -0.46 and for Fe(II)-lepidocrocite from 0.03 - 1.35. Although these data apply to 4-chloronitrobenzene rather than 2AcNB used in this current study, the log $\mathrm{k_B}$ values are in the same range as the log $\mathrm{k_{adj}}$ values for Fe(II)-associated with lepidocrocite and are greater than those observed for Fe(II) at silica or alumina surfaces. This supports our hypothesis that it is Fe(II) associated with the Fe-oxidation product may be responsible for the $\mathrm{k_B}$ phase of the reaction.

S3.16 Introduction to Mössbauer spectroscopy

Mössbauer spectroscopy is a method of nuclear absorption spectroscopy based on the Mössbauer effect of recoilless absorption of γ-radiation by solid phases. It is isotope specific and in our case a ^{57}Co source is used to probe the 14.41 keV nuclear transition in $^{5}7$Fe. In a transmission setup as used in this work, the source is mounted on a motor that oscillates, to probe small changes in absorption energies through Doppler shifting. The radiation passes through a collimator before the sample, which is often placed within a cryostat to allow variable temperature measurements, and is then received by a detector. Mössbauer spectroscopy can be used to determine the oxidation state and structural coordination of ^{57}Fe based upon three parameters relating to the perturbation and splitting of nuclear energy levels as described below and illustrated graphically in Figure S3.10

1. **Electric monopole interaction**, which reflects the effect of s-electrons within the nuclear envelope. This interaction is sensitive to nuclear volume and electron density and therefore is useful for determining the ^{57}Fe valence state. It appears as a single line (singlet) and is usually reported as Centre Shift (CS) with units of mm/s, relating to the difference from $^{5}7$Fe ground state (Isomer Shift), normalised for Doppler shifting.
2. **Electric quadrupole splitting** derives from the interaction between the Electric Field Gradient and the quadrupole moment of the nucleus. This leads to a splitting of the nuclear energy levels between the ground and first excited state leading to a symmetrical split in the spectra producing a doublet, with a central value determined by the Isomer Shift. It may be influenced both by the valence and structural coordination of ^{57}Fe and is mostly reported as Quadrupole Splitting (mm/s).
3. **Magnetic hyperfine field interaction**, which is the interaction between the net effective magnetic field and the nuclear magnetic moment. This interaction is temperature dependent and fully developed magnetic ordering in the spectra is often not visible except for under cryogenic conditions. These interactions remove degeneracy in the nuclear energy levels and under most circumstances produce sextet features although octets are also possible. The interaction may be reported as H with units of T and as it reflects the magnetic properties of the solid, is useful for phase identification.

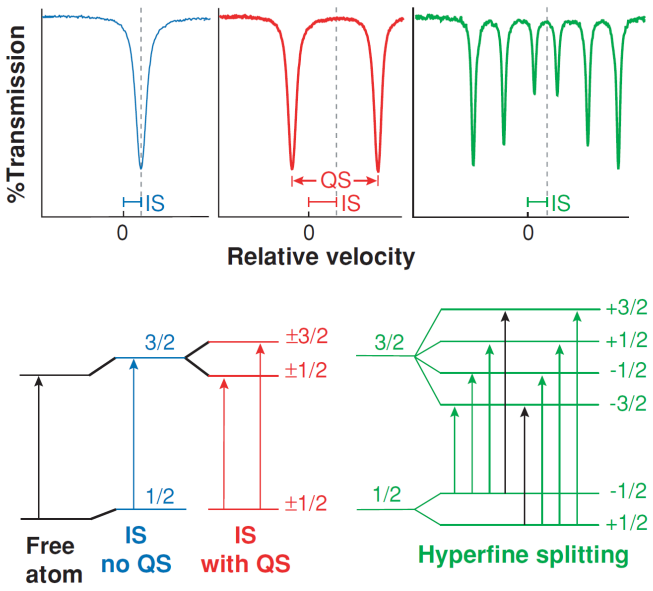

Figure S3.10: Illustration taken from Dyar *et al.*, (**?**) showing the Mössbauer parameters Isomer Shift, Quadrupole splitting and Zeeman splitting

Chapter 4
Assessing the influence of Fe(II)-organic complexes on the reactivity of Fe-bearing clay minerals

4.1 Introduction

Redox cycling of structural iron in clay minerals driven by microbial (38, 59, 76, 84, 159, 160) or chemical (65, 66, 69) processes has been shown to facilitate the reduction of a range of environmental contaminants including nitroaromatic compounds (20, 21, 50), halogenated hydrocarbons (48), pesticides (49, 161), nitrate (45) radionuclides (24) and hexavalent chromium (23). Aqueous Fe(II) is also ubiquitously present in anaerobic environments, as the result of dissimilatory iron-reducing bacteria such as *Shewanella* spp. using solid Fe(III) phases as a terminal electron acceptor (181). Recently, aqueous Fe(II) has also been shown to be capable of reducing Fe(III) in clay mineral structures resulting in the formation of Fe(II)-bearing clay minerals that are also reactive towards contaminants (47, 80, 81, 128, 166).

However, in complex natural environments Fe(II) in the aqueous phase is likely to be coordinated with ligand functional groups associated with natural organic matter (NOM) or microbial species (134, 140, 182, 183). NOM contains a range of Lewis base moities, commonly carboxylate and phenolate groups that are capable of donating free electron pairs to Fe(II) (137, 184) and microbial cell walls contain ligand functional groups such as carboxylate, thiolate and amine groups that may also form complexes with iron (185). Additionally, microbes are known to produce strongly Fe binding siderophores in order to solubilise and extract Fe as a nutrient from solid mineral phases (150).

These organic ligand species are of interest due to their abundance in natural systems and when complexing Fe species, they significantly lower the reduction potential (E_H^0) of the standard Fe(II)/Fe(III) redox couple (140). In the absence of mineral phases Fe(II)-organic complexes are also capable of reducing a range of contaminants that aqueous Fe(II) alone cannot including nitroaromatic compounds (1, 132, 136), pesticides (113), chromium (VI) (186) and chlorinated alkanes (187).

Furthermore, humic substances are important redox active phases in natural systems and may influence global nutrient cycling (139). It has been shown that humic substances can transfer electrons to Fe(III) oxide phases, particularly ferrihydrite (188, 189). However, little is currently known about whether metals bound to organic ligand moities in NOM may interact with mineral phases and whether other redox active minerals such as manganese oxides and clay minerals are capable of reacting with NOM (139).

Recent research has confirmed that Fe-bearing minerals and NOM are likely to coexist in natural environments (133, 190). However, it is currently unclear firstly, whether electron transfer can occur between Fe-bearing clay minerals and Fe(II)-organic ligand complexes and secondly, how reactive this combined system will be towards organic contaminants. In order to make predictions concerning the reactivity of real world systems towards environmental contaminants of interest, a mechanistic understanding of the reactivity of coexisting redox active phases is required.

In this study, we aim to determine the reactivity of combined mineral-ligand systems towards nitroaromatic compounds with the following objectives: (i) to determine how the presence of carboxylate ligands effects electron transfer to clay mineral Fe; (ii) to assess how the presence of carboxylate Fe(II)-complexes influences contaminant degradation in the presence of Fe-bearing clay minerals and, (iii) to investigate the effect of clay mineral Fe reduction extent on contaminant degradation in mixed systems of Fe-bearing clay minerals and organic ligands.

4.2 Materials and methods

4.2.1 Mineral preparation

A full list of chemicals used and a description of stock solution preparation is given in the Supporting Information (S4.1). Nontronite NAu-1, montmorillonite SWy-2 and synthetic Fe-free montmorillonite SYn-1 were purchased from the Source Clays Repository (http://www.clays.org) and the 0.1-0.5 μm size fraction of the minerals was obtained, as described in Chapter 3.

4.2.2 Kinetic batch experiments

All manipulation of oxygen sensitive solutions and reactors was undertaken in an anaerobic glovebox under an N_2 atmosphere ($\leq$1 ppm O_2). Aqueous Fe(II) stock solution was prepared by dissolving metallic Fe in HCl as previously described. Batch reactors were created by mixing 5 mM Fe(II), 10 mM MOPS (3-(N-morpholino)propanesulfonic acid) pH buffer, 50 mM NaCl ionic strength buffer, ligand of interest and if required, 2.0 $gL^{-}1$ clay mineral suspension. The pH was adjusted to 7.5 $\pm$ 0.1 using 5 M NaOH or 5 M HCl and batches were allowed to equilibrate for 24 hours prior to commencing kinetic experiments.

Batches were prepared containing 5 mM Fe(II) with 100 mM salicylic acid (FeSal), 50 mM L-(+)-tartaric acid ($FeTar_2$), 10 mM citric acid (FeCit) and 5 mM oxalic (FeOx) acid to produce the target Fe(II)-ligand species. Further batches were prepared containing SYn-1 or NAu-1 in either its native (fully oxidised) form, or reduced to give a 9 % or 91 % structural Fe(II)/Fe(tot) ratio. Mineral reduction was achieved using sodium dithionite as previously described (63). We also prepared control reactors containing either buffer only, ligand only or Fe(II) only and we did not observe any transformation of the NAC in these reactors.

In the case of citric acid, further batches were prepared where native NAu-1 - ligand batch reactors, with and without aqueous Fe(II), were prepared and allowed to equilibrate for

24 hours after which, the suspension was centrifuged for 30 minutes at 11,000 rpm. The supernatant was then used as a kinetic reactor. The extracted mineral was resuspended in 15 mL 10 mM MOPS, 50 mM NaCl solution and adjusted to pH 7.5 to be used as a reactor. Experiments were performed in triplicate and the aqueous Fe(II) concentration was measured using the 1,10-phenanthroline assay described previously (170). The extent of reduction and concentation of the mineral suspension was checked using both Mössbauer spectroscopy and HF digestion with the 1,10-phenanthroline assay (169).

Kinetic experiments were performed as previously described by spiking the batch reactors with an initial concentration of ~50 μM methanolic 2-acetylnitrobenzene (2AcNB) stock solution. Samples of 500 μL were taken as a time series and filtered using 0.22 μm nylon filters into 2 mL HPLC vials. The vials were loaded with 500 μL 50 mM hexacyanoferrate to quench the reaction as it preferentially complexes Fe(II) and is unreactive towards NACs. Samples were stored in the dark at 4 °C and HPLC analysis was undertaken as soon as possible following the reaction.

4.2.3 Analytical Methods

Reverse-phase HPLC with an LC-18 column was used to analyse the concentration of 2AcNB and the reduction product 2-acetylaniline, as in Chapter 3.

The supernatant collected from the citrate reactors, following reaction with NAu-1 was analysed for the concentration of citrate and Fe to determine whether sorption of the ligand/Fe(II) to the mineral had occurred. Citrate concentration was measured using ion chromatography and the concentration and speciation of Fe was measured using the 1,10-phenanthroline method (170). The concentration of Fe, Al, Si and Mg in the supernatant was also quantified using ICP-MS to determine whether any mineral dissolution had occurred.

Mössbauer spectroscopy was used to determine the structural coordination and reduction extent of NAu-1 as described in Chapter 3.

4.2.4 Speciation and kinetic modelling

The equilibrium speciation of the Fe(II)-ligand batches, before NAC addition, was calculated using the MICROQL software package (191). Stability constants were taken from the IUPAC stability constants database as listed in S4.3 (192) and corrected for the specific ionic strength conditions in our reactors (~0.1). The Nernst equation was then used to calculate the E_H of the reactive species in our reactors (Equations 4.1, 4.2).

$$\mathrm{E_H^0[\frac{Fe(III)L}{Fe(II)L}] = +0.77V - \frac{RT}{F}ln\frac{K_{Fe(III)L}}{K_{Fe(II)L}}} \tag{4.1}$$

$$\mathrm{E_H = E_H^0 - \frac{RT}{F}ln\left(\frac{\{Fe^{2+}\}}{\{Fe^{3+}\}}\right)} \tag{4.2}$$

Where $\mathrm{E_H^0}$ is the standard reduction potential of the Fe species, $\mathrm{E_H}$ is the reduction potential of the Fe species as calculated for our experimental conditions, $\mathrm{K_{Fe(x)L}}$ is the stability constant for the Fe species and $\{\mathrm{Fe^x}\}$ is the activity of the Fe species.

For the reactors containing only Fe(II)-ligand species, where no aqueous Fe(III) was measured we estimated the aqueous Fe(III) concentration using Henry's Law and the Ideal Gas Law to estimate the amount of oxidation that would occur in the aqueous phase from the 0.1 ppm O_2 concentration in our anaerobic chamber as 0.22 μM. Calculated $\mathrm{E_H}$ values and equilibrium plots of the speciation of each Fe(II)-ligand for varying pH and ligand concentration are presented in S4.3. In the case where more than one Fe(II)-ligand species was present, we adjusted the calculated $\mathrm{E_H}$ to reflect this using a weighted sum according to Equation 4.3.

$$\mathrm{E_H} = \sum_{\mathrm{i}} \mathrm{E_{Hi}} \alpha_{\mathrm{i}} \tag{4.3}$$

Reduction rate constants for the transformation of 2AcNB in Fe(II)-ligand and Fe(II)-ligand/NAu-1 reactors were modelled according to a pseudo-first order kinetic rate law (Equation 3.3. The pseudo-first rate constant ($\mathrm{k_{obs}}$, $\mathrm{h^{-1}}$) that can be converted to an equivalent second order rate constant ($\mathrm{k_{2nd}}$, $\mathrm{M^{-1}h^{-1}}$) using the measured reactive Fe(II) species concentration [Fe(II), M] (Equation 5.1).

$$\mathrm{k_{2nd}} = \frac{\mathrm{k_{obs}}}{[\mathrm{Fe(II)}]} \tag{4.4}$$

For reactors containing 91 %-reduced NAu-1 and Fe(II)-citrate, a pseudo-first order rate law did not provide a good fit for the data. In this case, a biphasic reduction model was used as proposed by Neumann *et al.*, 2008 (20) (Equation 3.1) as described in Chapter 3.

4.3 Results and Discussion

4.3.1 Reduction of Fe-bearing clay minerals by Fe(II)-carboxylate complexes

We evaluated whether complexing of aqueous Fe(II) with organic ligands would affect the extent of clay mineral iron reduction, to determine how the presence of ligands affects electron transfer and ultimately contaminant degradation. We chose oxalic acid, citric acid, L-(+)-tartaric acid and salicylic acid as carboxylate ligand species as they are known to be widely present in soil and groundwater as simple aliphatic acids (193) and as functional groups in a range of humic substances (194).

We used Mössbauer spectroscopy to quantify how the structrual Fe(II)/Fe(III) ratio of NAu-1 (nontronite, 21.5 wt. % Fe) changed in the presence of 5 mM Fe(II) and oxalic acid, citric acid, L-(+)-tartaric acid, and salicylic acid and SWy-2 (montmorillonite, 3.0 wt. % Fe)

in the presence of 5 mM Fe(II) and citric acid. Initially, we used aqueous Fe(II) enriched in ^{56}Fe to prepare our Fe(II)-ligand stocks, so that only changes in the naturally abundant ^{57}Fe in the clay mineral structure would be observed, as only ^{57}Fe is Mössbauer active.

As demonstrated by the formation of an Fe(II) doublet in the Mössbauer spectra (Figure S4.5), all carboxylate Fe(II)-ligand species tested were able to reduce structural Fe(III) in NAu-1, as summarized in Table 4.1. For NAu-1, the clay mineral reduction extent (%Fe(II)/Fe(tot)) ranged from 3 % for $FeTar_2$ to 6 % for FeSal (0.27 mM to 0.55 mM). The reduction measured in the mineral using Mössbauer spectroscopy was balanced by an equal amount of oxidation of the aqueous Fe-ligand species, as measured using the 1,10-phenanthroline method, for FeCit and FeSal. However, for $FeTar_2$ and FeOx, 0.075 mM and 1.15 mM Fe was measured to be removed from the aqueous phase indicating sorption to the clay mineral surface.

A higher reduction extent of 63.2 % Fe(II)/Fe(tot) was measured for SWy-2. However, due to the lower structural Fe concentration, this corresponds to a lower absolute concentration and 0.19 mM electron transfer was measured relative to 0.48 mM for NAu-1. It is possible that this is a result of Fe being more accessible in the dioctahedral nontronite lattice as more will be present at edge OH groups compared to Fe in the structure of low Fe-content SWy-2, where Fe is scattered throughout the lattice and therefore the majority of structural Fe is only accessible through the basal plane of the mineral (157).

It is well established that the speciation, and therefore reactivity, of Fe-organic complexes is influenced by both the organic ligand(s) present, ligand concentration, solution chemistry and pH (113). We used the MICROQL software package (191) and IUPAC published stability constants (192), adjusted for our solution conditions, to calculate the Fe speciation in our reactors (Table S4.3, Figures S4.1-4). Our modelling found that the predominant Fe species present in the reactors were Fe(oxalate)^{0}, Fe(citrate)$^{-1}$, Fe(tartrate)$_2{}^{2-}$ and Fe(salicylate)$^{+}$ (FeOx, FeCit, $FeTar_2$ and FeSal). We then used the Nernst equation (Equations 4.1, 4.2) to calculate the reduction potential (E_H) of the Fe(II)-ligand species (Table S4.3) (113).

Interestingly, for NAu-1 there is no relationship between the reduction potential of the ligand species and the amount of structural Fe reduction observed in the clay mineral (Table 4.1). However, the most electron transfer occurred for FeSal, which has has a positive charge charge and the least for $FeTar_2$, which has a charge of -2. It is possible that less reduction is observed for the more negatively charged species due to electrostatic repulsion by the negatively charged basal planes of the mineral despite electron transfer likely occurring through edge OH groups at pH 7.5.

We used the profiles developed by Gorski *et al.,* (2013) (123) to calculate the reduction potential of our clay minerals that had been reduced by Fe(II)-ligand species. We did not observe a relationship between either the E_H of the Fe(II)-ligand species and the final E_H of the clay minerals or between the final E_H of NAu-1 and SWy-2 that were both reduced by FeCit (Table 4.1).

Although organically complexed Fe(II) has a lower reduction potential than Fe(II) in the aqueous phase, we observed less reduction of structural Fe(III) in NAu-1 than was observed for

Table 4.1: Electron transfer from Fe(II)-ligand species to NAu-1 and SWy-2. The % Fe(II)/Fe(tot) ratios for reduced NAu-1 and SWy-2 were measured using Mössbauer spectroscopy and the resulting structural Fe(II) concentrations were calculated based upon the measured Fe content of NAu-1 of 4.5 mM/g. Changes in the aqueous speciation were measured spectrophotometrically using a modified 1,10-phenanthroline method.

		NAu-1	NAu-1 Fe(II)	ΔFe(II)$_{(aq)}$	ΔFe(tot)$_{(aq)}$	SWy-2	SWy-2 Fe(II)	ΔFe(II)$_{(aq)}$
Ligand species	**E^0_H (V)**	**% $\frac{Fe(II)}{Fe(tot)}$**	**mM**	**mM**	**mM**	**% $\frac{Fe(II)}{Fe(tot)}$**	**mM**	**mM**
$FeSalicylate^{+}$	0.20	6.2	0.56	-0.53	0.00	-		-
$FeTartrate_2^{2-}$	0.31	2.5	0.23	-0.22	-0.075		-	-
$FeCitrate^{-}$	0.07	5.3	0.48	-0.46	0.00	63.2	0.19	-0.12
$FeOxalate^{0}$	0.46	5.8	0.58	-1.15	-1.15	-	-	-

aqueous Fe(II) alone. This is likely because aqueous Fe(II) sorbs to mineral edge OH groups at circumneutral pHs and sorbed Fe(II) may more readily transfer electrons to the clay mineral structure than organically complexed Fe(II). In the presence of, salicylate and citrate we did not detect any removal of Fe(II) from the aqueous phase, and therefore sorption, following addition of the clay mineral and for L-(+)-tartrate only 0.075 mM sorbed (Table 4.1). This is less than would be expected for aqueous Fe(II) in the absence of any ligand species, based on our findings discussed in Chapter 3. However, in the presence of oxalate, 1.15 mM Fe(II) was removed from solution. According to our speciation modelling (Table S4.3, Figures S4.2), 1.64 mM Fe(II) remained complexed in the aqueous rather than organic phase. Interestingly, based on our previous findings, 1.15 mM of sorbed Fe(II) in the absence of any ligands would produce approximately the same reduction extent of NAu-1 (0.63 mM structural Fe(II) compared to 0.58 mM in the presence of oxalate, Table 4.1). Therefore, it is possible that only the aqueous rather than organically complexed Fe(II) contributes to mineral reduction in the presence of oxalate.

The reactivity of Fe(II)-reduced clay minerals is known to be influenced by the formation of a solid Fe oxidation product, the composition of which varies according to reaction conditions (47, 80, 172). Therefore, we used Fe(II)-ligand stock prepared from ^{57}Fe and Mössbauer spectroscopy to investigate the fate of sorbed Fe(II) in our reactors containing citrate, L-(+)-tartrate and oxalate.

Consistent with the absence of Fe(II) sorption in the FeCit-reduced NAu-1, at a temperature of 13 K, the Mössbauer spectrum resembled that for the spectra collected using ^{56}Fe and two doublets were observed corresponding to Fe(II) and octahedral Fe(III) (Figure S4.7). The collection time was also approximately the same as for ^{56}Fe reacted minerals indicating that the majority of the signal still came from the clay mineral rather than a solid phase formed from the enriched ^{57}Fe ligand species. No broadening of the spectra was observed and there were no sextet/octet phases to suggest that any iron-oxide or green rust-like phases had formed. However, the area of the Fe(II) doublet increased from 5.5 % to 16 %. After the isotopic enrichment factor of our ^{57}Fe stock was taken into account (95.06 %), this corresponds to an extra 0.1 μM of Fe(II), which is likely to comprise a small amount of sorption at the mineral surface not the formation of an Fe oxidation product.

In the case of FeTar and FeOx we observed the formation of distinct sorbed/precipitated phases. Due to the low Fe sorption extent measured for FeTar, after the enrichment factor of the ^{57}Fe stock was accounted for approximately 50 % of the Mössbauer spectral area corresponded to ^{57}Fe bound in NAu-1. However, at both 77 K and 4 K the spectra (Figure S4.10) resembles that of ferric tartrate (195), suggesting that some of the cationic Fe(III)-tartrate^{+} formed during NAu-1 reduction remained sorbed at the mineral surface. For FeOx, the precipitate accounted for 87 % of the contribution to the signal and clearly resembled that of ferrous oxalate mineral humboldtine (Figure S4.9) (196–198) with a smaller contribution from an Fe(III) doublet, which may comprise Fe(III)-oxalate species/structural Fe(III) and an Fe(III) sextet, which may comprise an Fe-(oxyhydr)oxide phase. Therefore, Fe(II)-complex-

reduced NAu-1 is likely to exhibit a differing reactivity to Fe(II)-reduced NAu-1 alone, either due to the lack of a solid oxidation product (FeCit, $FeTar_2$, FeSal) or because the oxidation product has a fundamentally different nature (FeOx).

To further investigate the interaction between coexisting Fe(II)-carboxylate ligand and Fe-bearing clay minerals we used ion chromotography to determine whether any sorption of citrate species to the clay mineral occurred, and ICP-MS to determine whether any dissolution of cations from the structure of NAu-1 occurred in the presence of citrate, as previous work has indicated that organic ligands may promote the dissolution of silicate minerals (76, 199). We did not measure any significant drop in citrate concentrations in our reactors, which would suggest sorption of the citrate to the mineral surface. We also did not measure dissolution of Fe, Al, Si or Mg from the structure of NAu-1 that had been suspended in 10 mM citrate solution at pH 7.5 for 1 - 7 days.

4.3.2 Reactivity of Fe-bearing clay minerals in the presence of carboxylate Fe(II)-complexes

To assess how organic contaminant reduction in the environment may be influenced by the presence of coexisting organic Fe(II)-complexes and redox active mineral phases, we used 2AcNB as a reactive probe compound to determine the reactivity of native (containing only structural Fe(III)) NAu-1 in the presence of FeOx, FeCit, $FeTar_2$ and FeSal. We used 5mM aqueous Fe(II) and a ligand concentration of 5 mM - 100 mM depending on the reactive species desired (S4.3).

Typical reduction kinetics of 2AcNB in the presence of NAu-1 and FeCit, $FeTar_2$ and FeSal are shown in Figure 4.1a. We observed rapid transformation ($<$ 2 hours) of 2AcNB into 2-acetylaniline, significantly faster than that measured for Fe(II)-reduced NAu-1 in the absence of an organic ligand ($\sim$ 1400 hours). Kinetics for $FeTar_2$ and FeCit, not shown here are included in Figure S4.11. The reduction kinetics were best modelled according to a pseudo-first order rate law rather than the biphasic model observed in the absence of a ligand. However, transformation of 2AcNB in the presence of NAu-1 and FeOx was found to be significantly slower (Figure 4.1b) and complete transformation was not reached within 1500 hours. Interestingly, the kinetics in this instance followed a biphasic rate law, as we observed for both dithionite- and Fe(II)-reduced NAu-1. Figure 4.1b shows the reduction kinetics of 2AcNB with FeOx and NAu-1 (5.8 % Fe(II)/Fe(tot)) relative to 5% dithionite- and 5.5% Fe(II)-reduced NAu-1 in the absence of a ligand. The modelled kinetic parameters for NAu-1 with FeOx are within error of those we modelled for 5 % dithionite-reduced NAu-1 (Table S4.8).

We also investigated the reactivity of structural Fe(II) in NAu-1 that had been reduced by Fe(II)-citrate to give a 5.5 % Fe(II)/Fe(tot) ratio. The reduced mineral was extracted through centrifugation and suspended in fresh buffer solution prior to spiking with 2AcNB solution. The reduced NAu-1 suspension slowly reacted with 2AcNB, although complete transformation was not observed after 1000 hours as shown in Figure S4.14. This is considerably slower

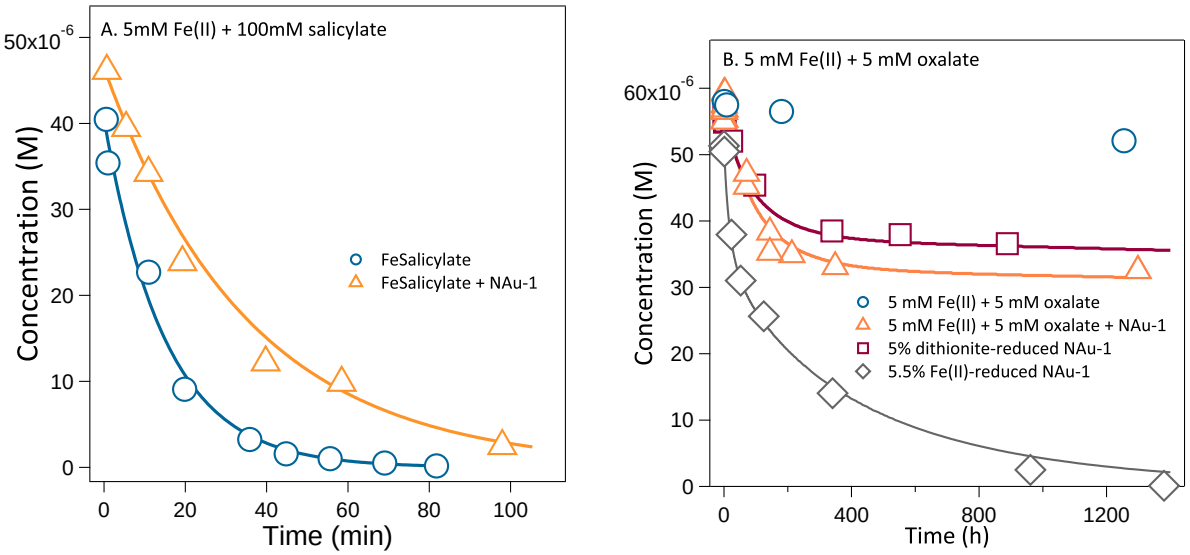

Figure 4.1: Typical reduction kinetics of 2AcNB in the presence of (a) FeSal with and without NAu-1. Kinetic fits shown follow a pseudo-first order rate law, and (b) FeOx with and without NAu-1. Kinetic plots showing the degradation of 2AcNB in the presence of 5.5 % Fe(II)-reduced NAu-1 and 5 % dithionite-reduced NAu-1 are shown for comparison. Kinetic fits shown follow a biphasic rate law.

than the reactivity of Fe(II)-reduced NAu-1 with 2AcNB, where complete transformation was observed within 1400 hours. However, a direct comparison cannot be made as this experiment was undertaken with excess aqueous Fe(II) present and our preliminary experiments indicated that Fe(II)-reduced NAu-1 that was similarly resuspended in fresh buffer also exhibited reduced reactivity towards NAu-1 under the same reaction conditions.

As we observed a significantly faster reduction rate of 2AcNB reduction in the presence of FeCit, $FeTar_2$ and FeSal, we also determined the reactivity of our carboxylate Fe(II)-complexes in the absence of a mineral phase in order to elucidate their contribution to the reactivity of the combined system.

In the absence of NAu-1, a faster transformation of 2AcNB into 2-acetylaniline was achieved ($<$ 90 minutes) with FeCit, $FeTar_2$ and FeSal and the kinetics again followed a pseudo-first order kinetic model (Figure 4.1, S4.11). Therefore, we propose that the carboxylate Fe(II)-ligands are the predominant reactive phase in the combined system.

However, transformation of 2AcNB in the presence of FeOx was found to be significantly slower (Figure 4.1b) with only a 10 % conversion measured after $>$ 4200 hours (approximately 6 months). It is therefore likely, that in this instance the clay mineral is the predominant reactive phase in the combined system hence the reaction kinetics matching those for dithionite-reduced NAu-1. Although we observed the formation of an Fe oxidation product with FeOx-reduced NAu-1, it was of a fundamentally different nature to that formed with Fe(II)-reduced NAu-1 and did not lead to the enhanced reactivity we observed for Fe(II)-reduced NAu-1 in the absence of a ligand.

The rapid transformation of 2AcNB in the presence of FeCit, $FeTar_2$ and FeSal in the absence of a mineral phase was unexpected, as previous work has found that although Fe(II)-carboxylate species are reactive towards more easily reducible contaminants such as Cr(VI)

(186) Fe(II) in the presence of salicylate and citrate did not show any reactivity towards NACs (1). However, our speciation modelling found that under the conditions used for Naka *et al.,*'s study (0.5 mM, 5 mM, pH 7.0) the maximum concentration of Fe(salicylate)^0 was 0.24 mM, with the majority of the rest present as Fe(OH)$^+$ (S4.3), which is unreactive towards NACs (42). As six electrons are required to transform the NAC to the corresponding aniline, 0.3 mM of Fe(II) is required to transform the 50 μM NAC spike. Therefore, in this instance there was not enough of the reactive species present for the reaction to proceed. In the case of citrate, although 0.45 mM of Fe(citrate)$^-$ was present (S4.3); enough to allow the reaction to proceed, at pH 7.0 the more highly reactive $Fe_2(OH)_2(citrate)_2^{-4}$ species is present in a much lower concentration than within our reactors (S3.4). Although it is not the dominant species in our reactors, it has a much lower (E_H) than Fe(citrate)$^-$ and therefore lowers the overall (E_H) of the reactors from 0.45 V (Naka *et al* 2006 (1)) to 0.07 V (our system).

It is generally expected that a linear free energy relationship will be observed between the reaction rate constant (log *k* ($M^{-1}h^{-1}$)) and the E_H^0 of structurally related ligand species with a specific reactive probe molecule with a slope of 1 if electron transfer is the rate limiting step (113, 140, 186). Figure 4.2b shows the relationship between the modelled log *k* values and E_H calculated for our reactors (orange circles). For FeCit, FeSal and $FeTar_2$ a linear trend is observed with an approximately horizontal slope. FeOx, where the reaction proceeded extremely slowly, plots significantly below this line.

The reduction of NACs to anilines proceeds through a series of electron and proton transfer steps (107) and it is generally thought that the transfer of the first electron to form a nitroaromatic radical anion can be mathematically thought of as the rate limiting step, although isotopic kinetic studies suggest that the actual rate limiting step is a dehydration reaction to form a nitrosobenzene species (Figure 2.3) (46, 107, 108, 200). The one-electron reduction potential (E_H^1 = -0.485 V, not pH dependent) for nitrobenzene is significantly more negative than the reduction potential for the overall reaction to aniline (E_H^0, (W) = 0.42 V at pH 7.0, [HCO_3^-] = 1 mM, [Cl^-] = 1 mM). The E_H^1 is also more negative than the E_H of the Fe(II)-ligand species in our reactors and therefore, the standard free energy of this first electron transfer step is positive. Although the E_H^0 for 2-acetylnitrobenzene is not known, it is likely to be of a similar magnitude to that of nitrobenzene, as the *ortho* acetyl group will not have a significant effect on the formation of the aniline. Therefore, although the transfer of the first electron is not favourable, the standard free energy for the entire reaction remains exergonic allowing the reaction to proceed spontaneously (10, 106, 201–204).

In this instance, we suggest that the approximately horizontal slope observed in the LFER is due to a dependence on the overall E_H^0 of the reaction rather than the E_H^1, i.e. the driving force to transfer 6 electrons and 6 protons to complete the transformation to the aniline rather than the first electron transfer to the first unstable intermediate phase. Therefore, the rate limiting step is not the transfer of the first electron but rather is limited by the formation/dissociation of precursor/successor complexes. It is likely that we do not see significant reactivity for FeOx as the E_H for FeOx lies close to or above the E_H^0.

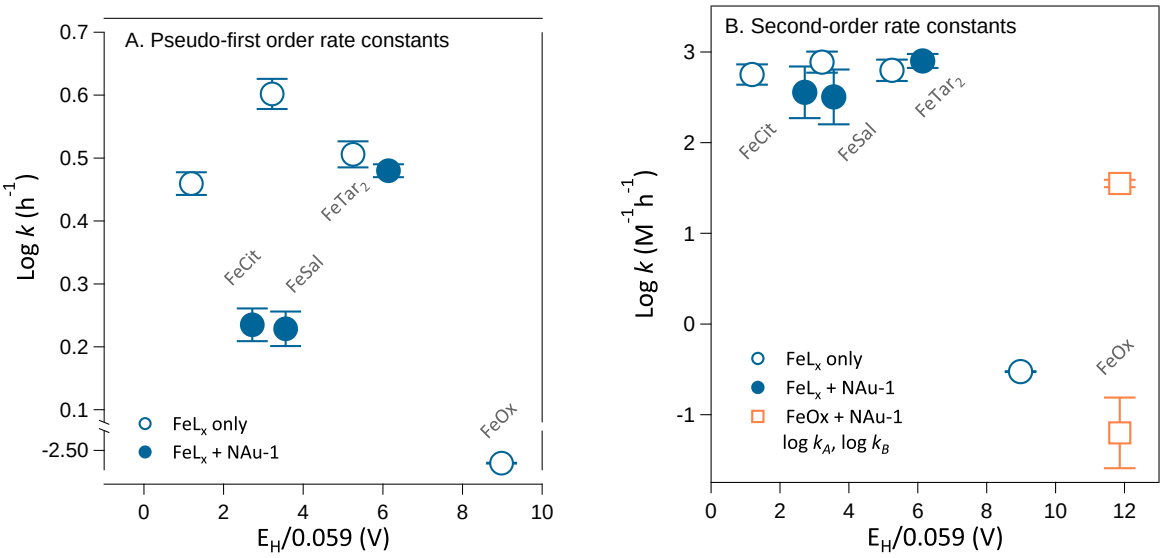

Figure 4.2: (a) Pseudo-first order reduction rate constants against $E_H/0.059$ for the reduction of 2AcNB by either Fe(II)-complexes alone (open circles) or Fe(II)-ligands in the presence of 2.0 g/L NAu-1 (filled circles), and (b) Second order reduction rate constants against $E_H/0.059$ with and without native NAu-1. In the case of FeOx + NAu-1, biphasic kinetics were observed indicating the presence of two reactive Fe(II)-species with differing intrinsic reactivities. Therefore, two second-order reduction rate constants are plotted (orange squares, $\log k_A$, higher reactivity and $\log k_B$, lower reactivity).

For FeCit, $FeTar_2$ and FeSal, we found that the in the presence of NAu-1, complete transformation of 2AcNB was slightly slower than in the absence of the mineral, reflected by the drop in the pseudo-first order rate constants in Figure 4.2a. However, we also calculated the second-order rate constants for the reaction using the measured aqueous Fe(II) concentrations after the addition of the mineral. As shown in Figure 4.2b, we did not observe a significant change in the second order rate constants. This suggests that the slight drop in reaction rate is due to the transfer of electrons from the Fe(II)-ligand species to the clay mineral and that the predominant reactive phase is the Fe(II)-ligand, the instrinsic reactivity of which is not affected by the clay mineral.

We remodelled the speciation of our reactors using MICROQL to account for this change and found that in our case this did not result in any significant changes the nature of the reactive species present or the E_H of the system (Table S3.4). However, as the reactivity of Fe(II)-ligand systems may be dramatically altered by changes in the speciation, in some cases electron transfer to mineral phases may also influence the reactivity of the combined system.

To confirm our hypothesis that the Fe(II)-ligand acts as the reductive phase in our reactors, we also investigated FeCit in the presence of synthetic, Fe-free montmorillonite SYn-1 and FeCit that had been allowed to equilibrate with native NAu-1 with the mineral phase removed by centrifugation. Figure 4.3 shows a comparison of the second order log k ($M^{-1}h^{-1}$) values for FeCit reacted in different conditions, individual kinetic plots are displayed in Figure S4.13.

Again, although we observed a drop in the reaction rate in the presence of native NAu-1 and SYn-1, reflected as a drop in the pseudo-first order rate contsants, we did not see a significant change in the magnitude of the second-order log k values. Therefore, we propose

that FeCit is the only phase in the system that reduces the NAC and the presence of the clay mineral act as a redox buffer, removing electrons from the carboxylate Fe(II)-complex and therefore slowing the rate of reaction without affecting the intrinsic reactivity of FeCit.

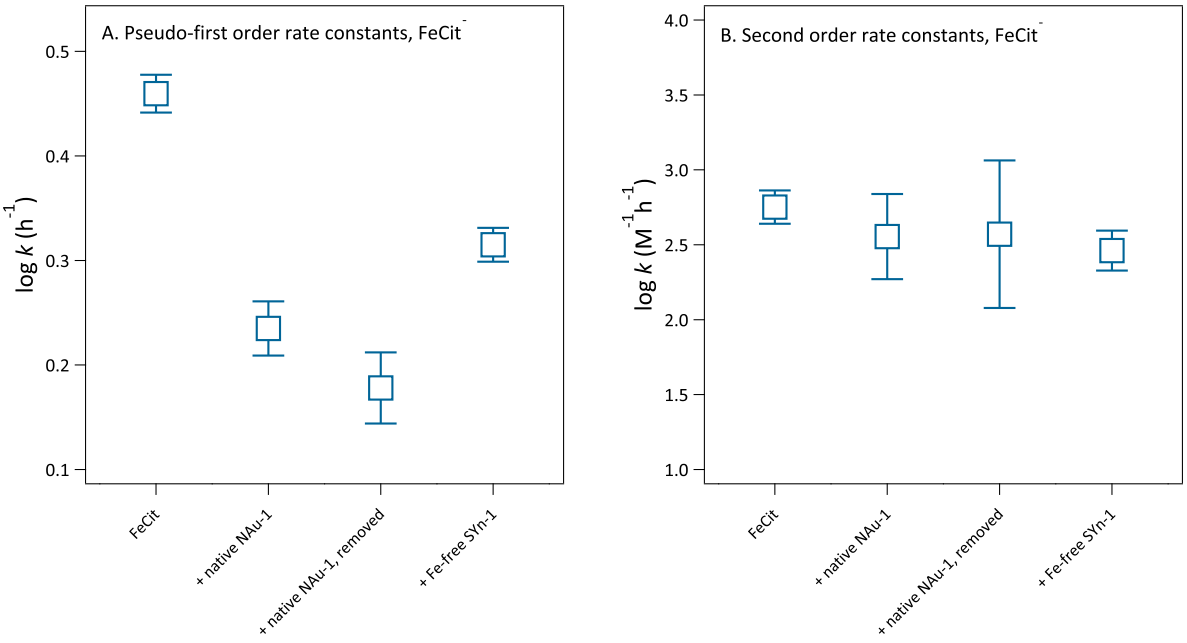

Figure 4.3: (a) Pseudo-first and (b) Second order rate constants for the reduction of 2AcNB by FeCit in various reaction conditions.

4.3.3 Dependence on clay mineral Fe reduction extent

To determine whether the redox buffering effect of Fe-bearing clay minerals is influenced by the structural Fe(II) content of the mineral, we also assessed the reactivity of FeCit in the presence of NAu-1 that had been previously reduced using dithionite to an extent of either 9 % or 91 % Fe(II)/Fe(tot). The reactivity of reduced Fe-bearing clay minerals towards NACs is already well documented in our previous work and others (20–22).

In the case of 9 %-reduced NAu-1, we did not observe a significant change in reactivity compared to FeCit alone (Figure fig:cat) despite the lower reduction potential of the NAu-1 (-0.18 V) (123). We also did not observe further electron transfer the FeCit to the mineral or other changes in the speciation of the aqueous phase.

Similarly, for 91 %-dithionite-reduced NAu-1 (E_H = -0.44 V) in the presence of FeCit, 2AcNB was completely transformed to 2-acetylanilinine in approximately the same timescale as that observed for the ligand only system. However, in this instance, the reduction kinetics of the 2AcNB transformation could not be modelled using a pseudo-first order rate law, as shown in Figure 4.4. Instead, we found that the reduction kinetics are best fit according to a biphasic kinetic model, indicating the presence of two types of reactive Fe(II) species (Equation 4). Biphasic kinetic models have previously been applied to describe the reduction of NACs in the presence of reduced, iron-rich nontronites (20). However, the reduction of 2AcNB in the

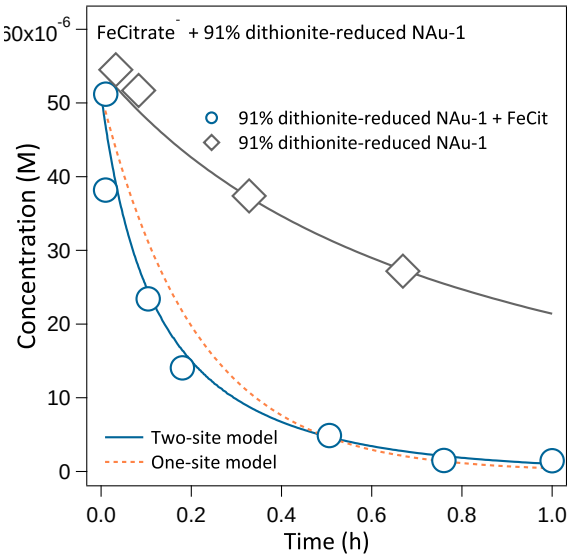

Figure 4.4: Reduction kinetics of 2-acetylnitrobenzene (blue circles) by FeCit in the presence of 91%-reduced NAu-1. The kinetics were best fit according to a biphasic rate law (blue solid line) rather than a pseudo-first order model (orange dashed line). For comparison, 91% dithionite-reduced NAu-1 alone, which also exhibits biphasic kinetics is shown (grey diamonds).

presence of 91 % reduced NAu-1 alone occurs more slowly taking approximately 48 hours for complete transformation to occur rather than the 60 minutes observed here. It is therefore likely that FeCit remains the predominant reactive phase.

We used Mössbauer spectroscopy and the 1,10-phenanthroline method to monitor the Fe(II)/Fe(tot) content of the NAu-1 and Fe-ligand species before and after reaction with 2AcNB. The Mössbauer spectra (Figure S4.8), indicate that the structural Fe(II)/Fe(tot) ratio has decreased from 91% to 87% (0.54 mM) whereas no measurable change occurs in the aqueous Fe speciation. Accounting for the stoichiometry of the reaction (6 moles Fe(II): 1 mole NAC), this is enough to completely transform the 50 μM 2AcNB spike with a large excess. This is surprising, as our hypothesis that the Fe(II)-ligand species is a reactive phase would suggest that the Fe(II) content of the ligand should be partially oxidised to Fe(III) through the reaction with 2AcNB.

As the reaction proceeds significantly more quickly than that observed for the reduced mineral alone, we suggest that the Fe(II)-ligand species is the predominant reactive phase although the reduced NAu-1 contributes to the reduction kinetics. As no change is measured in the aqueous speciation but a drop is measured in the Fe(II) content of the NAu-1, we suggest that the clay mineral may be recharging the reactive Fe(II)-ligand species. Alternatively, it possible that the clay mineral also transfers electrons directly to the NAC and one of the reactive Fe(II)-species comprises structural Fe(II). However, it is not possible to distinguish the actual mechanism.

4.4 Summary

To summarise, we have shown that Fe(II)-ligand complexes are generally more reactive towards NACs than clay mineral Fe(II). However, if a Fe(II)-complex of lower reactivity is present (e.g. FeOx), clay mineral Fe is the primary reductant and behaves similarly to dithionite-reduced NAu-1 with a comparable % Fe(II)/Fe(tot) ratio.

In the presence of more reactive Fe(II)-complexes, we observed the clay mineral to act as a redox buffer. In its native form, the clay mineral lowers the aqueous reactive Fe(II) concentration through sorption, electron transfer or precipitate formation therefore decreasing the observed rate of reduction (but not the second-order rate constant). In its reduced form, we found that NAu-1 recharged the Fe(II) of the reactive Fe(II)-complex species, enabling further contaminant transformation than would be predicted according to aqueous speciation alone.

Chapter S4
Assessing the influence of Fe(II)-organic complexes on the reactivity of Fe-bearing clay minerals: Supporting Information

S4.1 Chemicals and Reagents

All chemicals and reagents used in this study were of analytical grade and purchased from either Fisher Scientific/ACROS Organics (sodium chloride, sodium citrate, sodium bicarbonate, sodium dithionite, 1,10-phenanthroline, hydrofluoric acid, hydrochloric acid and hexacyanoferrate) or Sigma Aldrich (sodium hydroxide, 2-acetylnitrobenzene, 2-acetylaniline, citric acid, L-(+)-tartaric acid, oxalic acid, salicylic acid, HPLC grade methanol).

All stock solutions were purged with N_2 for at least an hour before introduction to the anaerobic chamber.

S4.2 Mineral preparation

Nontronite NAu-1 with the published unit cell formula of $M^+_{1.05}[Si_{6.98}Al_{1.02}][Al_{0.29}Fe_{3.68}Mg_{0.04}]O_{20}OH_4$, synthetic mica montmorillonite SYn-1 with the published unit cell formula of $M^+_{0.024}[Si_{6.5}Al_{1.5}][Al_{4.44}Mg_{0.04}Fe_{tr}]O_{20}OH_4$ and SWy-2, $(M^+_{0.61})[Si_{7.98}Al_{0.02}][Al_{3.01}Fe_{0.41}Mn_{0.01}Mg_{0.54}Ti_{0.02}]O_{20}OH_4$ were purchased from the Source Clays Repository. The cation exchange capacities of the minerals as determined at the basal planes are 125 meq/100 g, 70-140 meq/100 g and 76.4 meq/100 g respectively (205).

The 0.1-0.5 μm fraction of the mineral was obtained through repeated centrifugation according to Stoke's law. The fractionated mineral was then washed three times in 1 M NaCl solution, in order to achieve Na^+ homoionization and then washed twice with DI water. Finally, mineral impurities were removed by repeated centrifugation for 5 minutes at 8000 rpm, which preferentially leaves the impure fraction in the pellet and the clean fraction in the supernatant. FT-IR was then used to confirm removal of any Fe-oxide, carbonate and kaolin impurities (168).

S4.3 Figures and Tables

S4.4 Aqueous speciation

S4.4.1 Stability Constants

Table S4.1: Stability constants used to model the Fe speciation and E_H of our reactors. Values are valid for 25°C and are taken from the IUPAC stability constants database (192) and adjusted for $I = 0.11$ using the Davies Equation unless otherwise specified.

Reaction	log K
OH	
$Fe^{2+} + H_2O - H^+ = FeOH^+$	-9.41
$Fe^{2+} + 2\,H_2O - 2\,H^+ = Fe(OH)_2{}^0$	-23.8
$Fe^{2+} + 3\,H_2O - 3\,H^+ = Fe(OH)_3{}^-$	-27.79
$Fe^{3+} + H_2O - H^+ = FeOH^{2+}$	-2.82
$Fe^{3+} + 2\,H_2O - 2\,H^+ = Fe(OH)_2{}^+$	-5.56
$Fe^{3+} + 3\,H_2O - 3\,H^+ = Fe(OH)_3{}^0$	-11.14
$Fe^{3+} + 4\,H_2O - 4\,H^+ = Fe(OH)_4{}^-$	-20.72
$2\,Fe^{3+} + 2\,H_2O - 2\,H^+ = Fe_2(OH)_2{}^{4+}$	-3.06
$2\,Fe^{3+} + 4\,H_2O - 4\,H^+ = Fe_3(OH)_4{}^{5+}$	-6.12
Chloride	
$Fe^{2+} + Cl^- = FeCl^+$	-0.05
$Fe^{3+} + Cl^- = FeCl^{2+}$	0.67
$Fe^{3+} + 2\,Cl^- = FeCl_2{}^+$	1.37
$Na^+ + Cl^- = NaCl^0$	-0.38
Oxalate	
$H^+ + Ox^{2-} = HOx^-$	3.05
$2\,H^+ + Ox^{2-} = H_2Ox^0$	5.00
$Fe^{2+} + Ox^{2-} = FeOx^0$	3.13
$Fe^{2+} + 2\,Ox^{2-} = FeOx_2{}^{2-}$	6.07
$Fe^{2+} + 3\,Ox^{2-} = FeOx_3{}^{4-}$	6.41
$Fe^{3+} + Ox^{2-} = FeOx^+$	8.80
$Fe^{3+} + 2\,Ox^{2-} = FeOx_2{}^-$	15.4
$Fe^{3+} + 3\,Ox^{2-} = FeOx_3{}^{3-}$	19.8
$Na^+ + Ox^{2-} = NaOx^-$	0.90
Citrate	
$H^+ + Cit^{3-} = HCit^{2-}$	5.76
$2\,H^+ + Cit^{3-} = H_2Cit^-$	10.33
$3\,H^+ + Cit^{3-} = HCit^0$	13.34
$Fe^{2+} + Cit^{3-} = FeCit^-$	4.97

$Fe^{2+} + Cit^{3-} + H^+ = FeHCit^0$	5.96
$Fe^{2+} + Cit^{3-} + 2\,H^+ = FeH_2Cit^+$	9.91
$Fe^{2+} + 2\,Cit^{3-} + H^+ = FeHCit_2{}^{3-}$	11.99
$2\,Fe^{2+} + 2\,Cit^{3-} + 2\,H_2O - 2\,H^+ = Fe_2(OH)_2Cit_2{}^{4-}$	-2.53
$Fe^{3+} + Cit^{3-} = FeCit^0$	11.21
$Fe^{3+} + Cit^{3-} + H^+ = FeHCit^+$	12.28
$Fe^{3+} + 2\,Cit^{3-} + H^+ = FeHCit_2{}^+$	19.12
$Fe^{3+} + Cit^{3-} + H_2O - H^+ = FeOHCit^-$	8.51
$2\,Fe^{3+} + 2\,Cit^{3-} + 2\,H_2O - 2\,H^+ = Fe_2(OH)_2Cit_2{}^{2-}$	21.2
$Na^+ + Cit^{3-} = NaCit^{2-}$	1.39
L-(+)-Tartrate	
$H^+ + Tar^{2-} = HTar^-$	3.95
$2\,H^+ + Tar^{2-} = H_2Tar^0$	6.99
$Fe^{2+} + Tar^{2-} = FeTar^0$	2.24
$Fe^{2+} + 2\,Tar^{2-} = FeTar_2{}^{2-}$	2.63
$Fe^{2+} + Tar^{2-} + H^+ = FeHTar^+$	4.68
$Fe^{3+} + Tar^{2-} = FeTar^+$	5.68
$Fe^{3+} + Tar^{2-} + H^+ = FeHTar^{2+}$	10.53
$Na^+ + Tar^{2-} = NaTar^-$	0.50
Salicylate	
$H^+ + Sal^{2-} = HSal^-$	13.66
$2\,H^+ + Sal^{2-} = H_2Sal^0$	16.64
$Fe^{2+} + Sal^{2-} = FeSal^0$	6.55
$Fe^{2+} + 2\,Sal^{2-} = FeSal_2{}^{2-}$	11.2
$Fe^{2+} + Sal^{2-} + H^+ = FeHSal^+$	4.80
$2\,Fe^{2+} + Sal^{2-} + H^+ = Fe_2HSal^{3+}$	8.30
$Fe^{3+} + Sal^{2-} = FeSal^+$	16.45
$Fe^{3+} + 2\,Sal^{2-} = FeSal_2{}^-$	29.12
$Fe^{3+} + 3\,Sal^{2-} = FeSal_3{}^{3-}$	40.89
$Fe^{3+} + Sal^{2-} + H^+ = FeHSal^{2+}$	4.40
$Na^+ + Sal^{2-} = NaSal^-$	-0.50

S4.4.2 pK_a Values

Table S4.2: pK_a values for the acids used in this study, corrected for an ionic strength of 0.11 using the Davies Equation. Data is taken from ref (2).

Acid	$\mathbf{pK_a}$	$\mathbf{pK_b}$	$\mathbf{pK_c}$
Oxalic Acid	1.20	3.80	-
Citric Acid	2.90	4.35	5.70
Salicylic Acid	2.81	13.4	-
L-(+)-Tartaric Acid	2.82	3.97	-

S4.4.3 Equilibrium speciation plots

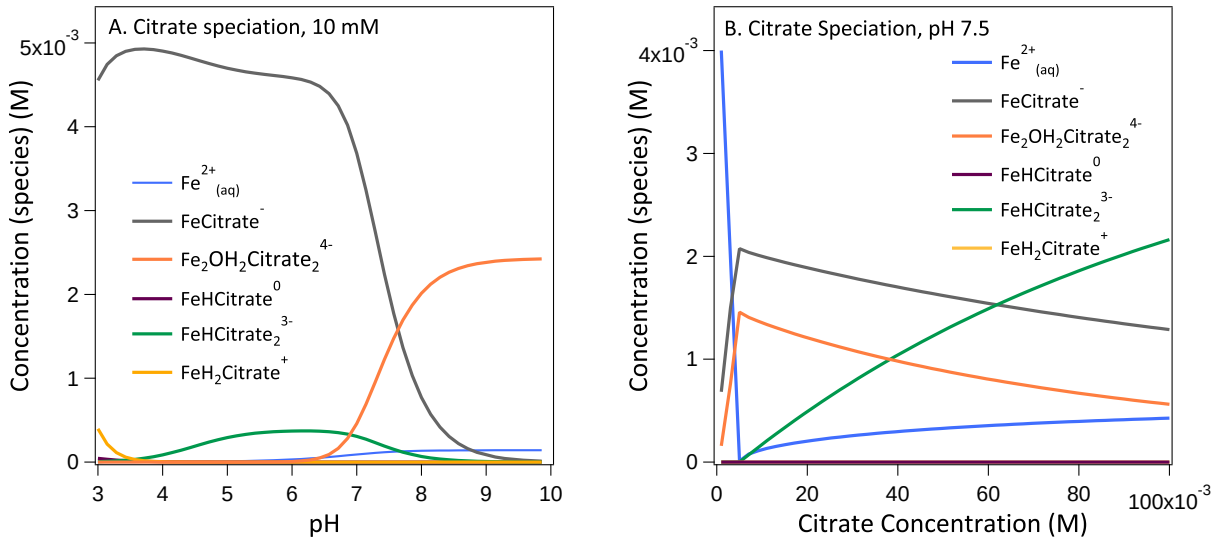

Figure S4.1: Equilibrium speciation plots as calculated using the MICROQL software package and published stability constants for (a) Fe(II)-Citrate speciation for a citrate concentration of 10 mM from pH 3.0 - 10.0 and (b) Fe(II)-Citrate speciation at pH 7.5 for citrate concentration from 0.001 to 0.1 M.

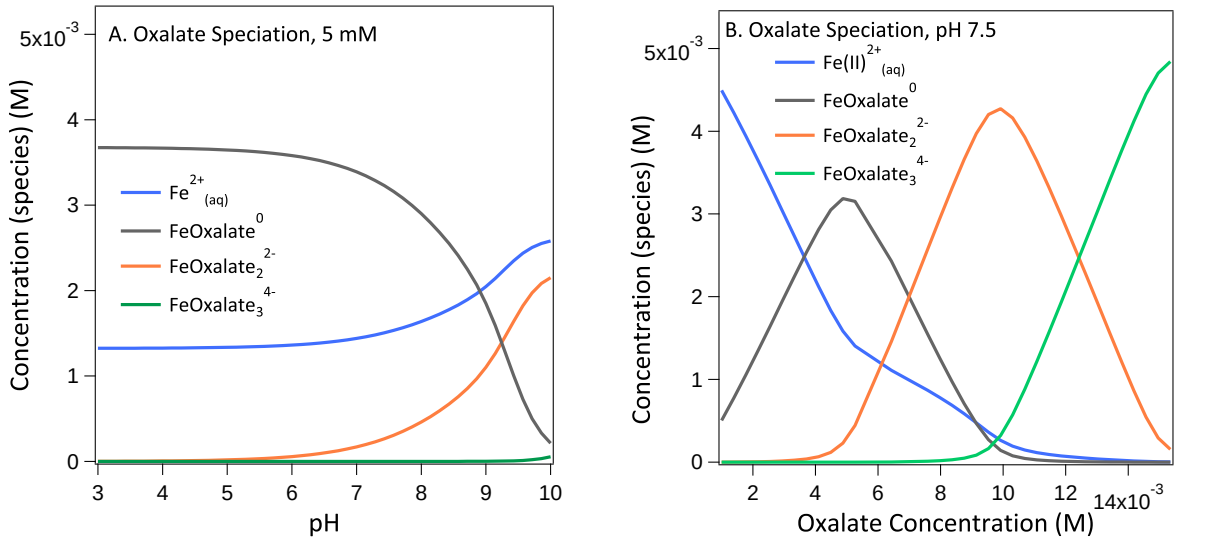

Figure S4.2: Equilibrium speciation plots as calculated using the MICROQL software package and published stability constants for (a) Fe(II)-Oxalate speciation for a oxalate concentration of 5 mM from pH 3.0 - 10.0 and (b) Fe(II)-Oxalate speciation at pH 7.5 for oxalate concentration from 0.001 to 0.015 M.

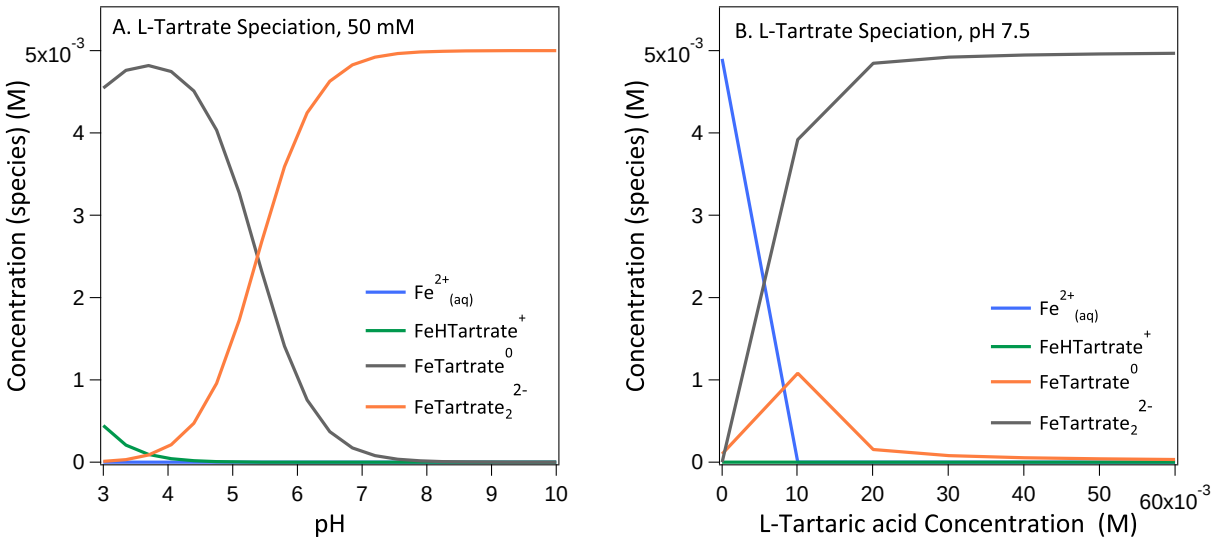

Figure S4.3: Equilibrium speciation plots as calculated using the MICROQL software package and published stability constants for (a) Fe(II)-Tartrate speciation for a tartrate concentration of 50 mM from pH 3.0 - 10.0 and (b) Fe(II)-Tartrate speciation at pH 7.5 for tartrate concentration from 0.001 to 0.06 M.

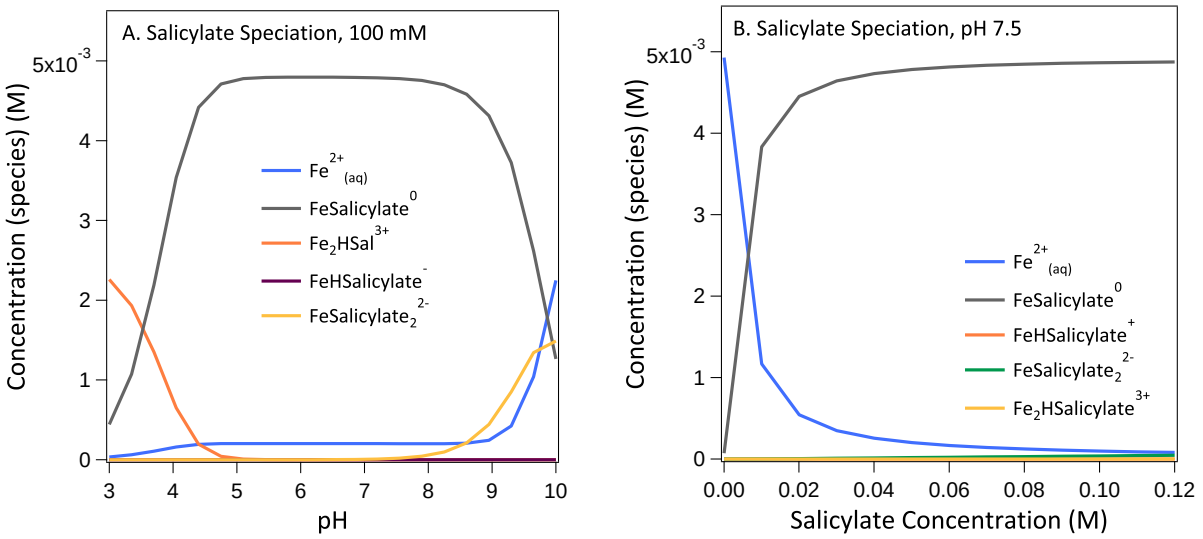

Figure S4.4: Equilibrium speciation plots as calculated using the MICROQL software package and published stability constants for (a) Fe(II)-Salicylate speciation for a salicylate concentration of 100 mM from pH 3.0 - 10.0 and (b) Fe(II)-Salicylate speciation at pH 7.5 for salicylate concentration from 0.001 to 0.12 M.

S4.4.4 Calculated Fe(II)-ligand species and E_H values

Table S4.3: Modelled concentrations of Fe(II)-ligand species in our reactors calculated using MICROQL (191) using the stability constants as displayed in Table S1.

Ligand	Calculated E_H (V)	Species	Modelled Concentration (M)	Modelled + NAu-1 Concentration (M)
Oxalate^{2-}	**0.46**	Fe(II)OH^{+}	4.61 x 10^{-4}	5.05 x 10^{-5}
		Fe(II)(OH)$_2$	5.94 x 10^{-11}	6.50 x 10^{-12}
		Fe(II)(OH)$_3^{-}$	1.92 x 10^{-7}	2.10 x 10^{-8}
		Fe(II)Cl^{+}	1.18 x 10^{-3}	1.05 x 10^{-3}
		Fe(II)Oxalate^{0}	2.90 x 10^{-3}	2.28 x 10^{-3}
		Fe(II)Oxalate$_2^{2-}$	1.45 x 10^{-4}	8.21 x 10^{-4}
		Fe(II)Oxalate$_3^{4-}$	3.17 x 10^{-4}	2.88 x 10^{-13}
		Fe(III)OH^{2+}	4.50 x 10^{-14}	1.00 x 10^{-10}
		Fe(III)(OH)$_2^{+}$	2.59 x 10^{-9}	5.77 x 10^{-6}
		Fe(III)(OH)$_3^{0}$	2.16 x 10^{-7}	4.80 x 10^{-4}
		Fe(III)(OH)$_4^{-}$	1.79 x 10^{-9}	4.50 x 10^{-14}
		Fe(III)$_2$(OH)$_2^{4+}$	7.71 x 10^{-25}	3.82 x 10^{-18}
		Fe(III)$_3$(OH)$_4^{5+}$	6.32 x 10^{-31}	6.98 x 10^{-21}
		Fe(III)Cl^{2+}	2.00 x 10^{-19}	3.61 x 10^{-15}
		Fe(III)Cl$_2^{+}$	4.53 x 10^{-20}	6.66 x 10^{-15}
		Fe(III)Oxalate^{+}	3.40 x 10^{-14}	5.46 x 10^{10}
		Fe(III)Oxalate$_2^{-}$	7.77 x 10^{-12}	8.96 x 10^{-7}
		Fe(III)Oxalate$_3^{3-}$	1.12 x 10^{-11}	9.29 x 10^{-6}
		HOxalate^{-}	2.03 x 10^{-9}	1.46 x 10^{-8}
		H$_2$Oxalate^{0}	5.73 x 10^{-15}	4.13 x 10^{-14}
		NaCl^{0}	4.88 x 10^{-2}	4.90 x 10^{-2}
		NaOxalate^{-}	1.18 x 10^{-3}	1.05 x 10^{-3}
Citrate^{3-}	**0.07**	Fe(II)OH^{+}	1.02 x 10^{-9}	8.48 x 10^{-10}
		Fe(II)(OH)$_2$	1.31 x 10^{-16}	1.09 x 10^{-16}
		Fe(II)(OH)$_3^{-}$	4.25 x 10^{-13}	3.54 x 10^{-13}
		Fe(II)Cl^{+}	1.20 x 10^{-4}	1.22 x 10^{-4}
		Fe(II)Citrate^{-}	2.00 x 10^{-3}	1.84 x 10^{-3}
		Fe(II)$_2$(OH)$_2$Citrate$_2^{4-}$	1.35 x 10^{-3}	1.15 x 10^{-3}
		Fe(II)H(Citrate)$_2^{3-}$	1.71 x 10^{-4}	1.75 x 10^{-4}
		Fe(II)H$_2$Citrate^{+}	1.74 x 10^{-13}	1.60 x 10^{-13}
		Fe(II)HCitrate^{0}	6.18 x 10^{-10}	5.69 x 10^{-10}
		Fe(III)OH^{2+}	3.96 x 10^{-18}	4.22 x 10^{-16}
		Fe(III)(OH)$_2^{+}$	2.28 x 10^{-13}	2.43 x 10^{-11}

		$Fe(III)(OH)_3^0$	1.89×10^{-11}	2.02×10^{-9}
		$Fe(III)(OH)_4^-$	1.57×10^{-13}	1.68×10^{-11}
		$Fe(III)_2(OH)_2^{4+}$	5.95×10^{-33}	6.76×10^{-29}
		$Fe(III)_3(OH)_4^{5+}$	4.28×10^{-43}	5.19×10^{-37}
		$Fe(III)Cl^{2+}$	6.30×10^{-19}	8.16×10^{-17}
		$Fe(III)Cl_2^+$	5.14×10^{-15}	8.10×10^{-13}
		$Fe(III)Citrate^0$	3.46×10^{-15}	4.09×10^{-10}
		$Fe(III)_2OH_2Citrate_2^{2-}$	7.23×10^{-10}	1.01×10^{-5}
		$Fe(III)HCitrate_2^{2-}$	2.30×10^{-12}	3.01×10^{-10}
		$Fe(III)HCitrate^+$	1.29×10^{-18}	1.52×10^{-16}
		$Fe(III)OHCitrate^+$	2.19×10^{-7}	2.58×10^{-5}
		$HCitrate^{2-}$	4.70×10^{-3}	5.21×10^{-3}
		$H_2Citrate^-$	5.53×10^{-6}	6.12×10^{-6}
		$H_3Citrate^0$	1.79×10^{-10}	1.98×10^{-10}
		$NaCitrate^{2-}$	1.20×10^{-4}	1.22×10^{-4}
		$NaCl^0$	4.99×10^{-2}	4.99×10^{-2}
$Salicylate^-$	**0.20**	$Fe(II)OH^+$	2.49×10^{-4}	2.25×10^{-4}
		$Fe(II)(OH)_2$	3.21×10^{-11}	2.90×10^{-11}
		$Fe(II)(OH)_3^-$	1.04×10^{-7}	9.38×10^{-8}
		$Fe(II)Cl^+$	5.91×10^{-6}	5.59×10^{-6}
		$Fe(II)Salicylate^+$	4.73×10^{-3}	4.23×10^{-3}
		$Fe(II)Salicylate_2^0$	1.39×10^{-5}	1.23×10^{-5}
		$Fe(II)HSalicylate^{2+}$	2.66×10^{-12}	2.38×10^{-12}
		$Fe(II)_2HSalicylate^{4+}$	2.66×10^{-16}	2.38×10^{-14}
		$Fe(III)OH^{2+}$	4.74×10^{-22}	1.18×10^{-18}
		$Fe(III)(OH)_2^+$	2.73×10^{-17}	6.80×10^{-14}
		$Fe(III)(OH)_3^0$	2.27×10^{-15}	5.66×10^{-12}
		$Fe(III)(OH)_4^-$	1.89×10^{-17}	4.71×10^{-14}
		$Fe(III)_2(OH)_2^{4+}$	8.55×10^{-41}	5.32×10^{-34}
		$Fe(III)_3(OH)_4^{5+}$	7.38×10^{-55}	1.14×10^{-44}
		$Fe(III)Cl^{2+}$	1.96×10^{-29}	1.13×10^{-26}
		$Fe(III)Cl_2^+$	4.15×10^{-32}	5.11×10^{-28}
		$Fe(III)Salicylate^{2+}$	1.84×10^{-17}	4.54×10^{-14}
		$Fe(III)Salicylate_2^+$	5.67×10^{-12}	1.38×10^{-8}
		$Fe(III)Salicylate_3^0$	2.20×10^{-7}	5.30×10^{-4}
		$Fe(III)HSalicylate^{3+}$	5.19×10^{-37}	1.28×10^{-33}
		$HSalicylate^0$	9.52×10^{-2}	9.42×10^{-2}
		$H_2Salicylate^+$	2.88×10^{-6}	2.84×10^{-6}
		$NaSalicylate^0$	5.91×10^{-6}	5.59×10^{-6}
		$NaCl^0$	5.00×10^{-2}	5.00×10^{-2}

L-(+)-Tartrate^{2-}	**0.31**	Fe(II)OH^{+}	2.02 x 10^{-9}	1.91 x 10^{-09}
		Fe(II)(OH)$_2$	2.61 x 10^{-16}	2.46 x 10^{-16}
		Fe(II)(OH)$_3^{-}$	8.44 x 10^{-13}	7.98 x 10^{-13}
		Fe(II)Cl^{+}	1.37 x 10^{-3}	1.34 x 10^{-3}
		Fe(II)Tartrate^{0}	3.63 x 10^{-3}	3.44 x 10^{-3}
		Fe(II)HTartrate^{+}	1.12 x 10^{-8}	1.06 x 10^{-8}
		Fe(III)OH^{2+}	4.44 x 10^{-14}	4.44 x 10^{-11}
		Fe(III)(OH)$_2^{+}$	2.55 x 10^{-9}	2.55 x 10^{-6}
		Fe(III)(OH)$_3^{0}$	2.12 x 10^{-7}	2.12 x 10^{-4}
		Fe(III)(OH)$_4^{-}$	1.77 x 10^{-9}	1.77 x 10^{-6}
		Fe(III)$_2$(OH)$_2^{4+}$	7.49 x 10^{-25}	7.48 x 10^{-19}
		Fe(III)$_3$(OH)$_4^{5+}$	6.05 x 10^{-31}	6.04 x 10^{-22}
		Fe(III)Cl^{2+}	5.24 x 10^{-14}	5.39 x 10^{-11}
		Fe(III)Cl$_2^{+}$	3.17 x 10^{-9}	3.35 x 10^{-6}
		Fe(III)Tartrate^{+}	2.24 x 10^{-11}	2.25 x 10^{-8}
		Fe(III)HTartrate^{2+}	4.47 x 10^{-14}	4.49 x 10^{-11}
		HTartrate^{-}	4.50 x 10^{-2}	4.52 x 10^{-2}
		H$_2$Tartrate^{0}	1.79 x 10^{-6}	1.80 x 10^{-6}
		NaTartrate^{-}	1.37 x 10^{-3}	1.34 x 10^{-3}
		NaHTartrate^{0}	4.35 x 10^{-11}	4.25 x 10^{-11}
		NaCl^{0}	4.86 x 10^{-2}	4.87 x 10^{-2}

S4.4.5 Modelled Fe(II)-ligand species and calculated E_H values for Naka *et al.*, (1)

Table S4.4: Modelled concentrations of Fe(II)-ligand species used by Naka *et al.*, (1) calculated using MICROQL (191).

Ligand	Species	Modelled Concentration (M)
Citrate^{3-}	Fe(II)OH^{+}	2.41 x 10^{-10}
	Fe(II)(OH)$_2$	9.38 x 10^{-18}
	Fe(II)(OH)$_3^{-}$	1.01 x 10^{-14}
	Fe(II)Cl^{+}	3.11 x 10^{-6}
	Fe(II)Citrate^{-}	4.47 x 10^{-4}
	Fe(II)$_2$(OH)$_2$Citrate$_2^{4-}$	6.78 x 10^{-6}
	Fe(II)H(Citrate)$_2^{3-}$	3.62 x 10^{-5}
	Fe(II)H$_2$Citrate^{+}	3.89 x 10^{-13}
	Fe(II)HCitrate^{0}	4.37 x 10^{-10}
	Fe(III)OH^{2+}	1.32 x 10^{-17}
	Fe(III)(OH)$_2^{+}$	2.41 x 10^{-13}

	$Fe(III)(OH)_3^0$	6.34×10^{-12}
	$Fe(III)(OH)_4^-$	1.67×10^{-14}
	$Fe(III)_2(OH)_2^{4+}$	6.66×10^{-32}
	$Fe(III)_3(OH)_4^{5+}$	5.07×10^{-42}
	$Fe(III)Cl^{2+}$	2.30×10^{-19}
	$Fe(III)Cl_2^+$	6.47×10^{-17}
	$Fe(III)Citrate^0$	1.10×10^{-11}
	$Fe(III)_2OH_2Citrate_2^{2-}$	7.23×10^{-10}
	$Fe(III)HCitrate^+$	1.29×10^{-17}
	$Fe(III)OHCitrate^+$	2.19×10^{-7}
	$HCitrate^{2-}$	4.44×10^{-3}
	$H_2Citrate^-$	1.65×10^{-5}
	$H_3Citrate^0$	1.69×10^{-9}
	$NaCitrate^{2-}$	3.11×10^{-6}
	$NaCl^0$	4.97×10^{-4}
Salicylate$^-$	$Fe(II)OH^+$	2.56×10^{-4}
	$Fe(II)(OH)_2$	1.04×10^{-11}
	$Fe(II)(OH)_3^-$	1.07×10^{-8}
	$Fe(II)Cl^+$	1.34×10^{-7}
	$Fe(II)Salicylate^+$	2.43×10^{-4}
	$Fe(II)Salicylate_2^0$	1.13×10^{-8}
	$Fe(II)HSalicylate^{2+}$	1.37×10^{-16}
	$Fe(II)_2HSalicylate^{4+}$	1.37×10^{-16}
	$Fe(III)OH^{2+}$	3.80×10^{-17}
	$Fe(III)(OH)_2^+$	6.92×10^{-13}
	$Fe(III)(OH)_3^0$	1.82×10^{-11}
	$Fe(III)(OH)_4^-$	4.79×10^{-14}
	$Fe(III)_2(OH)_2^{4+}$	5.50×10^{-31}
	$Fe(III)_3(OH)_4^{5+}$	1.20×10^{-40}
	$Fe(III)Cl^{2+}$	5.09×10^{-31}
	$Fe(III)Cl_2^+$	3.46×10^{-26}
	$Fe(III)Salicylate^{2+}$	7.37×10^{-14}
	$Fe(III)Salicylate_2^+$	3.59×10^{-10}
	$Fe(III)Salicylate_3^0$	2.20×10^{-7}
	$Fe(III)HSalicylate^{3+}$	6.57×10^{-33}
	$HSalicylate^0$	4.76×10^{-3}
	$H_2Salicylate^+$	4.54×10^{-7}
	$NaSalicylate^0$	1.34×10^{-7}
	$NaCl^0$	5.00×10^{-4}

S4.4.6 Reduction kinetics

S4.4.6.1 Modelled kinetic parameters

Table S4.5: Modelled kinetic parameters for the reduction of 2AcNB in suspensions containing Fe(II)-ligand species under varying reaction conditions.
* Biphasic kinetics observed, *k* values are provided in Table S6.
** E_H is not specified as both the partially reduced NAu-1 and the Fe(II)-ligand species have associated E_H values.

Reaction Condition	E_H	log k (h^{-1})	log k $(M^{-1}h^{-1})$
Fe(II)-ligand only			
FeOx	0.46	-2.82±0.01	-0.53±-0.005
FeCit	0.07	0.46±0.02	2.75±0.11
FeTar	0.31	0.51±0.02	2.79±0.12
FeSal	0.20	0.60±0.02	2.89±0.12
Fe(II)-ligand + 2 g/L NAu-1			
FeOx	0.46	-2.52±0.02	*
FeCit	0.07	0.26±0.03	2.58±0.26
FeTar	0.31	0.48±0.01	2.90±0.08
FeSal	0.20	0.23±0.03	2.51±0.30
FeCit			
Supernatant	0.07	0.18±0.03	2.57±0.49
+ SYn-1	0.07	0.31±0.02	2.46±0.13
+ NAu-1, 9 % dith-red	**	0.33±0.01	2.56±0.11

Table S4.6: Modelled kinetic parameters (biphasic) for the reduction of 2AcNB in suspensions containing Fe(II)-complexes under varying reaction conditions.
*Due to the rapid rate of reaction and low number of data points collected during the k_B phase of the reaction, error data is not provided.

Reaction Condition	log k_A $(M^{-1}h^{-1})$	log k_B $(M^{-1}h^{-1})$
FeOx + native NAu-1	1.56±0.05	0.39±0.44
FeCit + 91 % dith-red NAu-1	3.91±0.20	0.40*

S4.5 Mössbauer spectra

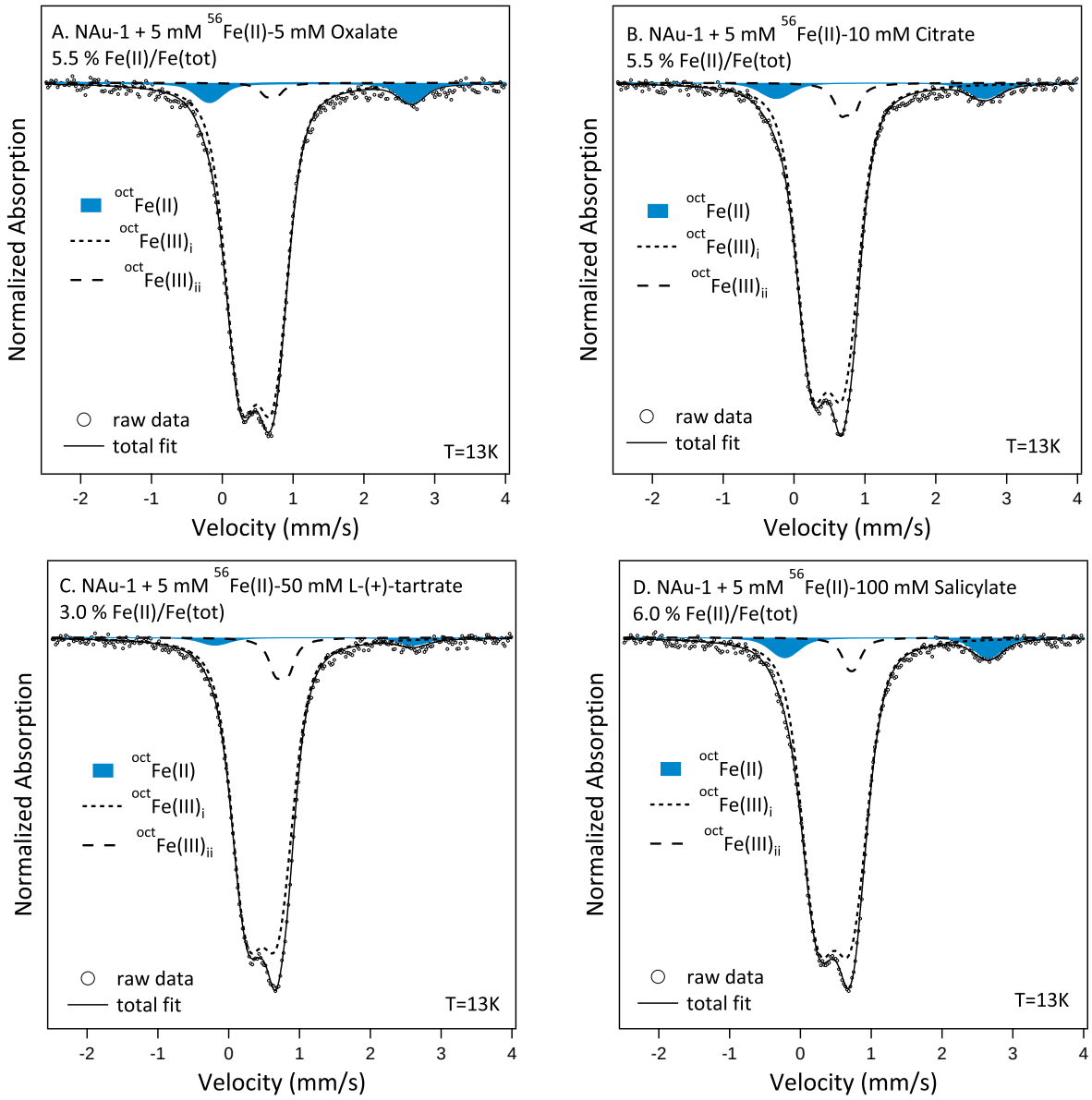

Figure S4.5: Mössbauer spectra of 5 mM ^{56}Fe(II) + (a) 5 mM oxalate, (b) 10 mM citrate, (c) 50 mM L-(+)-tartrate, and (d) 100 mM salicylate. As ^{56}Fe(II) is not Mössbauer active, only changes in the naturally abundant ^{57}Fe(II) in the clay mineral structure are visible.

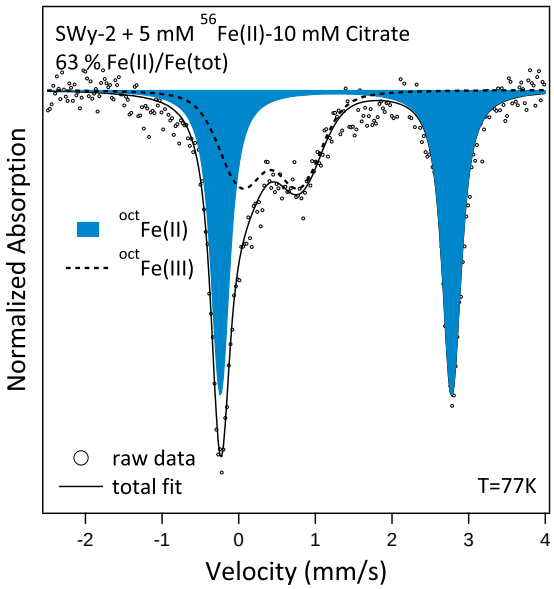

Figure S4.6: Mössbauer spectra of 5 mM ^{56}Fe(II) + 10 mM citrate + 8.0 g L–1 SWy-2.

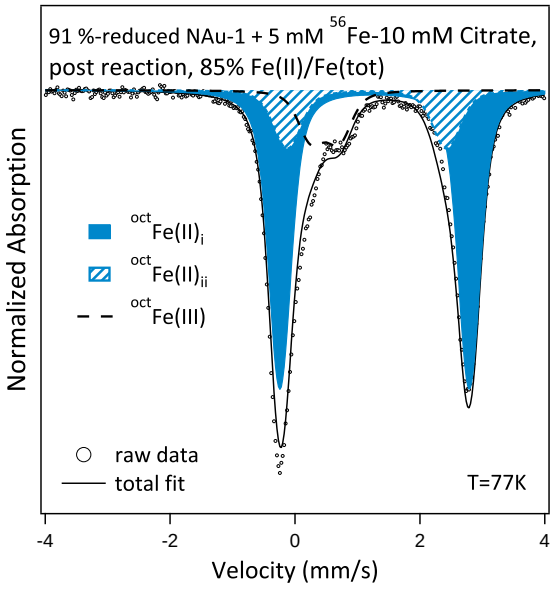

Figure S4.7: Mössbauer spectra of 91 %-reduced NAu-1 following reaction with 5 mM ^{56}Fe(II), 10 mM citrate and 2-acetylnitrobenzene. After the reaction the reduction extent has decreased to 85 % Fe(II)/Fe(tot).

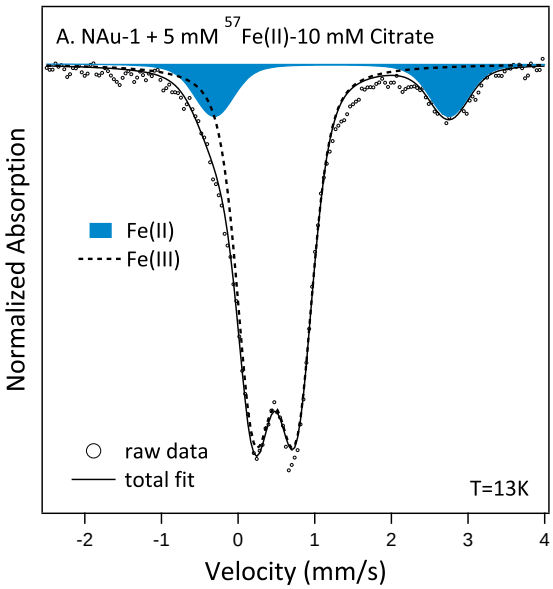

Figure S4.8: Mössbauer spectra of 5 mM ^{57}Fe(II) + 10 mM citrate + NAu-1.

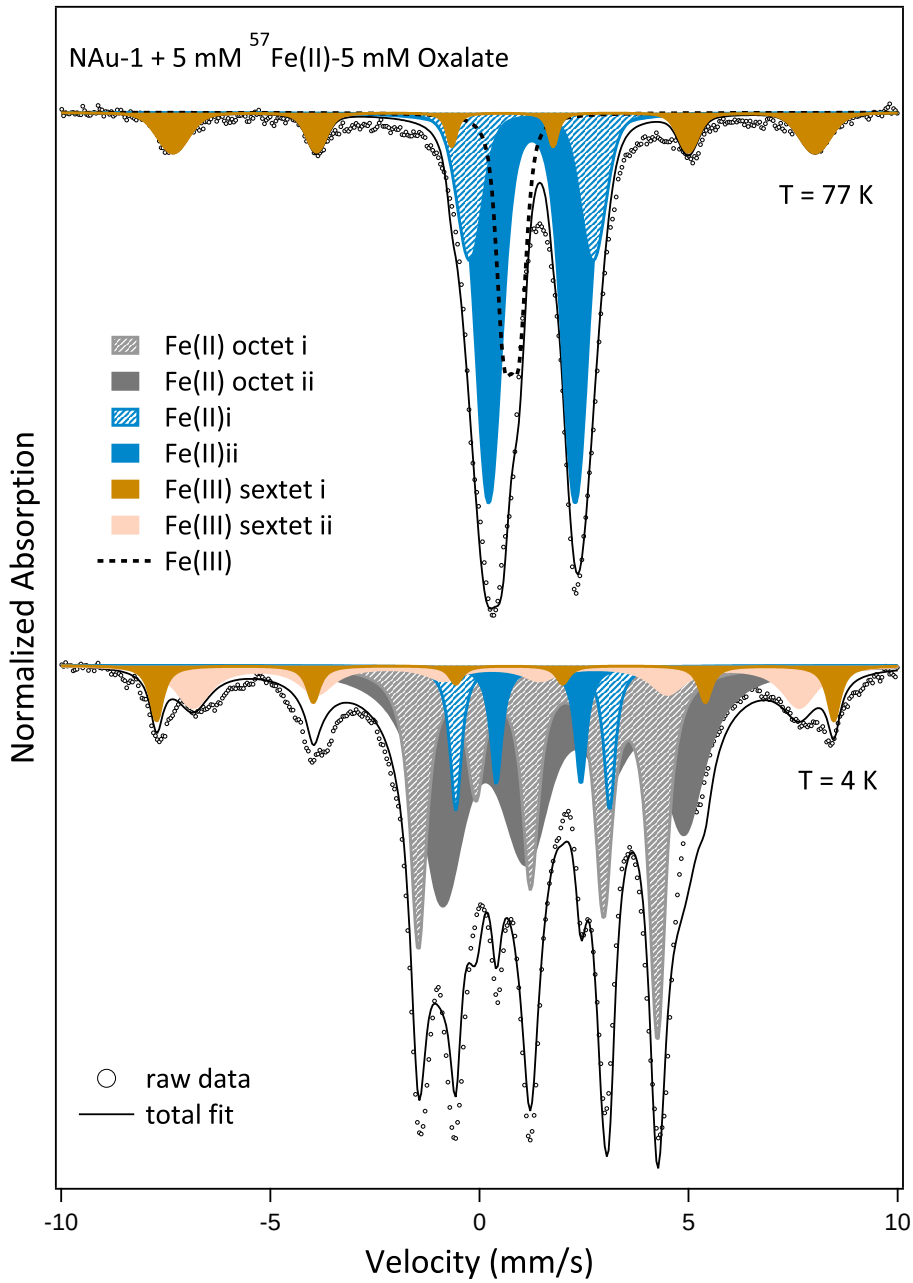

Figure S4.9: Mössbauer spectra of 5 mM ^{57}Fe(II) + 5 mM oxalate + NAu-1.

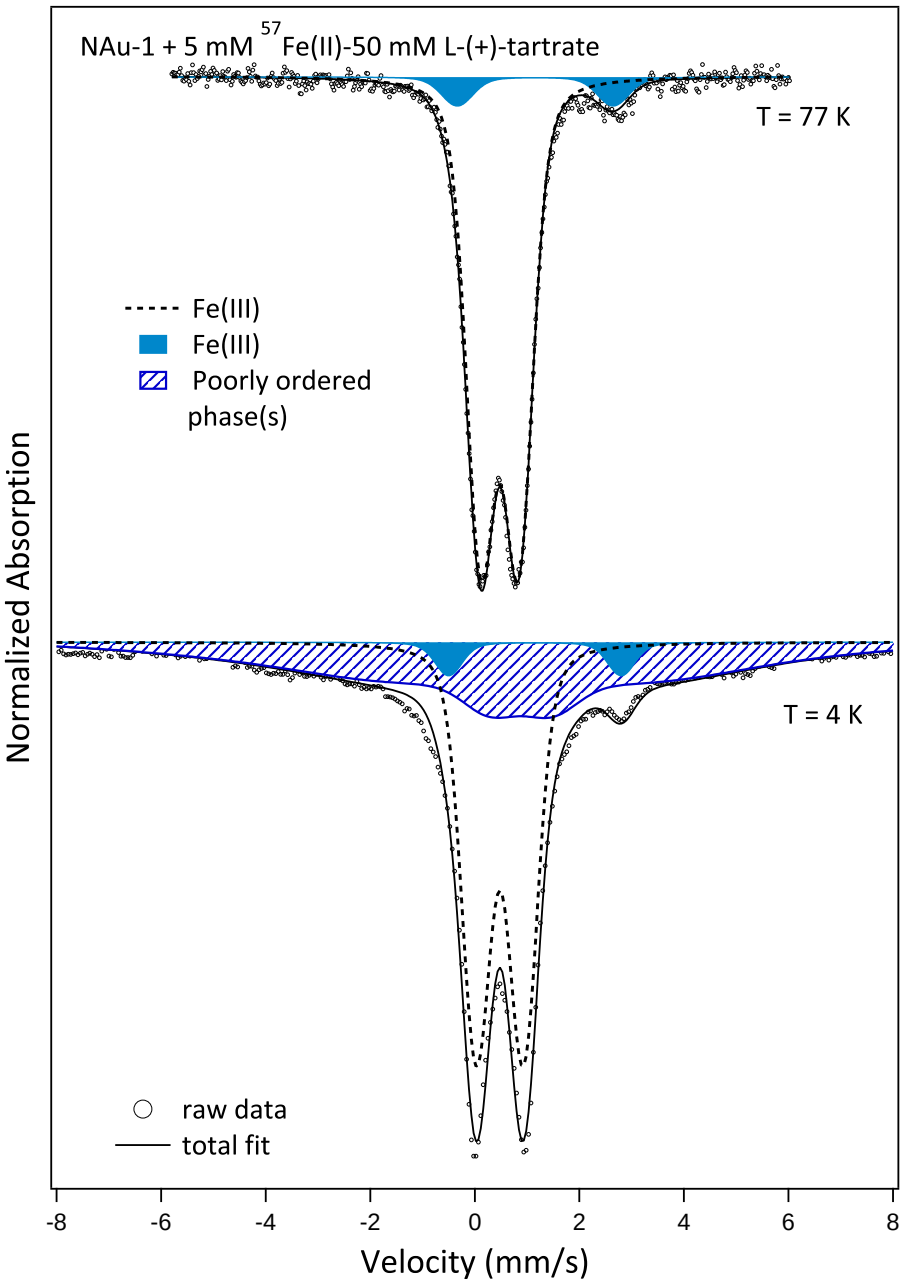

Figure S4.10: Mössbauer spectra of 5 mM ^{57}Fe(II) + 50 mM L-(+)-tartrate + NAu-1.

S4.5.1 Mössbauer fit parameters

Table S4.7: Mössbauer parameters for dithionite- and Fe(II)-reduced NAu-1, measured at 13 K or 77 K and fitted using a voigt based, fixed line width method.

Reaction Condition	χ^2	**Site**	**CS (mm/s)**	**QS (mm/s)**	**H (T)**	**Area (%)**
NAu-1 + 5 mM ^{56}Fe(II)						
+ 5 mM oxalate	0.56	oct Fe(III)i	0.48	0.49 ± 0.29		92.5 ± 0.87
		oct Fe(III)ii	0.69	0.15 ± 0.005		1.86 ± 0.65
		oct Fe(II)	1.25	2.86 ± 0.26		5.75 ± 0.62
+ 10 mM citrate	0.59	oct Fe(III)i	0.48	0.45 ± 0.29		90.0 ± 0.72
		oct Fe(III)ii	0.75	0.17 ± 0.03		4.68 ± 0.37
		oct Fe(II)	1.22	2.94 ± 0.07		5.32 ± 0.55
+ 50 mM L-(+)-tartrate	0.56	oct Fe(III)i	0.47	0.44 ± 0.01		91.51 ± 1.34
		oct Fe(III)ii	0.75	0.17 ± 0.03		5.97 ± 1.18
		oct Fe(II)	1.21	2.88 ± 0.13		2.52 ± 0.68
+ 100 mM salicylate	0.63	oct Fe(III)i	0.48	0.48 ± 0.01		90.25 ± 0.82
		oct Fe(III)ii	0.72	0.13 ± 0.04		3.59 ± 0.59
		oct Fe(II)	1.22	2.87 ± 0.06		6.20 ± 0.65
SWy-2 + 5 mM ^{56}Fe(II)	0.59	oct Fe(III)	0.41	0.76 ± 0.05		36.84 ± 2.48
+ 10 mM citrate		oct Fe(II)	1.27	3.01 ± 0.01		63.16 ± 2.46
91% dithionite-reduced	3.32	oct Fe(III)	0.48	0.57 ± 0.02		13.51 ± 0.33
NAu-1 + 5 mM ^{56}Fe(II)		oct Fe(II)i	1.27	3.03 ± 0.01		70.97 ± 5.06
+ 10 mM citrate		oct Fe(II)ii	1.15	2.55 ± 0.10		16.54 ± 4.05
NAu-1 + 5 mM ^{57}Fe(II)						
+ 5 mM oxalate	9.2	Fe(III)	0.76	0.38 ± 0.02		16.57 ± 0.04
		Fe(II)i	1.26	2.07 ± 0.05		51.79 ± 0.03
		Fe(II)ii	1.24	2.95 ± 0.05		18.97 ± 0.02
		Fe(III) sextet 1	0.45	-0.1 ± 0.2	47.6	12.68 ± 0.03
+ 50 mM L-(+)-tartrate	0.86	Fe(III)	0.48	0.75 ± 0.04		93.20 ± 0.02
		Fe(II)	1.16	2.97 ± 0.06		6.80 ± 0.02

Table S4.8: Mössbauer parameters for ^{57}Fe(II) + NAu-1, measured at 4 K using a variable line width fitting method (Full Static Hamitonian).

	CS (mm/s)	**H (T)**	$\mathbf{e^2qQ/2}$ **(mm/s)**	η **(-)**	θ **(-)**	**Area(%)**
5 mM ^{57}Fe(II) + NAu-1 + 50 mM L-(+)-tartrate						
Fe(III) sextet$_1$	0.73	22.6	-0.15	0	0	44.2
Fe(III) doublet	0.48	-	0.91	0	0	51.8
Fe(II) doublet	1.15	-	3.30	0	0	4.0
5 mM ^{57}Fe(II) + NAu-1 + 5 mM oxalate						
Fe(III) sextet$_1$	0.55	50.2	-0.34	0	0	4.6
Fe(III) sextet$_2$	0.35	44.9	0.10	0	0	9.4
Fe(II) doublet$_1$	1.28	-	-3.68	0	0	5.4
Fe(II) doublet$_2$	1.42	-	2.02	0	0	4.4
Collapsed Fe(II) octet$_1$	1.56	15.1	-2.42	0.02	90	43.7
Collapsed Fe(II) octet$_2$	1.75	10.8	3.50	0.03	90	32.6

S4.6 Reduction kinetics

S4.6.1 Modelled kinetic parameters

Table S4.9: Modelled kinetic parameters for the reduction of 2AcNB in suspensions containing Fe(II)-ligand species under varying reaction conditions.
* Biphasic kinetics observed, *k* values are provided in Table S6.
** E_H is not specified as both the partially reduced NAu-1 and the Fe(II)-ligand species have associated E_H values.

Reaction Condition	E_H	log k (h^{-1})	log k $(M^{-1}h^{-1})$
		Fe(II)-ligand only	
FeOx	0.46	-2.82±0.01	-0.53±-0.005
FeCit	0.07	0.46±0.02	2.75±0.11
FeTar	0.31	0.51±0.02	2.79±0.12
FeSal	0.20	0.60±0.02	2.89±0.12
		Fe(II)-ligand + 2 g/L NAu-1	
FeOx	0.46	-2.52±0.02	*
FeCit	0.07	0.26±0.03	2.58±0.26
FeTar	0.31	0.48±0.01	2.90±0.08
FeSal	0.20	0.23±0.03	2.51±0.30
		FeCit	
Supernatant	0.07	0.18±0.03	2.57±0.49
+ SYn-1	0.07	0.31±0.02	2.46±0.13
+ NAu-1, 9 % dith-red	**	0.33±0.01	2.56±0.11

Table S4.10: Modelled kinetic parameters (biphasic) for the reduction of 2AcNB in suspensions containing Fe(II)-complexes under varying reaction conditions.
*Due to the rapid rate of reaction and low number of data points collected during the k_B phase of the reaction, error data is not provided.

Reaction Condition	log k_A $(M^{-1}h^{-1})$	log k_B $(M^{-1}h^{-1})$
FeOx + native NAu-1	1.56±0.05	0.39±0.44
FeCit + 91 % dith-red NAu-1	3.91±0.20	0.40*

S4.6.2 Kinetic plots

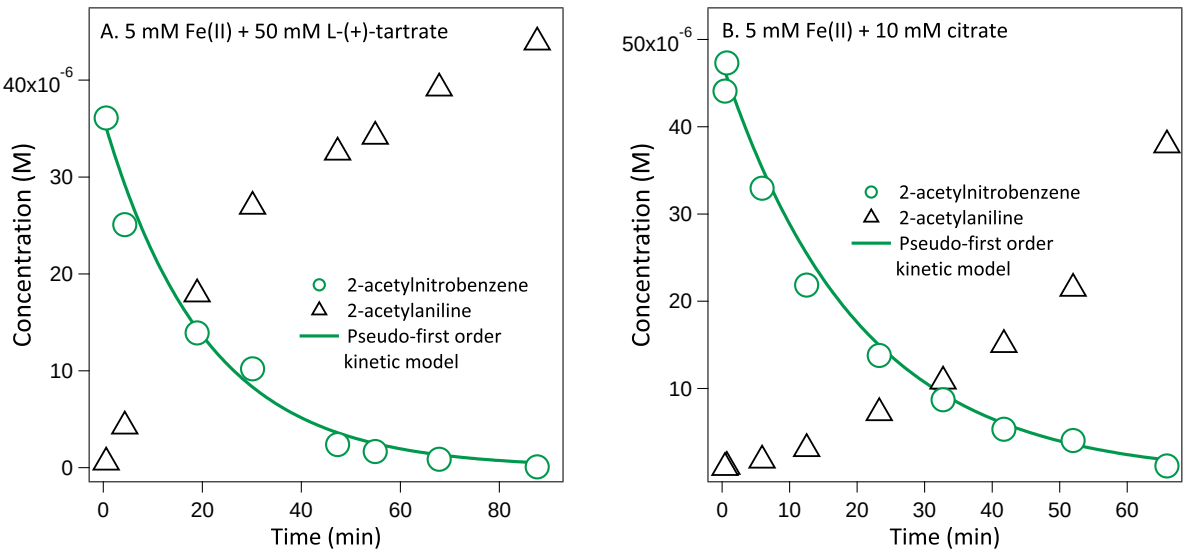

Figure S4.11: Typical reduction kinetics of 2-acetylnitrobenzene (blue circles) to 2-acetylaniline (black triangles) in suspensions containing 5 mM Fe(II) and (a) 50 mM L-(+)-tartrate, and (b) 10 mM citrate.

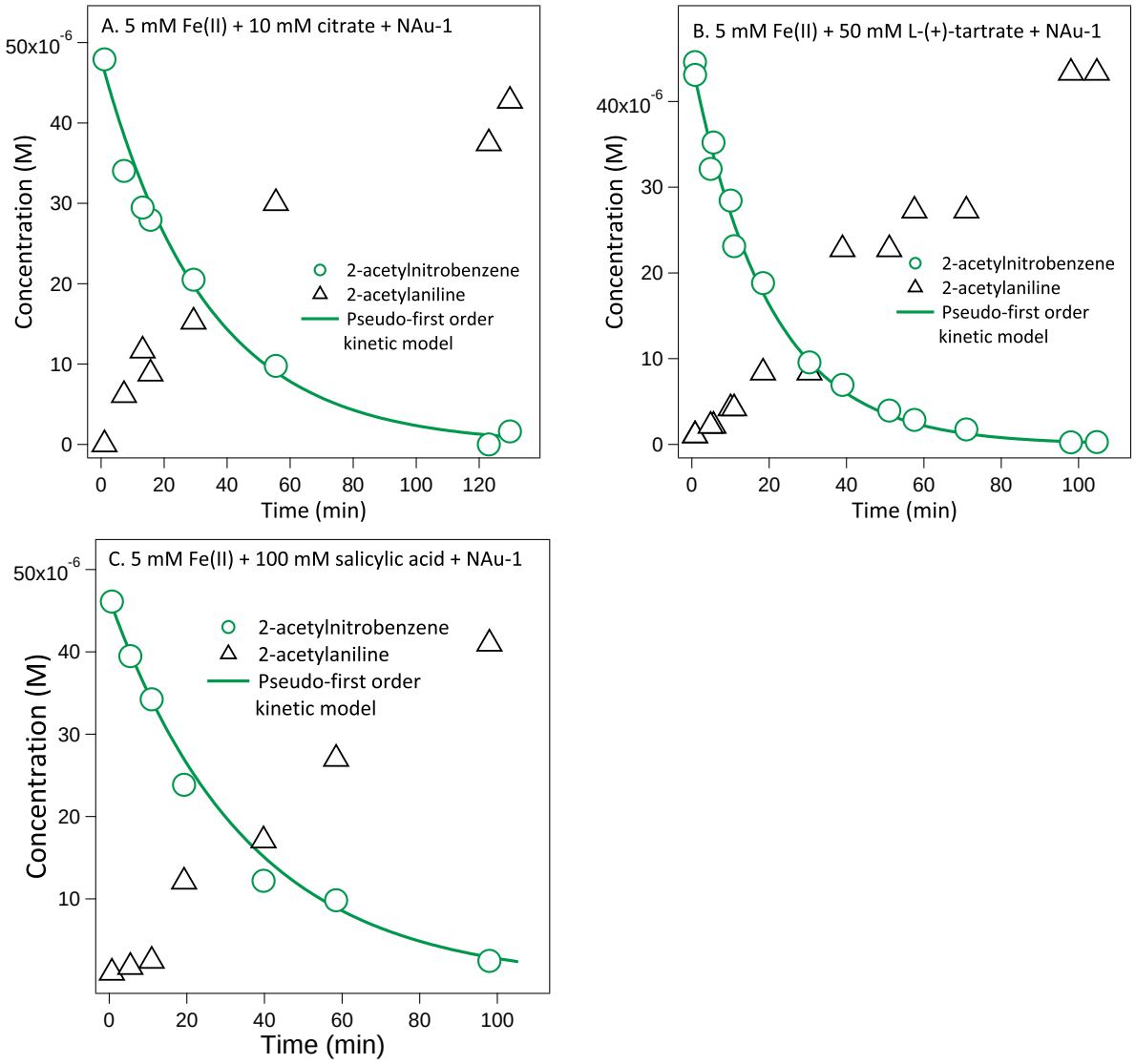

Figure S4.12: Typical reduction kinetics of 2-acetylnitrobenzene (blue circles) to 2-acetylaniline (black triangles) in suspensions containing 5 mM Fe(II), 2 g/L native NAu-1 and (a) 10 mM citrate, (b) 50 mM L-(+)-tartrate, and (c) 100 mM salicylate.

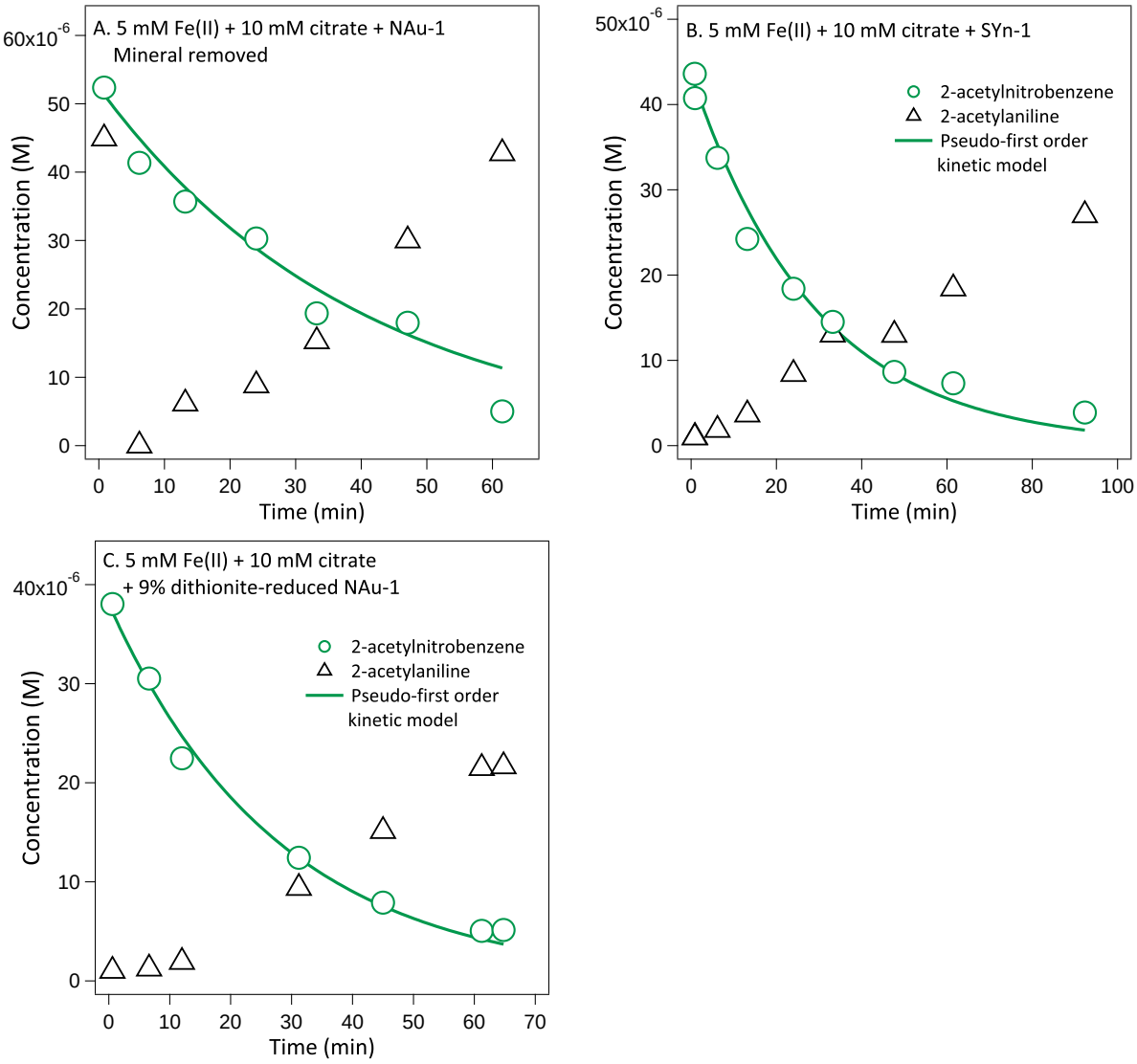

Figure S4.13: Typical reduction kinetics of 2-acetylnitrobenzene (blue circles) to 2-acetylaniline (black triangles) in suspensions containing 5 mM Fe(II), 10 mM citrate and (a) NAu-1, following removal of the mineral by centrifugation, (b) 2 g/L Fe-free montmorillonite SYn-1, and (c) 2 g/L NAu-1, 9 % dithionite-reduced.

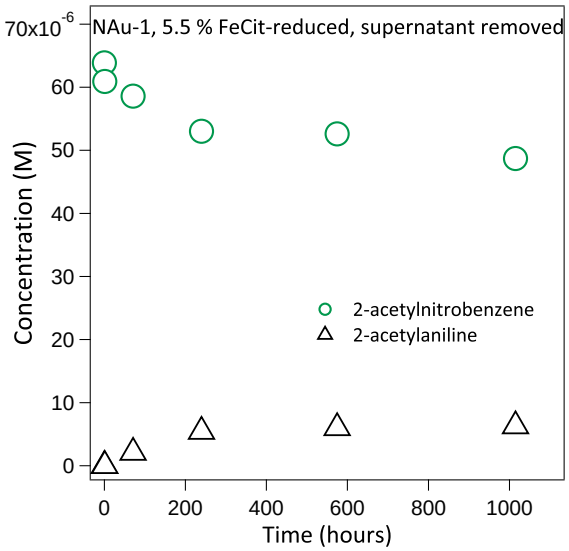

Figure S4.14: Typical reduction kinetics of 2-acetylnitrobenzene (blue circles) to 2-acetylaniline (black triangles) in suspensions containing NAu-1 that had been reduced in a suspension containing 5 mM Fe(II) + 10 mM citrate, removed by centrifugation and resuspended in fresh MOPS buffer solution before the addition of 2AcNB.

Chapter 5
Assessing the effect of electron transfer mediators on the reactivity of Fe-bearing clay minerals

5.1 Introduction

In the absence of oxygen, reductive transformation a major degradation pathway for contaminants (206). In complex natural environments, a variety of redox active microbes, minerals and organic phases can reductively transform a range of organic contaminants (193, 207). Fe-bearing clay minerals are of particular interest as they are capable of undergoing redox cycling without being subject to reductive dissolution as is the case for other Fe-containing minerals such as Fe-oxides (38, 59, 84). Ferrous iron is known to facilitate the reduction of contaminants including nitroaromatic compounds (20, 21, 50), halogenated hydrocarbons (48), pesticides (49, 161), nitrate (45) radionuclides (24) and hexavalent chromium (23).

To date, many studies have documented the influence of individual redox active components on contaminant degradation. However, in complex biogeochemical environments, several redox active components will be present, thus it is important to consider the reactivity of all coexisting redox active species to accurately assess likely degradation rates of contaminants in natural environments. For example, we and others have recently shown that the reactivity of Fe-bearing clay minerals towards nitroaromatic compounds (NACs) may be significantly influenced by the presence of aqueous Fe(II) and/or organically complexed Fe(II) depending on solution pH and speciation, which both affect the reduction potential of of the resulting Fe(II)-complexes. It is therefore important to consider the reactivity of all coexisting redox active species to accurately assess likely degradation rates of contaminants in natural environments.

Organic electron shuttling compounds are also ubiquitously present in natural environments and could affect the reactivity of clay mineral Fe (206). These may undergo rapid redox cycling and act as electron transfer mediators (ETMs) between a bulk electron donor and acceptor (e.g. Fe-bearing mineral and contaminant) are also ubiquitously present in natural environments (206). ETMs are known to increase the rates of redox processes by lowering the activation energy required for electron transfer (140, 208) and their enhancement of both microbial iron reduction and contaminant reduction has been widely documented (138, 139, 154, 208, 209). For example, ETMs facilitate NAC reduction by sulfide species (201) and enhance the rate of reduction of carbon tetrachloride by zero-valent iron (ZVI) (210) and thiol reductants (211). However, currently knowledge concerning the influence of ETMs on abiotic contaminant reduction is limited and particularly little is known about their influence on the redox reactivity

of Fe-bearing mineral phases despite work showing that quinone-containing ETMs can reduce Fe-oxide species (212).

Common naturally occurring ETMs include quinone functional groups present in humic substances (149, 156, 213, 214) and microbially produced quinone and flavin containing compounds (143, 155, 215). However, it is currently not known how the presence of ETMs may influence the reactivity of Fe-bearing clay minerals towards organic contaminants.

In this chapter, we aim to determine how the reactivity of Fe-bearing clay minerals towards NACs is affected by the presence of ETMs. To evaluate the system's reactivity we used quinones and flavins as model compounds representative of naturally occurring compounds. For reference, structures of the ETMs used in this study are provided in Figure S5.7. Specifically we aim to (i) determine the influence of quinones and flavins on the reactivity of dithionite-reduced NAu-1, using 2-acetylnitrobenzene (2AcNB) as a reactive probe molecule, and (ii) determine the influence of quinone and flavin ETMs on the reactivity of Fe(II)-reduced NAu-1.

5.2 Materials and methods

5.2.1 Mineral preparation

An inventory of chemicals and stock solutions used is provided in the Supporting Information (S5.1). Nontronite NAu-1 was purchased from the Source Clays Repository (http://www.clays.org) and the 0.1-0.5 μm size fraction was obtained, homoionized with Na^+ and purified as described in Chapter 3 (168).

5.2.2 Kinetic batch experiments

As described in previous chapters, all manipulation of oxygen sensitive solutions and reactors was undertaken in an anaerobic glovebox under an N_2 atmosphere ($\leq$1 ppm O_2). Aqueous Fe(II) stock solution was prepared by dissolving metallic Fe in HCl. Stocks of ETM solutions were prepared in 10 mM MOPS (3-(N-morpholino)propanesulfonic acid) pH buffer at pH 7.5. Due to the limited solubility of juglone and riboflavin in water, an ethanolic juglone stock was initially prepared and riboflavin was initially dissolved in dilute acetic acid before being diluted into the MOPS solution. Anthraquinone-2,6-disulfonate (AQDS) and 5-hydroxy-1,4-naphthalenedione (juglone) were individually added to reactors at a concentration of 30 μM whereas the three flavin compounds flavin mononucleotide (FMN), riboflavin and flavin adenine dinucleotide (FAD) were added together to a total concentration of 30 μM at a ratio of 49 %, 34 % and 17 % respectively. This ratio was chosen according to the flavin concentrations measured in the supernatant of *Shewanella oneidensis* MR-1 cultures (143). FMN and riboflavin are produced extracellularly by MR-1 whereas FAD is thought to be found in cell membranes but may be released into solution following cell lysis (143).

Batch reactors were created by mixing 10 mM MOPS pH buffer, 50 mM NaCl ionic strength buffer, shuttle(s) of interest, and 3 mM aqueous Fe(II) or 2.0 g L^{-1} NAu-1 suspension, either in its native (fully oxidised) form or 19 % or 91 %-dithionite reduced. Mineral Fe reduction

was achieved using sodium dithionite as previously described (63). The pH of the batch reactors was adjusted to 7.5 $\pm$ 0.1 using 1 M NaOH or 1 M HCl and batches were allowed to equilibrate for 24 hours prior to the initiation kinetic experiments. Aqueous Fe(II) concentration was measured using the 1,10-phenanthroline method described previously (170). The extent of reduction and concentration of the mineral suspension was checked using both Mössbauer spectroscopy and independently, HF digestion followed by the 1,10-phenanthroline assay (169).

Kinetic experiments were performed as before by spiking the batch reactors with an initial concentration of $\sim$50 μM methanolic 2-acetylnitrobenzene (2AcNB) stock solution. Samples of 500 μL were taken as a time series and filtered using 0.22 μm nylon filter into 2 mL HPLC vials loaded with 500 μL 50 mM hexacyanoferrate to quench the reaction by oxidising remaining ETMs. Samples were stored in the dark at 4 °C until HPLC analysis.

5.2.3 Analytical Methods

Again, we used reverse-phase HPLC to analyse the concentration of 2AcNB and 2-acetylaniline, and Mössbauer spectroscopy to determine the structural coordination and reduction extent of NAu-1 and precipitate phases (Chapter 3).

5.2.4 Kinetic modelling

Reduction rate constants for the transformation of 2AcNB in Fe(II)-ligand and Fe(II)-ligand/NAu-1 reactors were modelled according to a pseudo-first order kinetic rate law (Equation 3.3. The pseudo-first rate constant ($\mathrm{k_{obs}}$, $\mathrm{h^{-1}}$) that can be converted to an equivalent second order rate constant ($\mathrm{k_{2nd}}$, $\mathrm{M^{-1}h^{-1}}$) using the measured reactive Fe(II) species concentration [Fe(II), M] (Equation 5.1).

$$\mathrm{k_{2nd}} = \frac{\mathrm{k_{obs}}}{[\mathrm{Fe(II)}]} \tag{5.1}$$

For reactors containing 20 % or 91 %-reduced NAu-1, a pseudo-first order rate law did not provide a good fit for the data. In this case, a biphasic reduction model was used as proposed by Neumann *et al.,* 2008 (20) (Equation 3.1) as described in Chapter 3.

5.3 Results and Discussion

5.3.1 The effect of ETMs on the reactivity of dithionite-reduced NAu-1

To assess the reactivity of Fe-bearing clay minerals with organic contaminants in complex biogeochemical environments, we initially investigated whether the presence of electron transfer mediators (ETMs) could enhance the reactivity of dithionite-reduced NAu-1 by electron shuttling from clay mineral Fe(II) to a probe contaminant, 2-actylnitrobenzene (2AcNB). We chose anthraquinone-2,6-disulfonate (AQDS) and 5-hydroxy-1,4-naphthalenedione (juglone)

as quinone containing ETMs, as they have been previously used as analogues for quinone moities that are representative of natural humic substances (138). We also selected a mixture of flavin compounds, flavin mononucleotide (FMN), riboflavin and flavin adenine diphosphate (FAD). Flavins and other electron shuttling compounds are secreted by iron-reducing bacteria to enhance their ability to access solid-bound Fe(III) (215–217). *Shewanella oneidensis* species MR-1 has been the focus of recent research (155) and we selected the flavin mixture used in our experiments to match the ratio of what is produced by MR-1 (49% FMN, 34% riboflavin, 17% FAD) (143).

We investigated the effect of AQDS, juglone and flavins on the reactivity of fully (91 %) dithionite-reduced NAu-1 and AQDS only on the reactivity of partially (19 %) dithionite-reduced NAu-1 by comparison to dithionite-reduced NAu-1 that was explored in Chapter 3.

Typical reduction kinetics of 2AcNB in the presence of quinone and flavin containing ETMs and 91 % dithionite-reduced NAu-1 are shown in Figure 5.1. In the presence of the quinone containing ETMs AQDS and juglone and 91 % dithionite-reduced NAu-1, complete transformation of 2AcNB occurred within 24 hours, approximately the same time-scale as that observed for 91 % dithionite-reduced NAu-1 alone (Figure 5.1A).

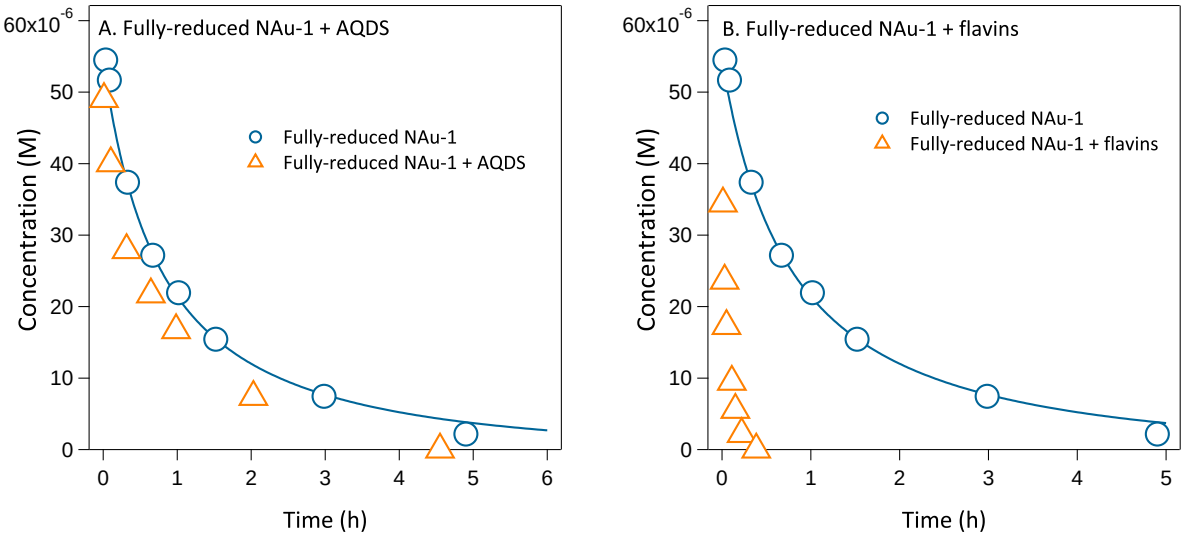

Figure 5.1: Typical reduction kinetics of 2AcNB in the presence of (a) 91 % dithionite-reduced NAu-1 and 30 μM AQDS, and (b) 91 % dithionite-reduced NAu-1 and 14.7 μM FMN, 10.2 μM riboflavin and 5.1 μM FAD. For comparison, data for 91 % dithionite-reduced NAu-1 alone is also shown.

As previously observed, the reduction of 2AcNB by 91 % dithionite-reduced NAu-1 alone was best modelled according to a biphasic, two-site kinetic model, attributed to the presence of two distinct mineral Fe(II) sites with different reactivities (20, 157). However, our kinetic modelling did not provide a clear indication of the best fit for the reaction kinetics in the presence of AQDS and juglone and both pseudo-first order (Equation 3.3) and biphasic kinetic models (Equation 3.1)) resulted in acceptable levels of error (Table 5.1), thus no kinetic fit is included in Figure 5.1. Therefore, it is unclear whether the clay mineral alone drives the reactivity towards the NACs or whether the quinone moieties act as shuttling compounds

between clay mineral Fe and the NAC. However, use of the two-site model (Equation 5.2), we can compare the resulting second-order rate constants to those of dithionite-reduced NAu-1 alone (Table 5.1). We found the presence of quinone-containing ETMs did not significantly affect the degradation rate of 2AcNB in the presence of fully-reduced NAu-1.

Table 5.1: Kinetic parameters for 2AcNB reduction in suspensions of dithionite-reduced NAu-1 in the presence and absence of AQDS, juglone and flavins. Reported values resulted from fitting measured data using Equation 3.1.
[a]Due to the rapid rate of reaction and low number of data points collected during the k_B phase of the reaction, error data is not provided.

	log k_A ($M^{-1}h^{-1}$)	**log k_B ($M^{-1}h^{-1}$)**
91 % dithionite-reduced NAu-1 alone	3.53±0.07	-0.47[a]
91 % dithionite-reduced NAu-1 + AQDS	3.46±0.16	-0.25[a]
91 % dithionite-reduced NAu-1 + juglone	3.60±0.04	-0.28[a]
91 % dithionite-reduced NAu-1 + flavins	4.78±0.05	-0.19[a]
19 % dithionite-reduced NAu-1 + AQDS	3.72±0.06	-0.38[a]
30 % dithionite-reduced NAu-1 alone	3.78±0.06	-0.16[a]

In contrast, in suspensions of the mixture of flavin containing ETMs (riboflavin, FMN and FAD) and 91 %-reduced NAu-1 we observed extremely rapid transformation of 2AcNB to 2-actylaniline within 30 minutes (Figure 5.1B), substantially quicker than what we observed 91 %-reduced NAu-1 alone (24 hours).

Again, this data set could equally well be fit with either a pseudo-first order or biphasic kinetic fit. As the rapid rate of degradation of 2AcNB suggests that the reaction was driven by the shuttling mechanism of the flavins, it is probable that a pseudo-first order, one site kinetic fit is most appropriate. However, it is equally possible that the two reactive sites in the clay mineral structure which lead to biphasic kinetics are both active in reducing the flavin compounds and this two-site regeneration could be reflected in the bulk 2AcNB reduction kinetics..

Although the flavin species generally have a more negative reduction potential than the quinone species, depending on their speciation (Table S5.7) (5, 211), it is unclear why they facilitate such a rapid degradation of 2AcNB in the presence of fully-reduced NAu-1.

While Shi *et al.,* initially found that the presence of flavin moities enhanced electron transfer rates to ferrihydrite and lepidocrocite more than AQDS (218), a later study concerning the dissolution of goethite and haematite indicated that the presence of AQDS led to a higher reaction rate than the presence of FMN (219). Consistent with these findings, work by Bae and Lee on the reduction of lepidocrocite in the presence of *Shewanella putrefaciens* CN32 with

quinone and flavin containing ETMs also found that the quinone moities generally provided the greatest enhancement in reaction rate (220). Similarly, a study investigating U(VI) reduction by *Shewanella putrefaciens* was more greatly enhanced by anthraquinone-2-sulfonate than by riboflavin.

However, these results are not necessarily applicable to real world systems, where the maximum reduction extent of nontronites would not be expected to exceed 40 % (65). Therefore, we also investigated the reduction kinetics of 2AcNB in the presence of 19 %-dithionite-reduced NAu-1 and AQDS. It is also approximately the reduction extent where we identified fundamental changes occurring within the mineral structure, as discussed in Chapter 3.

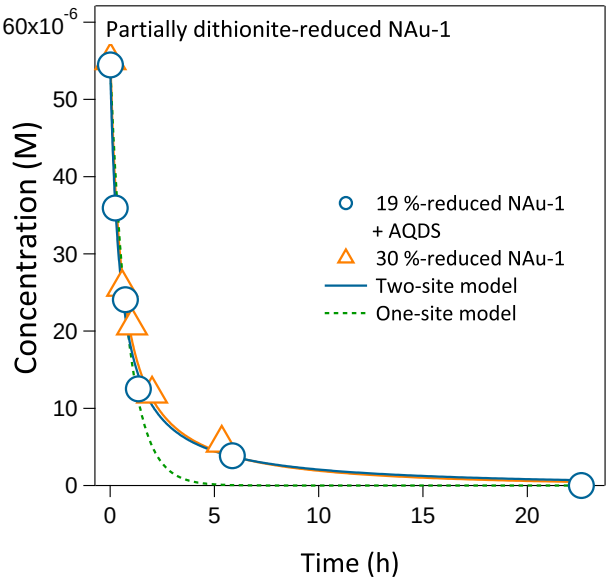

Figure 5.2: Typical reduction kinetics of 2AcNB in suspensions containing (blue circles) 19 % dithionite-reduced NAu-1 and 30 μM AQDS, and (orange triangles) 30 % dithionite-reduced NAu-1 alone. Solid lines represent the modelled biphasic reduction kinetics with the green dashed line showing a pseudo-first order fit for comparison

Reduction of 2AcNB in suspensions of partially dithionite-reduced NAu-1, with and without AQDS, was complete within 24 hours and exhibited distinctly biphasic transformation kinetics (Figure 5.2).

Our kinetic modelling showed that the kinetic rate constants (Table 5.1) for 19 % dithionite-reduced NAu-1 with AQDS are the same (within error) as for 30 % dithionite-reduced NAu-1 alone. We therefore suggest that the presence of AQDS does not make a significant contribution to the rate or kinetics of the reaction of reduced NAu-1 with 2AcNB. However, we do not have kinetic data for the reaction of 19 % dithionite-reduced NAu-1 alone to confirm this conclusion. It is possible that at this lower reduction extent, the reaction with NAu-1 alone would proceed more slowly and that the AQDS indeed enhanced the rate of 2AcNB reduction.

As AQDS/juglone did not significantly enhanced 2AcNB reduction rates by fully- or partially dithionite-reduced NAu-1, we propose that clay mineral Fe(II) is the rate determining species in our system and that it is unlikely that NOM/microbially-associated quinone moities will influence Fe-bearing clay mineral reactivity in real-world environments. In contrast, other

ETMs such as flavin-containing compounds may significantly increase the rate of NAC reduction by clay mineral Fe(II).

5.3.2 NAC reduction in the presence of native NAu-1, ETMs and aqueous Fe(II)

Our experiments with dithionite-reduced NAu-1 provide intriguing results that flavins efficiently shuttle electrons from clay mineral Fe(II) to NACs, whereas quinones largely did not affect NAC reduction by NAu-1. However, aqueous Fe(II) is the more relevant naturally occurring abiotic reductant for clay mineral Fe and we therefore investigated 2AcNB reduction in the presence of native NAu-1 (containing only structural Fe(III)), ETMs and aqueous Fe(II), as an example of a naturally occurring abiotic reductant.

Under our experimental conditions (3 mM $Fe(II)_{(aq)}$, pH 7.5, 2 g/L NAu-1), we measured a reduction extent of 5.8 % Fe(II)/Fe(tot) ratio in NAu-1 after 24 hours reaction with aqueous Fe(II) in the absence of any ETM compounds (Figure S5.7) and the same, or slightly greater reduction extents in the presence of the ETMs (5.8 % for juglone, 6.8 % for AQDS and 7.0 % for the flavin mixture, Figure S5.7, Table S5.2). Because we did not measure a difference in the amount of sorbed Fe(II) in the presence or absence of ETMs, we suggest that the increase in reduction extent is not statistically significant as the general uncertainty of Fe(II)/Fe(total) measurements from Mössbauer spectra is approximately 2 - 4 % (221).

As discussed in previous chapters, the reduction of clay mineral Fe(III) by aqueous Fe(II) also results in the formation of a solid Fe oxidation product. In our previous reactors containing only aqueous Fe(II) and NAu-1, Mössbauer spectroscopy indicated that this oxidation product contains a mixed valent Fe(II)-Fe(III) phase and we proposed that it contributes to the reactivity of the Fe(II)-clay mineral system towards NACs. Similarly to our previous study, we used Mössbauer spectroscopy in combination with Fe(II) enriched in the ^{57}Fe isotope, to determine if the nature of the Fe oxidation product changed due to the presence of AQDS (Figure S5.6). Before the addition of the NAC, the oxidation product in the presence and absence of AQDS contained the same ratio of Fe(II)/Fe(tot). However, in the presence of AQDS, we observed a shift of 10 % in the distribution of Fe(II) from the magnetically ordered octet phase to a doublet. This suggests that the presence of ETMs may alter the speciation and therefore the reactivity of Fe oxidation products formed due to interactions between aqueous Fe(II) and Fe-bearing minerals.

Indeed, 2AcNB transformation in the presence of ETMs was complete within 150 hours rather than 1000 hours as observed for Fe(II)-reduced NAu-1 alone (Figure 5.3, Table 5.2. However, 2AcNB reduction kinetics in the presence of ETMs were best fit according to a pseudo-first order rate law (Equation 3.3), in contrast to reactors containing only Fe(II) and NAu-1, where we observed typical biphasic reduction kinetics. Although, the order of addition of the ETM compound and the aqueous Fe(II) to the NAu-1 did not have a significant effect, our results are inconclusive whether the presence of ETMs or the difference in oxidation product was responsible for the observed difference in reactivity.

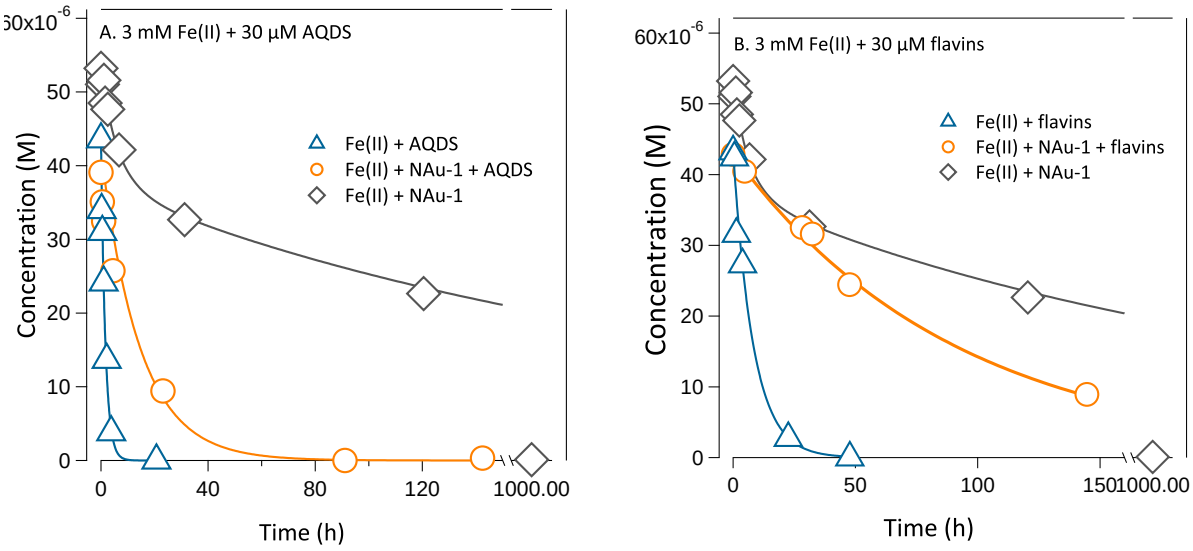

Figure 5.3: Typical reduction kinetics of 2AcNB in the presence of (a) 3 mM Fe(II) and AQDS, and (b) 3 mM Fe(II) and flavins, in the presence and absence of NAu-1. For comparison, data for 2AcNB reduction by 3.5 mM Fe(II) + NAu-1 is also shown.

To investigate the large differences in the reaction rates and kinetics we observed in the presence and absence of ETMs, we also examined the reactivity of aqueous Fe(II) and ETMs in the absence of mineral phases. It has been widely shown that aqueous Fe(II) alone does not show any reactivity towards NACs (16, 79, 173) and we also did not observe any transformation of 2AcNB in our control reactors containing only aqueous Fe(II) or ETMs in their oxidised form (Figure S5.4). In our control reactors containing ETMs that had been reduced by 91 % dithionite-reduced NAu-1 (removed before NAC addition), we observed ∼10 % transformation of 2AcNB (Figure S5.3). Assuming that all 30 μM of ETM had been reduced and transferred $2e^-$, the reduced ETMs could facilitate a 10 % transformation of the 50 μM NAC spike. However, as no bulk reductant was present to regenerate the ETM's reduced form the reduction stalled after ∼5 hours, once the maximum available reduction equivalents in the ETMs were oxidised.

In contrast, 2AcNB was transformed completely in $<$ 24 hours when quinone ETMs were added to reactors containing 3 mM aqueous Fe(II) (Figure 5.3). As six electrons are required to completely transform 2AcNB into 2-acetylaniline, 300 μM of reductant is required to react with the 50 μM 2AcNB in our reactors. Because, as the shuttle is initially present in its oxidised form and at a concentration of 30 μM, the aqueous Fe(II) must be acting as the bulk electron donor.

The reduction kinetics in the presence of Fe(II) and ETMs are of the same time scale and follow the same pseudo-first order rate law as also Fe(II), ETM and native NAu-1 rather than the slow, biphasic transformation observed for Fe(II)-reduced NAu-1 in the absence of an ETM. This suggests a common reactive species in both experiments and we suggest that once an ETM is present, the reduction of 2AcNB is facilitated by electron transfer from Fe(II) rather than from clay mineral Fe(II).

	- NAu-1	+ NAu-1
	log k $(\mathrm{M^{-1}h^{-1}})$	**log k** $(\mathrm{M^{-1}h^{-1}})$
AQDS	2.29±0.32	1.35±0.06
Juglone	2.15±0.24	1.42±0.04
Flavins	1.59±0.12	0.93±0.04

Table 5.2: Modelled kinetic parameters for 2AcNB reduction in suspensions of 3 mM Fe(II), 30 μM ETMs in the presence and absence of NAu-1.

Surprisingly, the ETM-facilitated reaction proceeds more slowly in the presence of the native NAu-1, compared to when it is absent. Even when the rate constants are correct for the removal of Fe(II) from the aqueous phase, due to interactions with NAu-1 (sorption/electron transfer/precipitate formation) we measured a decrease in the second-order log k value of between 0.6 - 1 order of magnitude (Table 5.2). It is unclear why the clay mineral has an inhibiting effect on the reactivity of the ETMs, although it is possible that sorption of the quinone species to the clay mineral is responsible.

Interestingly, we also observed the formation of a rust-coloured precipitate, we suspect is an iron-(oxyhydr)oxide phase, in the reactors containing quinone ETMs following reaction with the NAC. As the precipitate only formed after the NAC was added, it is plausible that it forms as a result of the oxidation of aqueous Fe(II) by the AQDS/juglone as it shuttles electrons from the bulk donor, Fe(II), to the NAC.

We used Mössbauer spectroscopy in combination with aqueous Fe(II) enriched in ^{57}Fe to characterise the precipitate. At a temperature of 4 K, both spectra (Figure 5.4) comprised a sextet characteristic of an iron (oxyhydr)oxide phase. Mössbauer parameters (Table S5.3) indicate that in the presence of AQDS the precipitate comprised 30 % ferrihydrite and 70 % lepidocrocite whereas in the presence of juglone two ferrihydrite sites are observed (180). In the case of juglone a small doublet (1.2 % of total area) with Mössbauer parameters typical for Fe(II) was required to achieve a satisfactory fit. Additionally, a similar small Fe(II) component resulting from electron shuttling via AQDS may also be present but could not be unambiguously determined due to the low signal:noise ratio.

Although iron (oxyhydr)oxide phases in the presence of aqueous Fe(II) are reactive towards NACs (42, 46), it is unlikely that the precipitates contribute towards the reactivity we observed here. Firstly, the precipitate absent before the addition of the NAC and thus it is unlikely that it would be capable of initiating the reaction. Secondly, our pseudo-first order kinetic fit suggests that only one reactive species is present, which is inconsistent with 2AcNB being facilitated by both ETM and Fe(II) and the precipitate with Fe(II). Thirdly, we measured an average removal of 284 $\pm$ 32 μM of Fe(II) from the aqueous phase, consistent with the 300 μM

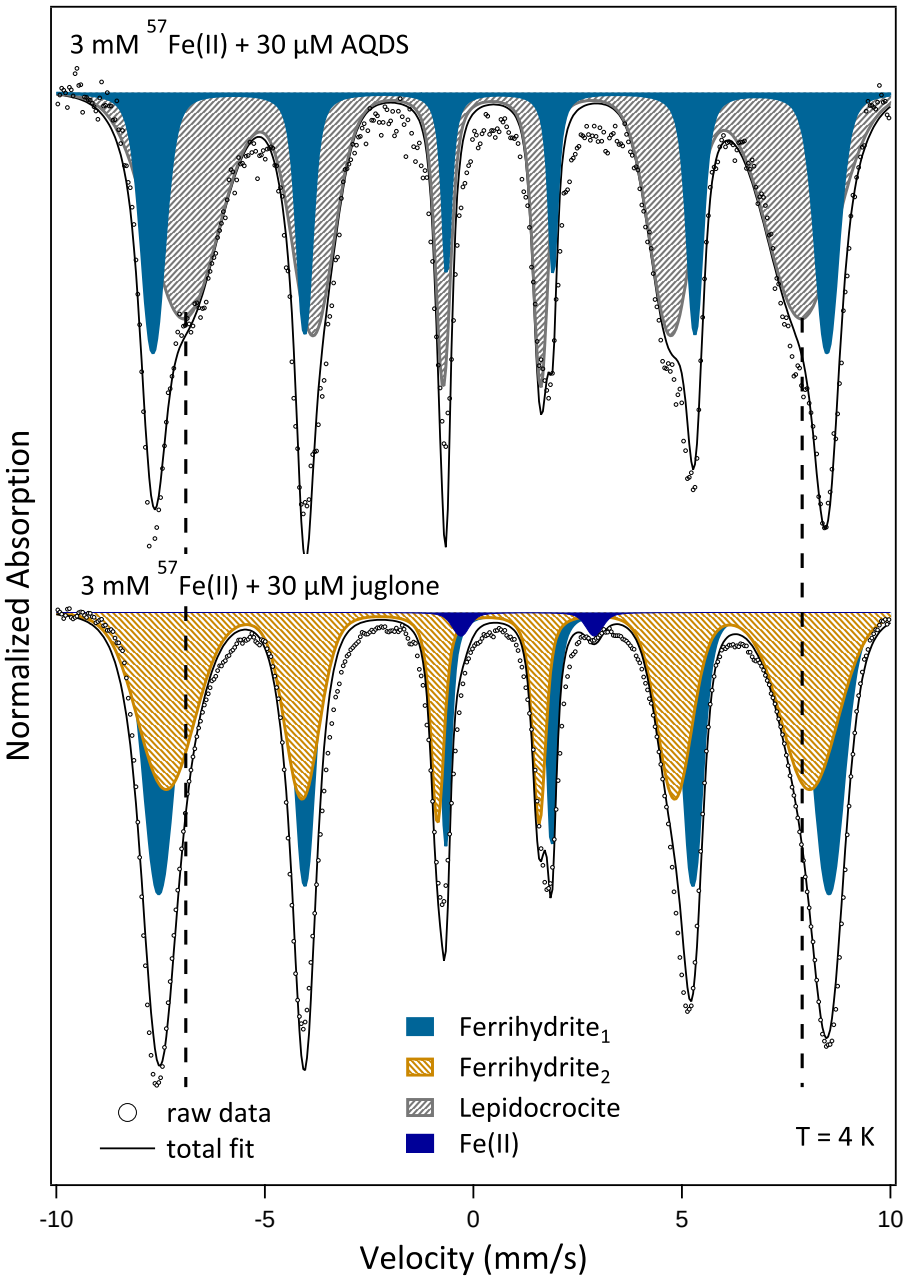

Figure 5.4: Mössbauer spectra of the precipitate formed from the reaction of 3 mM ^{57}Fe(II) and (top) AQDS or (bottom) juglone in the presence of 50 μM 2AcNB. Mössbauer fit parameters may be found in Table S5.3.

electron equivalents required to completely transform the 50 μM NAC present in the reactors, suggesting that aqueous Fe(II) was the only bulk electron donor in our system.

Further supporting evidence comes from comparing the Mössbauer spectra of NAu-1 before and after the reaction with with ^{57}Fe(II) AQDS and 2AcNB (Figure S5.6). We observed the formation of a new sextet (Table S5.4, sextet iii) that was not present in the spectra before NAC reaction (Figure S5.6) and an increase in spectral area of 15 % for sextet ii (Table S5.4). The fit parameters for these phases (Table S5.4) are similar to those for the ferrihydrite (sextet iii) and lepidocrocite (sextet ii) we observed in the absence of NAu-1 (Figure 5.4, Table S5.3) and the increase in spectral area of these sextets after NAC reaction (37 %: 63 %) is similar to the ratio of ferrihydrite:lepidocrocite in the absence of NAu-1 (30 %: 70%).

Despite the similarities observed for how ETMs affect 2AcNB transformation in the presence of dissolved Fe(II) and Fe(II)-reduced NAu-1, we found significant and surprising difference between ETMs with quinone and flavin groups. The quinone ETMs facilitated more rapid 2AcNB transformation, relative to the flavins (Figure 5.3b). This trend contrasts what we observed for dithionite-reduced NAu-1. Flavin compounds have been reported to form weak complexes with Fe (222, 223) and because these complexes have not been well characterised and no entries exist in published stability constant databases (192, 224) we could not determine the amount available for 2AcNB reduction. Lower aqueous Fe(II) concentrations would result in higher second-order rate constants (Equation 5.1). In the reactors containing Fe(II), flavins and 2AcNB we did not observe an iron (oxyhydr)oxide product suggest that the oxidised iron remained in a complex in the aqueous phase rather than forming a precipitate.

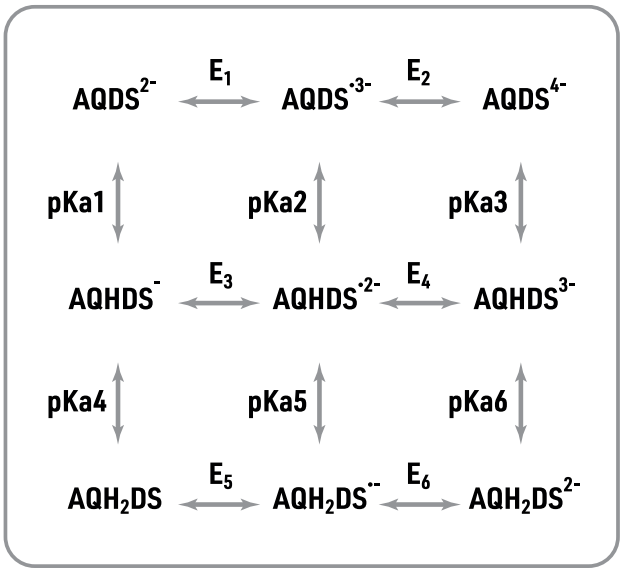

Figure 5.5: Scheme of squares illustrating AQDS speciation. The same scheme applies to juglone and to the flavin compounds. A table of the E_H^0 values for all species relevant for our reactions are found in Table SI.

Previously, work investigating the reduction of azo dyes by reduced (hydro)quinone species has shown that a linear relationship (LFER) should exist between second-order reduction rate constants and the reduction potentials (E_H^0) of the hydroquinone-quinone redox couple (225). Therefore, it is surprising that we did not observe a significant difference between the reactivity of reactors containing AQDS and juglone, despite the fully reduced, deprotonated hydroquinone species of AQDS having a more negative reduction potential (Tables 5.2, S5.6) (211, 225). However, Rau *et al.*,'s work was undertaken in controlled conditions with single ETM species, where the speciation of the (hydro)quinone could be precisely determined. In more complex

systems the efficacy of quinone species as electron shuttles is governed by the extent of protonation of the species (3, 4) and also the ratio at which the semiquinone radical ($Q^{\bullet-}$) is produced in comparison to the fully-reduced hydroquinone species (Q^{2-}) (211), as illustrated in Figure 5.5. As our experiments were undertaken at pH 7.5, close to the pK_a 6 of AQDS (Table S5.5), this further complicates our analysis and as highlighted in Figure 5.5 and Table S5.5, there are 4 different possible semiquinone/hydroquinone species that may contribute to the reaction with 2AcNB, each with an intrinsic E_H^0 ranging from -0.351 V to 0.253 V (Table S5.5) that will influence the equilibrium E_H of the system. To our knowledge, complete E_H^0 values for juglone semiquinone/hydroquinone species are not currently available preventing further quantitative comparison between the different ETMs.

Alternatively, the identity of the Fe (oxyhydr)oxide precipitate resulting from aqueous Fe(II) oxidation by ETMs could determine the overall thermodynamics, which in turn could influence the kinetics (if electron transfer is rate limiting). Lepidocrocite, which accounts for 70 % of the precipitate in the presence of AQDS, has a more negative free energy of formation than ferrihydrite (226), which comprises 100 % of the oxidation product in the reactors containing juglone. This suggests that, as expected from the reduction potentials of the deprotonated hydroquinone species, Fe(II) oxidation is energetically more favourable in the presence of AQDS than juglone. However, we did not observe a correspondingly enhanced reduction rate constant for 2AcNB. Comparison between flavins and quinones is difficult because complexation stability constants and aqueous speciation. are not known. Therefore, we cannot decisively conclude whether the reactivity of the ETMs in our reactors is dependent on their reduction potential or whether other interactions such as Fe(II) complexation of flavin compounds have an impact.

5.4 Summary

Overall, we have shown that quinone ETMs do not influence electron transfer from clay mineral Fe(II) to NACs. However we observed a strong enhancement of 2AcNB reduction in the presence of flavins. It is uncertain why flavins are able to enhance the reduction more than quinones, although it is possible that this is due to sorption of quinone ETMs to the clay mineral.

In the presence of Fe(II)-reduced NAu-1 we observed strongly enhanced reactivity, due to shuttling from otherwise inert aqueous Fe(II) to the NAC. Again, the clay mineral acts as a redox buffer and removes Fe(II) from the aqueous phase and stores electron equivalents. However, we also observed an additional inhibiting effect in the presence of the clay mineral, again which could be due to ETM sorption to the clay mineral. In contrast the trend observed for dithionite-reduced NAu-1, we found that flavins enhance 2AcNB reduction less than quinones in the presence of Fe(II)-reduced NAu-1 and it is plausible that this is due to complexing of Fe(II).

Chapter S5
Assessing the effect of electron transfer mediators on the reactivity of Fe-bearing clay minerals: Supporting Information

S5.1 Chemicals and Reagents

All chemicals and reagents used in this study were of analytical grade and purchased from either Fisher Scientific/ACROS Organics (sodium chloride, sodium citrate, sodium bicarbonate, sodium dithionite, 1,10-phenanthroline, hydrofluoric acid, hydrochloric acid and hexacyanoferrate) or Sigma Aldrich (sodium hydroxide, 2-acetylnitrobenzene, 2-acetylaniline, AQDS, juglone, riboflavin, flavin mononucleotide, flavine adenine phosphate, HPLC grade methanol).

All stock solutions were purged with N_2 for at least an hour before introduction to the anaerobic chamber.

S5.2 Mineral preparation

Nontronite NAu-1 with the published unit cell formula of $M^{+}{}_{1.05}[Si_{6.98}Al_{1.02}][Al_{0.29}Fe_{3.68}Mg_{0.04}]O_{20}OH_4$ was purchased from the Source Clays Repository.

The 0.1-0.5 μm fraction of the mineral was obtained through repeated centrifugation according to Stoke's law. The fractionated mineral was then washed three times in 1 M NaCl solution, in order to achieve Na^+ homoionization and then washed twice with DI water. Finally, mineral impurities were removed by repeated centrifugation for 5 minutes at 8000 rpm, which preferentially leaves the impure fraction in the pellet and the clean fraction in the supernatant. FT-IR was then used to confirm removal of any Fe-oxide, carbonate and kaolin impurities (168).

S5.3 Figures and Tables

S5.3.1 Modelled kinetic parameters for dithionite-reduced NAu-1

Table S5.1: Two-site and one-site modelled kinetic parameters for dithionite-reduced NAu-1.

	Two-site model		One-site model
	log k_A	log k_B	log k
	$(M^{-1}h^{-1})$	$(M^{-1}h^{-1})$	$(M^{-1}h^{-1})$
91 % dithionite-reduced NAu-1 alone	3.53±0.07	-0.47[a]	-
91 % dithionite-reduced NAu-1 + AQDS	3.46±0.16	-0.25[a]	2.38±0.63
91 % dithionite-reduced NAu-1 + juglone	3.60±0.04	-0.28[a]	2.32±0.41
91 % dithionite-reduced NAu-1 + flavins	4.78±0.05	-0.19[a]	3.24±0.05
19 % dithionite-reduced NAu-1 + AQDS	3.72±0.06	-0.38[a]	-
30 % dithionite-reduced NAu-1 alone	3.78±0.06	-0.16[a]	-

S5.3.2 Kinetic Plots

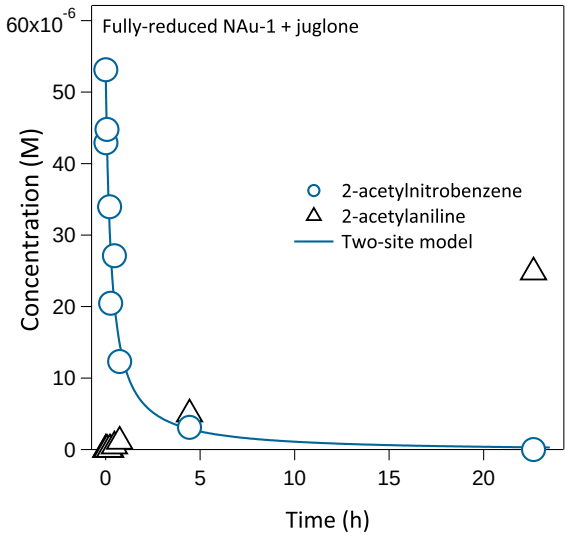

Figure S5.1: Typical reduction kinetics of 2AcNB in suspensions of 91 % dithionite-reduced NAu-1 and 30 μM juglone.

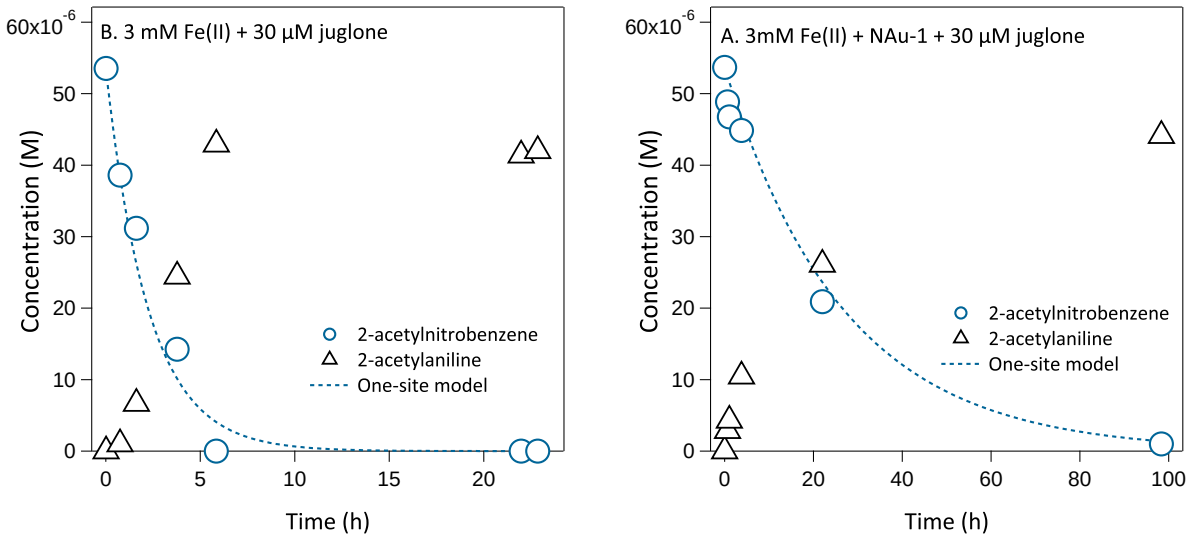

Figure S5.2: Typical reduction kinetics of 2AcNB in suspensions of 3 mM Fe(II) and 30 μM juglone in the presence/absence of NAu-1.

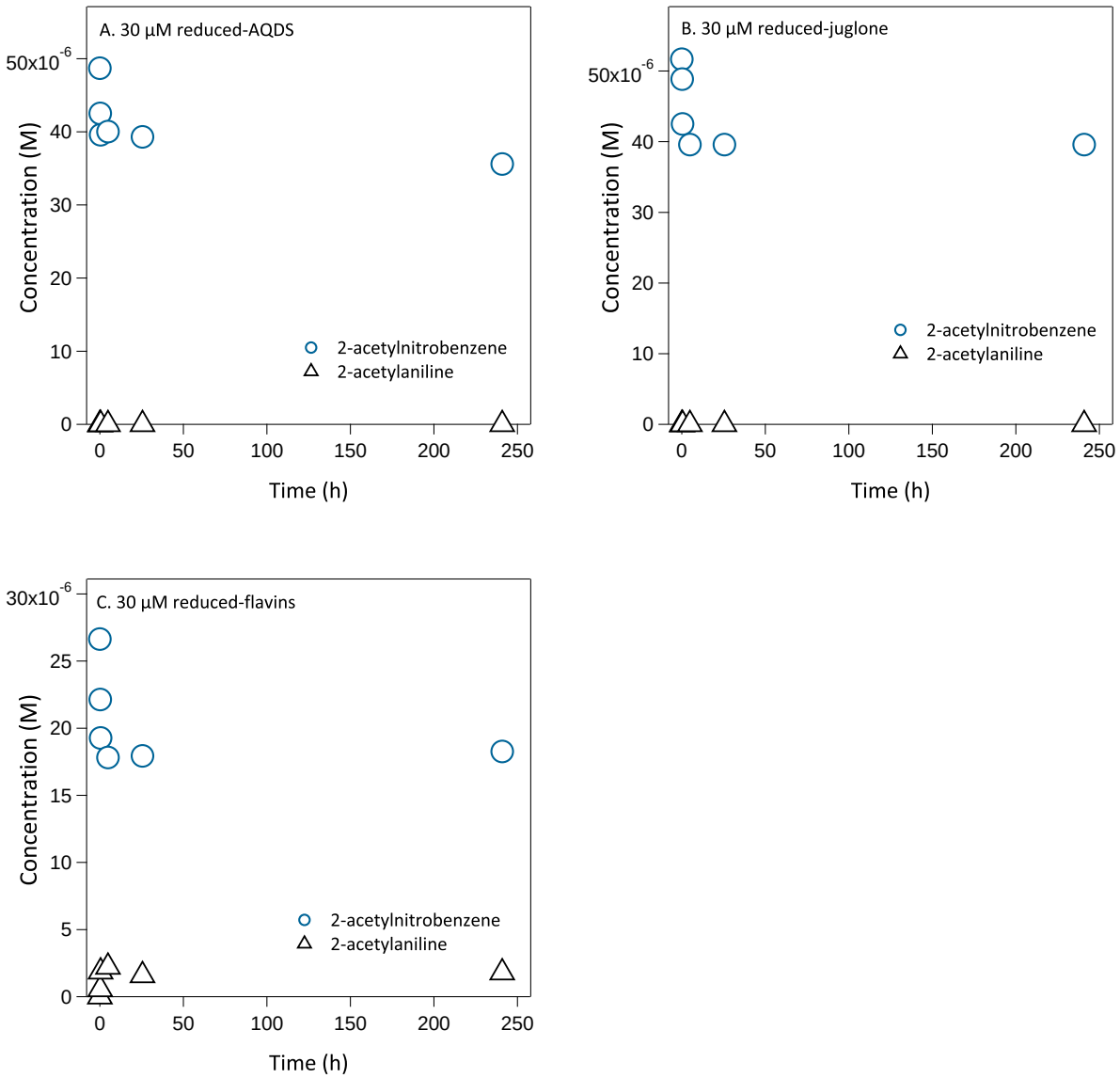

Figure S5.3: Typical reduction kinetics of 2AcNB in suspensions of (a) reduced AQDS, (b) reduced juglone, and (c) reduced flavins. ETMs were reduced by reacting with 91 %-dithionite-reduced NAu-1.

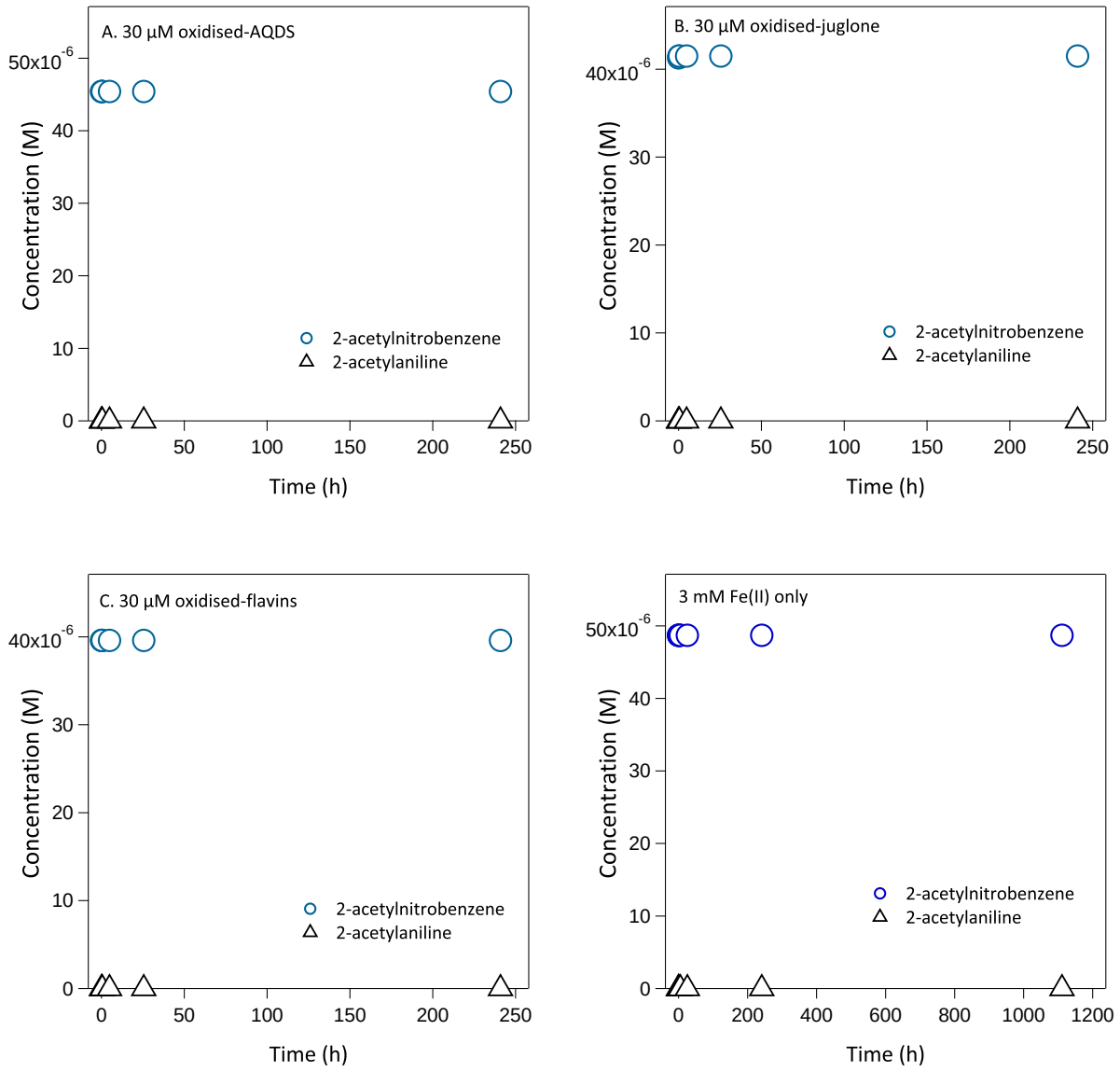

Figure S5.4: Typical concentration-time profiles of 2AcNB and 2-acetylaniline in suspensions of (a) oxidised AQDS, (b) oxidised juglone, (c) oxidised flavins, and (d) 3 mM Fe(II) alone.

S5.3.3 Mössbauer spectra

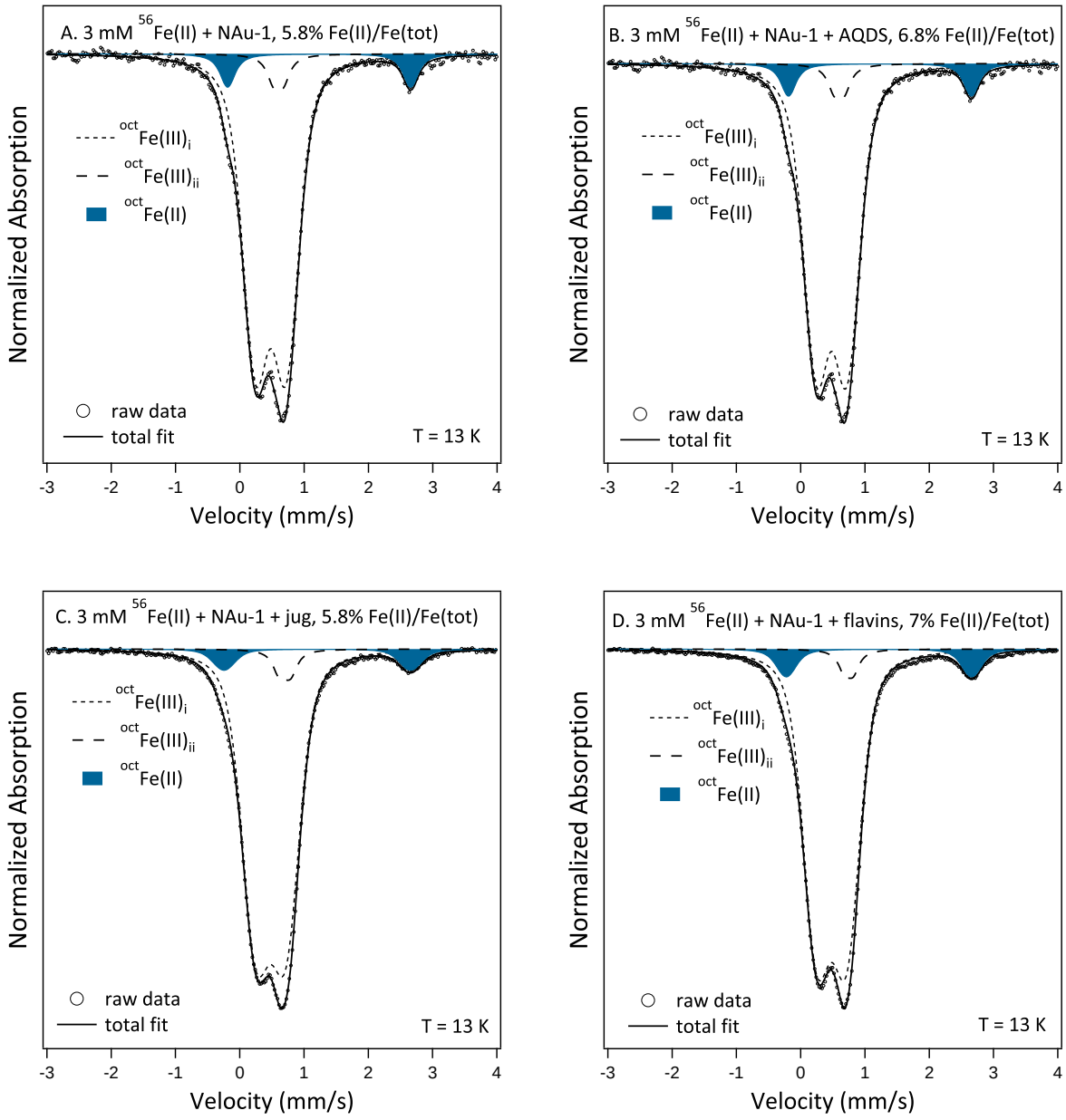

x

Figure S5.5: Mössbauer spectra of 3 mM ^{56}Fe(II) + NAu-1 + (a) alone, (b) AQDS, (c) juglone, and (d) flavins. As ^{56}Fe(II) is not Mössbauer active, only changes in the naturally abundant ^{57}Fe(II) in the clay mineral structure are visible.

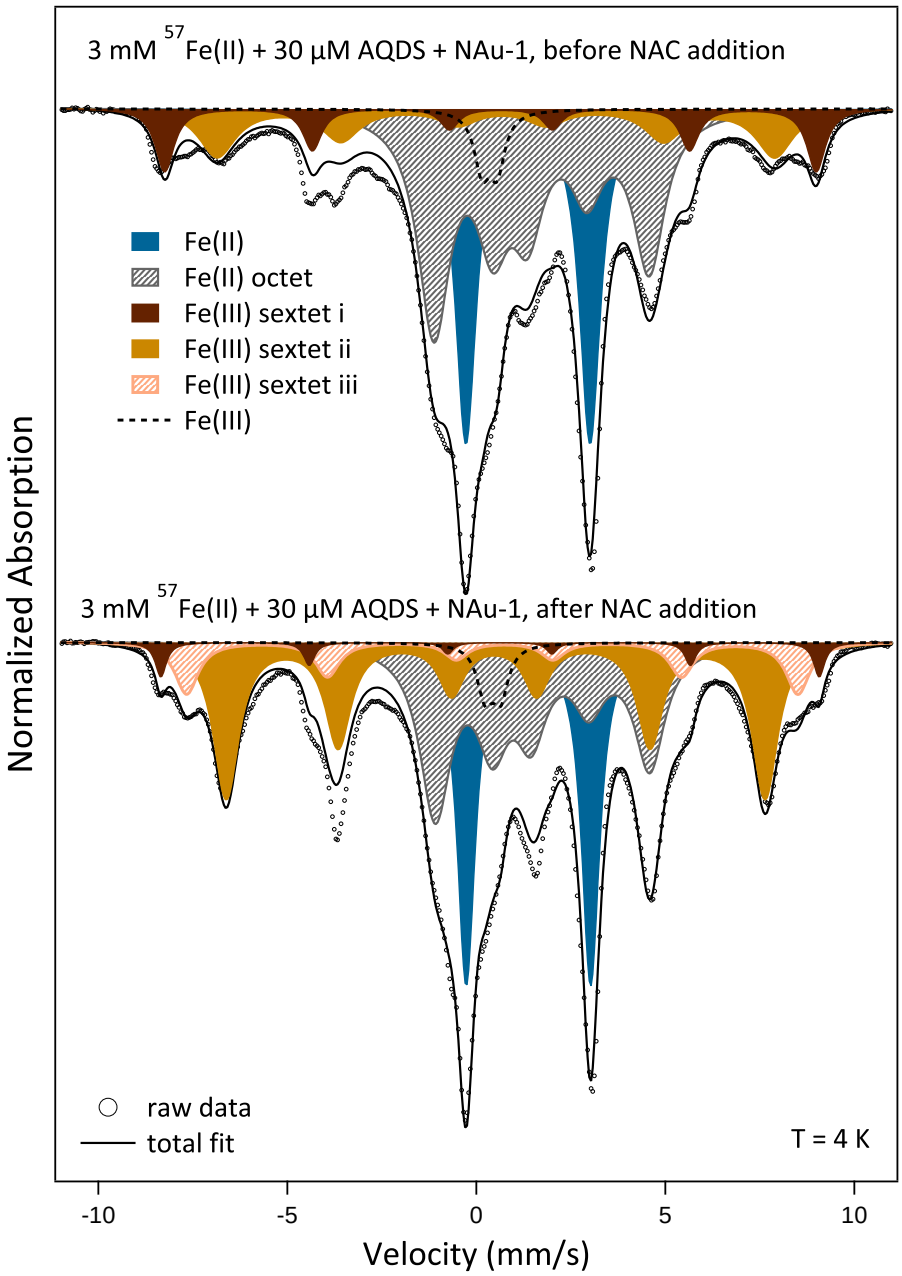

Figure S5.6: Mössbauer spectra of (top) 3 mM ^{57}Fe(II) + NAu-1 + AQDS before NAC addition and (bottom) after NAC addition.

S5.3.4 Mössbauer fit parameters

Table S5.2: Mössbauer parameters for ^{56}Fe(II)-reduced NAu-1, in the presence and absence of ETMs, measured at 13 K and fitted using a voigt based, fixed line width method.

Reaction Condition	χ^2	Site	CS (mm/s)	QS (mm/s)	Area (%)
3 mM ^{56}Fe(II) + NAu-1	0.63	oct Fe(III)i	0.48	0.47 ± 0.01	91.6 ± 0.9
		oct Fe(III)ii	0.76	0.15 ± 0.04	2.5 ± 0.7
		oct Fe(II)	1.22	2.90 ± 0.04	5.8 ± 0.5
3 mM ^{56}Fe(II) + NAu-1 + AQDS	0.63	oct Fe(III)i	0.48	0.49 ± 0.01	88.6 ± 0.5
		oct Fe(III)ii	0.60	0.14 ± 0.03	4.6 ± 0.3
		oct Fe(II)	1.23	2.84 ± 0.02	6.8 ± 0.5
3 mM ^{56}Fe(II) + NAu-1 + juglone	0.91	oct Fe(III)i	0.48	0.49 ± 0.01	90.0 ± 0.3
		oct Fe(III)ii	0.71	0.17 ± 0.01	4.2 ± 0.3
		oct Fe(II)	1.21	2.90 ± 0.02	5.8 ± 0.3
3 mM ^{56}Fe(II) + NAu-1 + flavins	1.30	oct Fe(III)i	0.48	0.47 ± 0.01	89.6 ± 0.3
		oct Fe(III)ii	0.75	0.14 ± 0.01	3.5 ± 0.2
		oct Fe(II)	1.22	2.88 ± 0.01	7.0 ± 0.5

Table S5.3: Mössbauer parameters for the precipitate formed by the reaction of 3 mM ^{57}Fe(II), quinone ETMs and 2AcNB, measured at 4 K and fitted using a voigt based, fixed line width method.

Reaction Condition	χ^2	Site	CS (mm/s)	QS (mm/s)	H (T)	Area (%)
3 mM ^{57}Fe(II)	3.07	Ferrihydrite	0.52	-0.12 ± 0.01	50.1 ± 0.1	29.7 ± 1.2
+ AQDS		Lepidocrocite	0.45	0.01 ± 0.01	45.9 ± 0.2	70.3 ± 1.2
3 mM ^{57}Fe(II)	29.9	Ferrihydrite i	0.55	-0.06 ± 0.01	49.8 ± 0.1	46.2 ± 3.9
+juglone		Ferrihydrite ii	0.35	-0.01 ± 0.01	47.8 ± 0.1	70.3 ± 3.9
		Fe(II)	1.30	3.20 ± 0.05	-	1.2 ± 0.96

Table S5.4: Mössbauer parameters for ^{57}Fe(II)-reduced NAu-1 in the presence of AQDS, before and after reaction with 2AcNB, measured at 4 K and fitted using a Full Static Hamiltonian method.

	χ^2	**Site**	**CS (mm/s)**	**QS (mm/s)**	**H (T)**	θ (°)	**Area (%)**
Pre-2AcNB	58.0	Fe(II)	1.37	3.30 ± 0.01	-	0	28.7 ± 4.4
		Fe(II) octet	1.31	-2.90 ± 0.01	13.15 ± 0.1	90	42.9 ± 6.8
		Fe(III) sextet i	0.51	-0.28 ± 0.01	53.40 ± 0.1	0	9.7 ± 0.72
		Fe(III) sextet ii	0.60	-0.17 ± 0.01	45.74 ± 0.1	0	15.0 ± 0.80
		Fe(III)	0.35	0.40 ± 0.01	-	0	3.6 ± 0.6
After reaction with 2AcNB	81.9	Fe(II)	1.37	3.29 ± 0.01	-	0	23.7 ± 1.2
		Fe(II) octet	1.34	-3.00 ± 0.01	12.70 ± 0.2	90	30.6 ± 5.8
		Fe(III) sextet i	0.49	-0.26 ± 0.01	54.01 ± 0.1	0	2.9 ± 0.49
		Fe(III) sextet ii	0.49	0.04 ± 0.01	44.20 ± 0.1	0	30.4 ± 6.9
		Fe(III) sextet iii	0.58	-0.32 ± 0.01	50.15 ± 0.1	0	9.4 ± 0.69
		Fe(III)	0.44	0.41 ± 0.01	-	0	3.0 ± 0.4

S5.3.5 ETM speciation

pK_a 1	0
pK_a 2	3.2
pK_a 3	10.5
pK_a 5	4.8
pK_a 6	7.6

Table S5.5: AQDS pK_a values (3).

Half reaction	$\mathbf{E_H^0}$ **(V)**
$AQDS^{2-} + 2e^- + 2H^+ \rightleftharpoons AQH_2DS^{2-}$	0.253
$AQDS^{2-} + 2e^- \rightleftharpoons AQDS^{4-}$	-0.298
$AQDS^{2-} + e^- \rightleftharpoons AQDS^{\bullet 3-}$	-0.244
$AQDS^{\bullet 3-} + e^- \rightleftharpoons AQDS^{4-}$	-0.351

Table S5.6: Theoretical E_H^0 values for relevant AQDS half reactions (4).

Half reaction	$\mathbf{E_H^0}$ **(V)**
$FMNH^- + e^- \rightleftharpoons (FMN^{\bullet -})H^-$	-0.345
$(FMN^{\bullet -})H^- + e^- \rightleftharpoons (FMN^{2-})H^-$	-0.410
$(FMN^{\bullet -})H^- + e^- \rightleftharpoons (FMN^-)H^-$	-0.0125
$(FMN)^{2-} + e^- \rightleftharpoons (FMN^{-\bullet})^{2-}$	-0.540
$(FMN^{-\bullet})^{2-} + e^- \rightleftharpoons (FMN^{2-})^{2-}$	-0.570
$(FMN^{2-})^{2-} + e^- \rightleftharpoons (FMN^{2-\bullet})^{2-}$	-0.600
$(FMN^{2-\bullet})^{2-} + e^- \rightleftharpoons (FMN^{3-\bullet})^{2-}$	-0.600

Table S5.7: Theoretical E_H^0 values for relevant FMN half reactions (5).

S5.4 ETM Structures

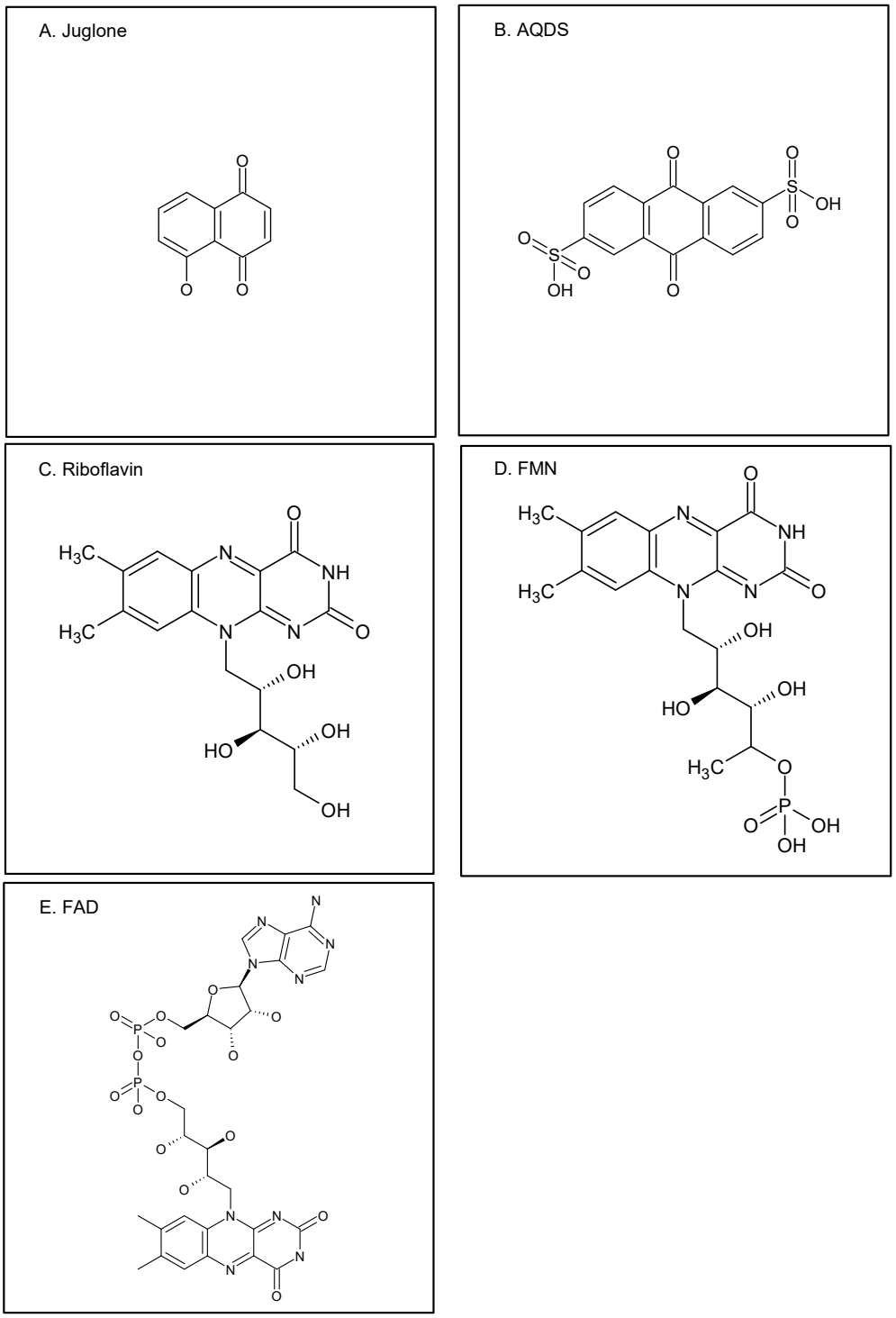

Figure S5.7: Structures of the Electron Transfer Mediation Compounds used in this study including (a) Juglone (5-hydroxy-1,4-naphthalenedione), (b) AQDS (anthraquinone-2,6-disulfonate), (c) riboflavin, (d) FMN (flavin mononucleotide), and, (e) FAD (flavin adenine dinucleotide).

Chapter 6
Summary of Results and Environmental Implications

Our research has highlighted that in complex biogeochemical environments, a range of naturally occurring inorganic and organic species may influence the reactivity of Fe-bearing clay minerals. Based on the knowledge gaps we identified in our literature review (Chapter 2), we have investigated:

i The influence of aqueous Fe(II) and of the formation of Fe(III)-containing oxidation products on Fe-bearing clay mineral reactivity (Chapter 3);

ii The influence of carboxylate Fe(II)-complexes, as analogues of Natural Organic Matter (NOM), on Fe-bearing clay mineral reactivity (Chapter 4); and,

iii The influence of electron shuttling compounds representative of functional groups in microbial exudates on Fe-bearing clay mineral reactivity (Chapter 5).

Our main findings and the environmental implications of our research detailed within each chapter is summarised below.

6.1 The influence of aqueous Fe(II) and of the formation of Fe(III)-containing oxidation products on Fe-bearing clay mineral reactivity

Our findings from this chapter confirm the importance of abiotic reductants for clay mineral Fe reduction in natural environments. Our results highlight the potential of a dynamic, biologically mediated system of contaminant degradation where dissimilatory iron-reducing bacteria respire on Fe-oxide phases and produce aqueous Fe(II), which is then able to reduce Fe-bearing clay minerals creating reactive, structural Fe(II) that is able to reductively transform contaminants.

We have shown that Fe(II)-reduced nontronite facilitates the transformation of NACs more rapidly than dithionite- or bio-reduced clay minerals with similar structural Fe(II)/Fe(tot) ratios (21). We propose that the differences in reactivity are due to differences in reactive Fe(II) entities and our kinetic modelling indicates that Fe(II)- and dithionite-reduced NAu-1 contain the same highly reactive species in their structure. We suggest that these comprise dioctahedral Fe(II) at reduction extents between 5% and 30% Fe(II)/Fe(total). Reduction extents higher than 30% Fe(II)/Fe(total) are achieved in NAu-1 only using dithionite and at these reduction extents we observed significant changes in the mineral structure and propose that the highly reactive sites change from dioctahedral Fe(II) to trioctahedral Fe(II) domains.

Despite the similarities between Fe(II)- and dithionite-reduced NAu-1, the reductant used governs the nature of the less reactive Fe(II) sites. In dithionite-reduced minerals, these may

comprise dioctahedral Fe(II)-other cation pairs as suggested before,(157) whereas in Fe(II)-reduced NAu-1 these comprise Fe(II) bound in or to Fe-containing phases formed during the electron transfer reaction. Most importantly, the presence of residual aqueous Fe(II) apparently increases the redox capacity of Fe(II)-reduced clay minerals over that of dithionite-reduced NAu-1 of the same reduction extents and even at the very low reduction extent of 3.5% Fe(II)/Fe(total), Fe(II)-reduced NAu-1 was capable of completely transforming 2AcNB, although our evidence suggest that the reduction was in-fact determined by the low reactivity site.

Taken together, our results highlight the importance of clay mineral Fe(II) for contaminant transformation in the environment, as the highly reacitive Fe(II) entities in the clay mineral structure form at reduction extents as low as 5% Fe(II)/Fe(total) and during interaction with natural reductants such as Fe(II). The characteristic two-site kinetics of Fe-rich clay minerals are thus expected to be found in natural environments and not just fully dithionite-reduced minerals that are often used as surrogates for their naturally reduced counterparts.

The markedly different reaction kinetics of dithionite and bio-reduced Fe-rich clay minerals over a range of environmentally relevant Fe reduction extents suggest that dithionite-reduced clay minerals are inadequate models for deriving the redox reactivity of bio-reduced clay minerals. Nevertheless, similar trends for dithionite- and Fe(II)-reduced nontronite suggest that the same reactive species are responsible and that data from dithionite-reduced samples can be used to estimate reactivity for Fe(II)-reduced clay minerals, applicable clearly only at low reduction extents.

6.2 The influence of carboxylate Fe(II)-complexes on Fe-bearing clay mineral reactivity

Our work in this chapter provides an insight into the reactivity of combined systems of Fe-bearing clay minerals, aqueous Fe(II) and carboxylate organic ligand species representative of NOM, which are all likely to coexist in complex natural environments. Previously, research has tended to focus on assessing the reactivity of single soil/groundwater components.

We have shown that aqueous carboxylate Fe(II)-ligand species tend to be more reactive than Fe(II) in clay mineral structures. This result was unexpected due to the lower reduction potential of clay mineral Fe(II). However, the reactivity of these complexes is highly dependent on their speciation which is in turn influenced by pH and solution composition.

If an Fe(II)-complex is present that is less reactive than the clay mineral Fe(II), as observed for Fe(II)-oxalate, the complexes reduces the clay mineral Fe and the resulting structural Fe(II) is the predominant reactive species and behaves similarly to dithionite-reduced notronite.

In the presence of reactive Fe(II)-complexes, the clay mineral acts as a redox buffering phase. In its native form clay mineral Fe lowers the aqueous Fe(II) concentration through sorption and electron transfer, thereby decreasing the NAC transformation rate. Note that the rate constant of the reaction remains unaffected because the reactive species (i.e. the Fe(II)-complex) is the same but reduced in concentration.

In its reduced form we suggest that clay mineral Fe may recharge the reactive Fe(II)-complex species and enable further contaminant transformation than could be predicted based on aqueous speciation alone. This recharge effect may be an important mechanism in natural groundwater and soil environments that undergo periodic reduction and oxidation cycles. Here, Fe-bearing clay minerals may store electrons that can replenish the reactivity of more reactive organically complexed Fe(II) species. This work highlights the importance of considering both inorganic and organic redox-active phases when making predictions concerning contaminant transformation rates in real world systems.

6.3 The influence of electron transfer mediators (ETMs) on Fe-bearing clay mineral reactivity

This chapter highlights the importance of ETMs for the abiotic reduction of contaminants in complex natural environments extending the range of research showing ETMs enhance microbial Fe-reduction processes and microbial degradation of contaminants (138).

For NAu-1 that had been previously partially or fully-reduced using dithionite, the presence of quinone-containing shuttling compounds did not significantly affect the rate of 2AcNB reduction. However, in the presence of flavin compounds the rate of 2AcNB reduction by fully-reduced NAu-1 was substantially increased despite reacting more slowly than the quinone-moities in the presence of aqueous Fe(II) and native NAu-1. Therefore, we have shown the importance of reaction conditions, which have a controlling influence on the efficiency of different classes of shuttling compounds that cannot be explained according to differing reduction potentials of the ETMs. The reasons behind this are not clearly understood and elucidating these mechanisms would create a better understanding of ETMs and their impact on contaminant degradation, nutrient cycling and other fundamentally important, naturally occurring redox processes.

We have shown that the presence of a small concentration of ETMs enables otherwise unreactive aqueous Fe(II) to completely transform our nitroaromatic probe compound in less than 24 hours, suggesting that other phases that may be considered inert towards contaminants may be capable of facilitating contaminant reduction in the presence of electron shuttling compounds characteristic of naturally ubiquitous microbial exudates and natural organic matter. This process also resulted in the formation of an iron (oxyhydr)oxide oxidation product, which will also contribute to the redox behaviour of complex natural systems although it did not affect NAC transformation rates in our experiments. Again, we have highlighted the importance of considering the impact of all redox active components in complex natural systems when assessing the likely fate of contaminants in the environment.

6.4 Conceptual Model

Our work has identified several novel interactions between Fe-bearing clay minerals and inorganic as well as organic components characteristic of complex biogeochemical environments.

We found that all components influenced the reactivity of clay mineral Fe towards NACs, and presumably also other contaminants. Our work therefore significantly progresses and compliments previous research primarily focussed on the reactivity of single-redox active phases. In the conceptual model illustrated in Figure 6.1 we summarise all of the processes and interactions discussed in this thesis. The processes may occur concurrently, and the predominant reactive phases may change as a result of fluctuating solution and/or redox conditions.

Our model centres on structural Fe in clay minerals (clay mineral Fe reduction pathways are depicted as green lines), which can be reduced either abiotically, by aqueous Fe(II) or organic Fe(II)-complexes, or microbially. The resulting octahedral Fe(II) facilitates NAC reduction (depicted as purple lines) and its reactivity depends on the mechanism of clay mineral Fe reduction. Abiotic reduction may result in the formation of a secondary Fe(III)-containing product (secondary phase formation is depicted as orange lines), which may enhance NAC reduction by Fe(II)-bearing clay minerals, depending on the composition of the precipitate.

Dissimilatory iron-reducing bacteria (DIRB) increase the aqueous concentration of Fe(II) through the reductive dissolution of solid-bound Fe(III) (47), therefore increasing the Fe(II) available to facilitate abiotic clay mineral Fe reduction.

Aqueous Fe(II) associated with Fe-(oxyhydr)oxide phases (associations are depicted as light blue lines) is also known to facilitate NAC reduction (42) and in complex biogeochemical environments, this process may occur alongside NAC reduction by clay minerals. DIRB are also known to produce electron transfer mediating compounds (ETMs), that enhance NAC reduction by Fe-bearing clay minerals and facilitate NAC reduction by otherwise inert phases, such as aqueous Fe(II).

Finally, in the presence of NOM, aqueous Fe(II)-organic complexes can form and facilitate NAC reduction while interacting with Fe-bearing clay minerals that can act as redox buffers; by either reducing the available aqueous Fe(II) pool or recharging reactive Fe(II)-complexes.

Overall, our research has taken the first steps towards assessing the redox reactivity of Fe-bearing clay minerals in complex biogeochemical environments. We have used batch experiments of increasing complexity to identify previously unknown interactions between Fe-bearing clay minerals and various components that are ubiquitously present in natural systems. As summarised in Figure 6.1, these processes may occur concurrently with Fe-bearing clay minerals either facilitating NAC reduction or acting as redox buffers, which influence NAC reduction by other reactive Fe-species. We highlight the importance of considering all coexisting redox active phases that occur in complex natural environments when assessing the feasibility of engineered remedial solutions.

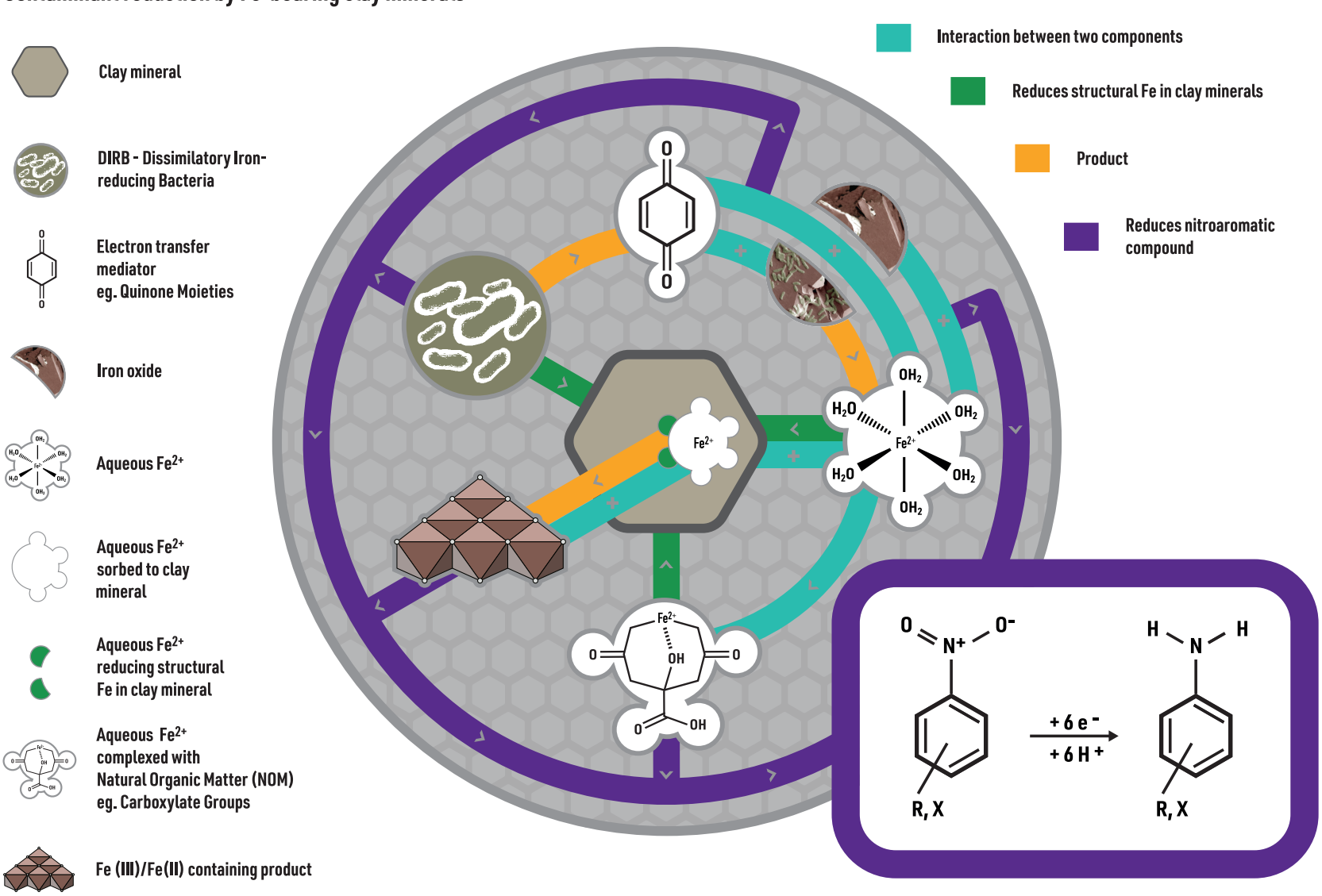

Figure 6.1: Conceptual model illustrating NAC reduction by Fe-bearing clay minerals in complex biogeochemical environments

Bibliography

(1) Daisuke Naka, Dongwook Kim, and Timothy J Strathmann. Abiotic reduction of nitroaromatic compounds by aqueous iron (ii)- catechol complexes. *Environmental science & technology*, 40(9):3006–3012, 2006.

(2) AE Martell, RM Smith, and RJ Motekaitis. Nist standard reference database 46. *Critical Stability Constants of Metal Complexes Database Version*, 8, 2004.

(3) Christopher Batchelor-McAuley, Qian Li, Sophie M Dapin, and Richard G Compton. Voltammetric characterization of dna intercalators across the full ph range: Anthraquinone-2, 6-disulfonate and anthraquinone-2-sulfonate. *The Journal of Physical Chemistry B*, 114(11):4094–4100, 2010.

(4) Kevin M Rosso, Dayle MA Smith, Zheming Wang, Calvin C Ainsworth, and Jim K Fredrickson. Self-exchange electron transfer kinetics and reduction potentials for anthraquinone disulfonate. *The Journal of Physical Chemistry A*, 108(16):3292–3303, 2004.

(5) Serena LJ Tan, Jia Min Kan, and Richard D Webster. Differences in proton-coupled electron-transfer reactions of flavin mononucleotide (fmn) and flavin adenine dinucleotide (fad) between buffered and unbuffered aqueous solutions. *The Journal of Physical Chemistry B*, 117(44):13755–13766, 2013.

(6) Panos Panagos, Marc Van Liedekerke, Yusuf Yigini, and Luca Montanarella. Contaminated sites in europe: review of the current situation based on data collected through a european network. *Journal of Environmental and Public Health*, 2013, 2013.

(7) Edkardt C Beck. The love canal tragedy. *EPA J.*, 5:17, 1979.

(8) CB Doty and CC Travis. Can contaminated aquifers at superfund sites be remediated. *Environmental Science and Technology ESTHAG,*, 24(10), 1990.

(9) Mary E Barth and Maureen F McNichols. Estimation and market valuation of environmental liabilities relating to superfund sites. *Journal of Accounting Research*, pages 177–209, 1994.

(10) Stefan B Haderlein and René P Schwarzenbach. Environmental processes influencing the rate of abiotic reduction of nitroaromatic compounds in the subsurface. In *Biodegradation of nitroaromatic compounds*, pages 199–225. Springer, 1995.

(11) Jim C Spain. Biodegradation of nitroaromatic compounds. *Annual Reviews in Microbiology*, 49(1):523–555, 1995.

(12) Thomas A Lewis, David A Newcombe, and Ronald L Crawford. Bioremediation of soils contaminated with explosives. *Journal of Environmental Management*, 70(4):291–307, 2004.

(13) Deyi Hou and Abir Al-Tabbaa. Sustainability: a new imperative in contaminated land remediation. *Environmental Science & Policy*, 39:25–34, 2014.

(14) JE Amonette, JE Szecsody, HT Schaef, YA Gorby, JS Fruchter, and JC Templeton. Abiotic reduction of aquifer materials by dithionite: a promising in-situ remediation technology. Technical report, Pacific Northwest Lab., 1994.

(15) Donald L Macalady, Paul G Tratnyek, and Timothy J Grundl. Abiotic reduction reactions of anthropogenic organic chemicals in anaerobic systems: a critical review. *Journal of Contaminant Hydrology*, 1(1-2):1–28, 1986.

(16) Thomas B Hofstetter, Cornelis G Heijman, Stefan B Haderlein, Christof Holliger, and René P Schwarzenbach. Complete reduction of tnt and other (poly) nitroaromatic compounds under iron-reducing subsurface conditions. *Environmental science & technology*, 33(9):1479–1487, 1999.

(17) Joseph W Stucki and Joel E Kostka. Microbial reduction of iron in smectite. *Comptes Rendus Geoscience*, 338(6):468–475, 2006.

(18) Junjie Yang, Ravi K Kukkadapu, Hailiang Dong, Evgenya S Shelobolina, Jing Zhang, and Jinwook Kim. Effects of redox cycling of iron in nontronite on reduction of technetium. *Chemical Geology*, 291:206–216, 2012.

(19) Linduo Zhao, Hailiang Dong, Ravi K Kukkadapu, Qiang Zeng, Richard E Edelmann, Martin Pentraĺk, and Abinash Agrawal. Biological redox cycling of iron in nontronite and its potential application in nitrate removal. *Environmental Science & Technology*, 49(9):5493–5501, 2015.

(20) Anke Neumann, Thomas B Hofstetter, Maja Luĺssi, Olaf A Cirpka, Sabine Petit, and René P Schwarzenbach. Assessing the redox reactivity of structural iron in smectites using nitroaromatic compounds as kinetic probes. *Environmental science & technology*, 42(22):8381–8387, 2008.

(21) Fubo Luan, Yan Liu, Aron M Griffin, Christopher A Gorski, and William D Burgos. Iron (iii)-bearing clay minerals enhance bioreduction of nitrobenzene by shewanella putrefaciens cn32. *Environmental science & technology*, 2015.

(22) Fubo Luan, Christopher A Gorski, and William D Burgos. Linear free energy relationships for the biotic and abiotic reduction of nitroaromatic compounds. *Environmental science & technology*, 49(6):3557–3565, 2015.

(23) Diana R Brookshaw, Victoria S Coker, Jonathan R Lloyd, David J Vaughan, and Richard AD Pattrick. Redox interactions between cr (vi) and fe (ii) in bioreduced biotite and chlorite. *Environmental science & technology*, 48(19):11337–11342, 2014.

(24) Michael E Bishop, Hailiang Dong, Ravi K Kukkadapu, Chongxuan Liu, and Richard E Edelmann. Bioreduction of fe-bearing clay minerals and their reactivity toward pertechnetate (tc-99). *Geochimica et Cosmochimica Acta*, 75(18):5229–5246, 2011.

(25) Adele M Jones, Cassandra A Murphy, T David Waite, and Richard N Collins. Fe (ii) interactions with smectites: temporal changes in redox reactivity and the formation of green rust. *Environmental Science & Technology*, 51(21):12573–12582, 2017.

(26) Willard L Lindsay. Solubility and redox equilibria of iron compounds in soils. In *Iron in Soils and Clay Minerals*, pages 37–62. Springer, 1988.

(27) Enver Murad and Walter R Fischer. The geobiochemical cycle of iron. In *Iron in soils and clay minerals*, pages 1–18. Springer, 1988.

(28) Raymond T Pollard, Ian Salter, Richard J Sanders, Mike I Lucas, C Mark Moore, Rachel A Mills, Peter J Statham, John T Allen, Alex R Baker, Dorothee CE Bakker, et al. Southern ocean deep-water carbon export enhanced by natural iron fertilization. *Nature*, 457(7229):577, 2009.

(29) Tim I Eglinton. Geochemistry: A rusty carbon sink. *Nature*, 483(7388):165, 2012.

(30) Yichun Li, Shen Yu, James Strong, and Hailong Wang. Are the biogeochemical cycles of carbon, nitrogen, sulfur, and phosphorus driven by the âfe iii–fe ii redox wheelâ in dynamic redox environments? *Journal of Soils and Sediments*, 12(5):683–693, 2012.

(31) Victor Smetacek, Christine Klaas, Volker H Strass, Philipp Assmy, Marina Montresor, Boris Cisewski, Nicolas Savoye, Adrian Webb, Francesco dâOvidio, Jesús M Arrieta, et al. Deep carbon export from a southern ocean iron-fertilized diatom bloom. *Nature*, 487(7407):313, 2012.

(32) Werner Stumm and Barbara Sulzberger. The cycling of iron in natural environments: considerations based on laboratory studies of heterogeneous redox processes. *Geochimica et Cosmochimica Acta*, 56(8):3233–3257, 1992.

(33) Kirsten Rügge, Thomas B Hofstetter, Stefan B Haderlein, Poul L Bjerg, Søren Knudsen, Claudia Zraunig, Hans Mosbæk, and Thomas H Christensen. Characterization of predominant reductants in an anaerobic leachate-contaminated aquifer by nitroaromatic probe compounds. *Environmental science & technology*, 32(1):23–31, 1998.

(34) Drew E Latta, Christopher A Gorski, and Michelle M Scherer. Influence of fe2+-catalysed iron oxide recrystallization on metal cycling, 2012.

(35) Aaron GB Williams and Michelle M Scherer. Kinetics of cr (vi) reduction by carbonate green rust. *Environmental Science & Technology*, 35(17):3488–3494, 2001.

(36) JE Amonette. Iron redox chemistry of clays and oxides: environmental applications. In *CMS WORKSHOP LECTURES*, volume 10, pages 89–148. Clay Minerals Society, 2002.

(37) Alain Meunier. *Clays*. Springer Science & Business Media, 2005.

(38) JW Stucki. Properties and behaviour of iron in clay minerals. *Developments in Clay Science*, 1:423–475, 2006.

(39) Ralph Early Grim. Applied clay mineralogy. 1962.

(40) YT He, JT Wilson, C Su, and RT Wilkin. Review of abiotic degradation of chlorinated solvents by reactive iron minerals in aquifers. *Groundwater Monitoring & Remediation*, 35(3):57–75, 2015.

(41) Marco C Mangayayam, Knud Dideriksen, and Dominique J Tobler. Can or cannot green rust reduce chlorinated ethenes? *Energy Procedia*, 146:173–178, 2018.

(42) Martin Elsner, René P Schwarzenbach, and Stefan B Haderlein. Reactivity of fe (ii)-bearing minerals toward reductive transformation of organic contaminants. *Environmental science & technology*, 38(3):799–807, 2004.

(43) Christopher A Gorski, James T Nurmi, Paul G Tratnyek, Thomas B Hofstetter, and Michelle M Scherer. Redox behavior of magnetite: Implications for contaminant reduction. *Environmental science & technology*, 44(1):55–60, 2009.

(44) Johnathan D Culpepper, Michelle M Scherer, Thomas C Robinson, Anke Neumann, David Cwiertny, and Drew E Latta. Reduction of pce and tce by magnetite revisited. *Environmental Science: Processes & Impacts*, 20(10):1340–1349, 2018.

(45) Vibeke Ernstsen. Reduction of nitrate by fe^ 2^+ in clay minerals. *Clays and Clay Minerals*, 44(5):599–608, 1996.

(46) Sydney M Stewart, Thomas B Hofstetter, Prachi Joshi, and Christopher A Gorski. Linking thermodynamics to pollutant reduction kinetics by fe2+ bound to iron oxides. *Environmental science & technology*, 52(10):5600–5609, 2018.

(47) Sergey Tsarev, T David Waite, and Richard N Collins. Uranium reduction by fe (ii) in the presence of montmorillonite and nontronite. *Environmental Science & Technology*, 50(15):8223–8230, 2016.

(48) Anke Neumann, Thomas B Hofstetter, Marita Skarpeli-Liati, and René P Schwarzenbach. Reduction of polychlorinated ethanes and carbon tetrachloride by structural fe (ii) in smectites. *Environmental science & technology*, 43(11):4082–4089, 2009.

(49) Javiera Cervini-Silva, Jun Wu, Richard A Larson, and Joseph W Stucki. Transformation of chloropicrin in the presence of iron-bearing clay minerals. *Environmental science & technology*, 34(5):915–917, 2000.

(50) Thomas B Hofstetter, Anke Neumann, and René P Schwarzenbach. Reduction of nitroaromatic compounds by fe (ii) species associated with iron-rich smectites. *Environmental science & technology*, 40(1):235–242, 2006.

(51) Christopher A Schultz and Timothy J Grundl. ph dependence on reduction rate of 4-cl-nitrobenzene by fe (ii)/montmorillonite systems. *Environmental science & technology*, 34(17):3641–3648, 2000.

(52) Javiera Cervini-Silva, Richard A Larson, Jun Wu, and Joseph W Stucki. Transformation of chlorinated aliphatic compounds by ferruginous smectite. *Environmental science & technology*, 35(4):805–809, 2001.

(53) Claresta Joe-Wong, Gordon E Brown Jr, and Kate Maher. Kinetics and products of chromium (vi) reduction by iron (ii/iii)-bearing clay minerals. *Environmental science & technology*, 51(17):9817–9825, 2017.

(54) Fabienne Favre, Daniel Tessier, Mustapha Abdelmoula, Jean-Marie Génin, Will P Gates, and Pascal Boivin. Iron reduction and changes in cation exchange capacity in intermittently waterlogged soil. *European Journal of Soil Science*, 53(2):175–183, 2002.

(55) Anke Neumann, Michael Sander, and Thomas B Hofstetter. Redox properties of structural fe in smectite clay minerals. *Aquatic Redox Chemistry*, 1071:361–379, 2011.

(56) Dieke Postma. Kinetics of nitrate reduction by detrital fe (ii)-silicates. *Geochimica et Cosmochimica Acta*, 54(3):903–908, 1990.

(57) J Rae and A Parker. Environmental interactions of clays. In *Environmental Interactions of Clays*, pages 1–6. Springer, 1998.

(58) P Fletcher and Garrison Sposito. Chemical modeling of clay/electrolyte interactions of montmorillonite. *Clay Minerals*, 24(2):375–391, 1989.

(59) Joseph W Stucki, Bernard A Goodman, and Udo Schwertmann. *Iron in soils and clay minerals*, volume 217. Springer Science & Business Media, 1985.

(60) I Rozenson and L Heller-Kallai. Reduction and oxidation of fe (super 3+) in dioctahedral smectites; 2, reduction with sodium sulphide solutions. *Clays and clay minerals*, 24(6):283–288, 1976.

(61) Douglas B Hunter and Paul M Bertsch. In situ measurements of tetraphenylboron degradation kinetics on clay mineral surfaces by ir. *Environmental science & technology*, 28(4):686–691, 1994.

(62) I Rozenson and L Heller-Kallai. Reduction and oxidation of fe3+ in dioctahedral smectites-1: Reduction with hydrazine and dithionite. *Clays and Clay Minerals*, 24:271–282, 1976.

(63) Joseph W Stucki, DC Golden, and Charles B Roth. Preparation and handling of dithionite-reduced smectite suspensions. *Clays Clay Miner*, 32(3):191–197, 1984.

(64) Stephen G Mayhew. The redox potential of dithionite and so- 2 from equilibrium reactions with flavodoxins, methyl viologen and hydrogen plus hydrogenase. *European journal of biochemistry*, 85(2):535–547, 1978.

(65) Peter Komadel, Paul R Lear, Joseph W Stucki, et al. Reduction and reoxidation of nontronite: Extent of reduction and reaction rates. *Clays and Clay Minerals*, 38(2):203–208, 1990.

(66) Claire-Isabelle Fialips, Dongfang Huo, Laibin Yan, Jun Wu, and Joseph W Stucki. Infrared study of reduced and reduced-reoxidized ferruginous smectite. *Clays and Clay Minerals*, 50(4):455–469, 2002.

(67) Paul R Lear and Joseph W Stucki. Intervalence electron transfer and magnetic exchange in reduced nontronite. *Clays and Clay Minerals*, 35(5):373–378, 1987.

(68) Fabiana R Ribeiro, José D Fabris, Joel E Kostka, Peter Komadel, and Joseph W Stucki. Comparisons of structural iron reduction in smectites by bacteria and dithionite: Ii. a variable-temperature mössbauer spectroscopic study of garfield nontronite. *Pure and Applied Chemistry*, 81(8):1499–1509, 2009.

(69) Peter Komadel, Jana Madejová, and Joseph W Stucki. Structural fe (iii) reduction in smectites. *Applied Clay Science*, 34(1):88–94, 2006.

(70) JD Russell, BA Goodman, and AR Fraser. Infrared and mössbauer studies of reduced nontronites. *Clays and Clay Minerals*, 27(1):63–71, 1979.

(71) Deb P Jaisi, Ravi K Kukkadapu, Dennis D Eberl, and Hailiang Dong. Control of fe (iii) site occupancy on the rate and extent of microbial reduction of fe (iii) in nontronite. *Geochimica et Cosmochimica Acta*, 69(23):5429–5440, 2005.

(72) JW Stucki and PJ Getty. Microbial reduction of iron in nontronite. *Proceedings of the Agronomy Abstracts*, page 279, 1986.

(73) L Pentráková, K Su, M Pentrák, and JW Stucki. A review of microbial redox interactions with structural fe in clay minerals. *Clay Minerals*, 48(3):543–560, 2013.

(74) Yu N Vodyanitskii. Reductive biogenic transformation of fe (iii)-containing phyllosilicates (review of publications). *Eurasian Soil Science*, 40(12):1355–1363, 2007.

(75) Hailiang Dong, Deb P Jaisi, Jinwook Kim, and Gengxin Zhang. Microbe-clay mineral interactions. *American Mineralogist*, 94(11-12):1505–1519, 2009.

(76) Joel E Kostka, Eberhard Haefele, Ralf Viehweger, and Joseph W Stucki. Respiration and dissolution of iron (iii)-containing clay minerals by bacteria. *Environmental Science & Technology*, 33(18):3127–3133, 1999.

(77) A Manceau, B Lanson, VA Drits, D Chateigner, Will P Gates, J Wu, D Huo, and JW Stucki. Oxidation-reduction mechanism of iron in dioctahedral smectites: I. crystal chemistry of oxidized reference nontronites. *American Mineralogist*, 85(1):133–152, 2000.

(78) A Manceau, VA Drits, B Lanson, D Chateigner, J Wu, D Huo, Will P Gates, and JW Stucki. Oxidation-reduction mechanism of iron in dioctahedral smectites: Ii. crystal chemistry of reduced garfield nontronite. *American Mineralogist*, 85(1):153–172, 2000.

(79) Thomas B Hofstetter, René P Schwarzenbach, and Stefan B Haderlein. Reactivity of fe (ii) species associated with clay minerals. *Environmental science & technology*, 37(3):519–528, 2003.

(80) Michael V Schaefer, Christopher A Gorski, and Michelle M Scherer. Spectroscopic evidence for interfacial fe (ii)- fe (iii) electron transfer in a clay mineral. *Environmental science & technology*, 45(2):540–545, 2011.

(81) Daniela Soltermann, Maria Marques Fernandes, Bart Baeyens, Rainer Dà lhn, Prachi A Joshi, Andreas C Scheinost, and Christopher A Gorski. Fe (ii) uptake on natural montmorillonites. i. macroscopic and spectroscopic characterization. *Environmental science & technology*, 48(15):8688–8697, 2014.

(82) Linduo Zhao, Hailiang Dong, Ravi Kukkadapu, Abinash Agrawal, Deng Liu, Jing Zhang, and Richard E Edelmann. Biological oxidation of fe (ii) in reduced nontronite coupled with nitrate reduction by pseudogulbenkiania sp. strain 2002. *Geochimica et Cosmochimica Acta*, 119:231–247, 2013.

(83) Evgenya S Shelobolina, Hiromi Konishi, Huifang Xu, Jason Benzine, Mai Yia Xiong, Tao Wu, Marco Blöthe, and Eric Roden. Isolation of phyllosilicate–iron redox cycling microorganisms from an illite–smectite rich hydromorphic soil. *Frontiers in microbiology*, 3:134, 2012.

(84) Joseph W Stucki. A review of the effects of iron redox cycles on smectite properties. *Comptes Rendus Geoscience*, 343(2):199–209, 2011.

(85) Qiang Zeng, Hailiang Dong, Xi Wang, Tian Yu, and Weihua Cui. Degradation of 1, 4-dioxane by hydroxyl radicals produced from clay minerals. *Journal of hazardous materials*, 331:88–98, 2017.

(86) Songhu Yuan, Xixiang Liu, Wenjuan Liao, Peng Zhang, Xiaoming Wang, and Man Tong. Mechanisms of electron transfer from structrual fe (ii) in reduced nontronite to oxygen for production of hydroxyl radicals. *Geochimica et Cosmochimica Acta*, 223:422–436, 2018.

(87) Man Tong, Songhu Yuan, Sicong Ma, Menggui Jin, Deng Liu, Dong Cheng, Xixiang Liu, Yiqun Gan, and Yanxin Wang. Production of abundant hydroxyl radicals from oxygenation of subsurface sediments. *Environmental science & technology*, 50(1):214–221, 2015.

(88) Alexandre S Anastácio, Amina Aouad, Patrik Sellin, José Domingos Fabris, Faïza Bergaya, and Joseph W Stucki. Characterization of a redox-modified clay mineral with respect to its suitability as a barrier in radioactive waste confinement. *Applied Clay Science*, 39(3-4):172–179, 2008.

(89) Vibeke Ernstsen, Will P Gates, and Joseph W Stucki. Microbial reduction of structural iron in claysâa renewable source of reduction capacity. *Journal of Environmental Quality*, 27(4):761–766, 1998.

(90) Huichun Zhang and Eric J Weber. Identifying indicators of reactivity for chemical reductants in sediments. *Environmental science & technology*, 47(13):6959–6968, 2012.

(91) Per H Nielsen, Helga Bjarnadóttir, Pia L Winter, and Thomas H Christensen. In situ and laboratory studies on the fate of specific organic compounds in an anaerobic landfill leachate plume, 2. fate of aromatic and chlorinated aliphatic compounds. *Journal of Contaminant Hydrology*, 20(1-2):51–66, 1995.

(92) John F Kenneke and Eric J Weber. Reductive dehalogenation of halomethanes in iron- and sulfate-reducing sediments. 1. reactivity pattern analysis. *Environmental science & technology*, 37(4):713–720, 2003.

(93) Inseong Hwang, Bill Batchelor, Mark A Schlautman, and Renjin Wang. Effects of ferrous iron and molecular oxygen on chromium (vi) redox kinetics in the presence of aquifer solids. *Journal of hazardous materials*, 92(2):143–159, 2002.

(94) Ashok Chilakapati, Mark Williams, Steve Yabusaki, Charlie Cole, and Jim Szecsody. Optimal design of an in situ fe (ii) barrier: Transport limited reoxidation. *Environmental science & technology*, 34(24):5215–5221, 2000.

(95) Woojin Lee and Bill Batchelor. Reductive capacity of natural reductants. *Environmental science & technology*, 37(3):535–541, 2003.

(96) Woojin Lee. Removal of trichloroethylene in reduced soil columns. *Journal of hazardous materials*, 113(1-3):175–180, 2004.

(97) Paul G Tratnyek, Richard L Johnson, Gregory V Lowry, and Richard A Brown. In situ chemical reduction for source remediation. In *Chlorinated Solvent Source Zone Remediation*, pages 307–351. Springer, 2014.

(98) Linda Davis Anderson, Douglas B Kent, and James A Davis. Batch experiments characterizing the reduction of chromium (vi) using suboxic material from a mildly reducing sand and gravel aquifer. *Environmental science & technology*, 28(1):178–185, 1994.

(99) John C Seaman, Paul M Bertsch, and L Schwallie. In situ cr (vi) reduction within coarse-textured, oxide-coated soil and aquifer systems using fe (ii) solutions. *Environmental Science & Technology*, 33(6):938–944, 1999.

(100) Patricia M Fox, James A Davis, Ravi Kukkadapu, David M Singer, John Bargar, and Kenneth H Williams. Abiotic u (vi) reduction by sorbed fe (ii) on natural sediments. *Geochimica et Cosmochimica Acta*, 117:266–282, 2013.

(101) Yuanyuan Liu, Chongxuan Liu, Ravi K Kukkadapu, James P McKinley, John Zachara, Andrew E Plymale, Micah D Miller, Tamas Varga, and Charles T Resch. 99tc (vii) retardation, reduction, and redox rate scaling in naturally reduced sediments. *Environmental science & technology*, 49(22):13403–13412, 2015.

(102) Charles E Schaefer, Paul Ho, Erin Berns, and Charles J Werth. Mechanisms for abiotic dechlorination of tce by ferrous minerals under oxic and anoxic conditions in natural sediments. *Environmental science & technology*, 2018.

(103) Jason Benzine, Evgenya Shelobolina, Mai Yia Xiong, David W Kennedy, James P McKinley, Xueju Lin, and Eric Roden. Fe-phyllosilicate redox cycling organisms from a redox transition zone in hanford 300 area sediments. *Frontiers in microbiology*, 4:388, 2013.

(104) TS Peretyazhko, John M Zachara, Ravi K Kukkadapu, Steve M Heald, Igor V Kutnyakov, Charles T Resch, Bruce W Arey, Chong M Wang, Libor Kovarik, Jerry L Phillips, et al. Pertechnetate (tco4-) reduction by reactive ferrous iron forms in naturally anoxic, redox transition zone sediments from the hanford site, usa. *Geochimica et Cosmochimica Acta*, 92:48–66, 2012.

(105) Amanda M Stemig, Tram Anh Do, Virany M Yuwono, William A Arnold, and R Lee Penn. Goethite nanoparticle aggregation: effects of buffers, metal ions, and 4-chloronitrobenzene reduction. *Environmental Science: Nano*, 1(5):478–487, 2014.

(106) Philip M Gschwend et al. *Environmental organic chemistry*. John Wiley & Sons, 2016.

(107) Akané Hartenbach, Thomas B Hofstetter, Michael Berg, Jakov Bolotin, and René P Schwarzenbach. Using nitrogen isotope fractionation to assess abiotic reduction of

nitroaromatic compounds. *Environmental science & technology*, 40(24):7710–7716, 2006.

(108) Akané E Hartenbach, Thomas B Hofstetter, Michael Aeschbacher, Michael Sander, Dongwook Kim, Timothy J Strathmann, William A Arnold, Christopher J Cramer, and René P Schwarzenbach. Variability of nitrogen isotope fractionation during the reduction of nitroaromatic compounds with dissolved reductants. *Environmental science & technology*, 42(22):8352–8359, 2008.

(109) Klaus Pecher, Stefan B Haderlein, and René P Schwarzenbach. Reduction of polyhalogenated methanes by surface-bound fe (ii) in aqueous suspensions of iron oxides. *Environmental science & technology*, 36(8):1734–1741, 2002.

(110) Ida Damgaard, Poul L Bjerg, Jacob Bælum, Charlotte Scheutz, Daniel Hunkeler, Carsten S Jacobsen, Nina Tuxen, and Mette M Broholm. Identification of chlorinated solvents degradation zones in clay till by high resolution chemical, microbial and compound specific isotope analysis. *Journal of contaminant hydrology*, 146:37–50, 2013.

(111) James Entwistle, David Werner, Drew E Latter, Michelle M Scherer, and Anke Neumann. Formation of mixed-valent nano-precipitates due to electron transfer: impact on chlorinated solvent degradation. *Clay Minerals Society Annual Meeting, University of Illinois at Urbana-Champaign*.

(112) Woojin Lee and Bill Batchelor. Abiotic reductive dechlorination of chlorinated ethylenes by iron-bearing phyllosilicates. *Chemosphere*, 56(10):999–1009, 2004.

(113) Timothy J Strathmann and Alan T Stone. Reduction of oxamyl and related pesticides by feii: influence of organic ligands and natural organic matter. *Environmental science & technology*, 36(23):5172–5183, 2002.

(114) Peter J Vikesland and Richard L Valentine. Reaction pathways involved in the reduction of monochloramine by ferrous iron. *Environmental science & technology*, 34(1):83–90, 2000.

(115) Robert W Taylor, Siyuan Shen, William F Bleam, and Shu-I Tu. Chromate removal by dithionite-reduced clays: evidence from direct x-ray adsorption near edge spectroscopy (xanes) of chromate reduction at clay surfaces. *Clays and Clay Minerals*, 48(6):648–654, 2000.

(116) Michael E Bishop, Paul Glasser, Hailiang Dong, Bruce Arey, and Libor Kovarik. Reduction and immobilization of hexavalent chromium by microbially reduced fe-bearing clay minerals. *Geochimica et Cosmochimica Acta*, 133:186–203, 2014.

(117) FT Madsen. Clay mineralogical investigations related to nuclear waste disposal. *Clay minerals*, 33(1):109–129, 1998.

(118) Deb P Jaisi, Hailiang Dong, Andrew E Plymale, James K Fredrickson, John M Zachara, Steve Heald, and Chongxuan Liu. Reduction and long-term immobilization of technetium by fe (ii) associated with clay mineral nontronite. *Chemical Geology*, 264(1-4):127–138, 2009.

(119) Drew E Latta, Maxim I Boyanov, Kenneth M Kemner, Edward J OâLoughlin, and Michelle M Scherer. Abiotic reduction of uranium by fe (ii) in soil. *Applied geochemistry*, 27(8):1512–1524, 2012.

(120) Mavrik Zavarin, Brian A Powell, Mathilde Bourbin, Pihong Zhao, and Annie B Kersting. Np (v) and pu (v) ion exchange and surface-mediated reduction mechanisms on montmorillonite. *Environmental science & technology*, 46(5):2692–2698, 2012.

(121) Christopher A Gorski, Michael Aeschbacher, Daniela Soltermann, Andreas Voegelin, Bart Baeyens, Maria Marques Fernandes, Thomas B Hofstetter, and Michael Sander. Redox properties of structural fe in clay minerals. 1. electrochemical quantification of electron-donating and-accepting capacities of smectites. *Environmental science & technology*, 46(17):9360–9368, 2012.

(122) Christopher A Gorski, Laura Kluìpfel, Andreas Voegelin, Michael Sander, and Thomas B Hofstetter. Redox properties of structural fe in clay minerals. 2. electrochemical and spectroscopic characterization of electron transfer irreversibility in ferruginous smectite, swa-1. *Environmental science & technology*, 46(17):9369–9377, 2012.

(123) Christopher A Gorski, Laura E Kluìpfel, Andreas Voegelin, Michael Sander, and Thomas B Hofstetter. Redox properties of structural fe in clay minerals: 3. relationships between smectite redox and structural properties. *Environmental science & technology*, 47(23):13477–13485, 2013.

(124) Michael Sander, Thomas B Hofstetter, and Christopher A Gorski. Electrochemical analyses of redox-active iron minerals: a review of nonmediated and mediated approaches. *Environmental science & technology*, 49(10):5862–5878, 2015.

(125) Christopher A Gorski, Rebecca Edwards, Michael Sander, Thomas B Hofstetter, and Sydney M Stewart. Thermodynamic characterization of iron oxide–aqueous fe2+ redox couples. *Environmental science & technology*, 50(16):8538–8547, 2016.

(126) Jim E Szecsody, Jonathan S Fruchter, Mark D Williams, Vince R Vermeul, and Debbie Sklarew. In situ chemical reduction of aquifer sediments: Enhancement of reactive iron phases and tce dechlorination. *Environmental science & technology*, 38(17):4656–4663, 2004.

(127) Aaron GB Williams and Michelle M Scherer. Spectroscopic evidence for fe (ii)-fe (iii) electron transfer at the iron oxide-water interface. *Environmental science & technology*, 38(18):4782–4790, 2004.

(128) Anke Neumann, Lingling Wu, Weiqiang Li, Brian L Beard, Clark M Johnson, Kevin M Rosso, Andrew J Frierdich, and Michelle M Scherer. Atom exchange between aqueous fe (ii) and structural fe in clay minerals. *Environmental science & technology*, 49(5):2786–2795, 2015.

(129) Garrison Sposito. *The chemistry of soils*. Oxford university press, 2008.

(130) Johannes Lehmann and Markus Kleber. The contentious nature of soil organic matter. *Nature*, 528(7580):60, 2015.

(131) Frank J Stevenson. *Humus chemistry: genesis, composition, reactions*. John Wiley & Sons, 1994.

(132) Dalizza Colón, Eric J Weber, and James L Anderson. Effect of natural organic matter on the reduction of nitroaromatics by fe (ii) species. *Environmental science & technology*, 42(17):6538–6543, 2008.

(133) Bjorn P von der Heyden, Emily J Hauser, Bhoopesh Mishra, Gustavo A Martinez, Andrew R Bowie, Tolek Tyliszczak, Thato N Mtshali, Alakendra N Roychoudhury, and Satish CB Myneni. Ubiquitous presence of fe (ii) in aquatic colloids and its association with organic carbon. *Environmental Science & Technology Letters*, 1(10):387–392, 2014.

(134) Ellen E Daugherty, Benjamin Gilbert, Peter S Nico, and Thomas Borch. Complexation and redox buffering of iron (ii) by dissolved organic matter. *Environmental science & technology*, 51(19):11096–11104, 2017.

(135) Maria Szilagyi. Reduction of fe3+ ion by humic acid preparations. *Soil Science*, 111(4):233–235, 1971.

(136) J Alexandra Hakala, Yu-Ping Chin, and Eric J Weber. Influence of dissolved organic matter and fe (ii) on the abiotic reduction of pentachloronitrobenzene. *Environmental science & technology*, 41(21):7337–7342, 2007.

(137) Michael Aeschbacher, Daniele Vergari, René P Schwarzenbach, and Michael Sander. Electrochemical analysis of proton and electron transfer equilibria of the reducible moieties in humic acids. *Environmental science & technology*, 45(19):8385–8394, 2011.

(138) Frank P Van der Zee and Francisco J Cervantes. Impact and application of electron shuttles on the redox (bio) transformation of contaminants: a review. *Biotechnology advances*, 27(3):256–277, 2009.

(139) Thomas Borch, Ruben Kretzschmar, Andreas Kappler, Philippe Van Cappellen, Matthew Ginder-Vogel, Andreas Voegelin, and Kate Campbell. Biogeochemical redox processes and their impact on contaminant dynamics. *Environmental Science & Technology*, 44(1):15–23, 2009.

(140) Timothy J Strathmann. Redox reactivity of organically complexed iron (ii) species with aquatic contaminants. In *Aquatic redox chemistry*, pages 283–313. ACS Publications, 2011.

(141) Tamara Polubesova and Benny Chefetz. Dom-affected transformation of contaminants on mineral surfaces: a review. *Critical Reviews in Environmental Science and Technology*, 44(3):223–254, 2014.

(142) JB Neilands. Siderophores: structure and function of microbial iron transport compounds. *Journal of Biological Chemistry*, 270(45):26723–26726, 1995.

(143) Harald Von Canstein, Jun Ogawa, Sakayu Shimizu, and Jonathan R Lloyd. Secretion of flavins by shewanella species and their role in extracellular electron transfer. *Applied and environmental microbiology*, 74(3):615–623, 2008.

(144) Karrie A Weber, Laurie A Achenbach, and John D Coates. Microorganisms pumping iron: anaerobic microbial iron oxidation and reduction. *Nature Reviews Microbiology*, 4(10):752, 2006.

(145) PE Powell, GR Cline, CPP Reid, and PJ Szaniszlo. Occurrence of hydroxamate siderophore iron chelators in soils. *Nature*, 287(5785):833, 1980.

(146) Derek R Lovley. Dissimilatory fe (iii) and mn (iv) reduction. *Microbiological reviews*, 55(2):259–287, 1991.

(147) Engy Ahmed and Sara JM Holmström. The effect of soil horizon and mineral type on the distribution of siderophores in soil. *Geochimica et Cosmochimica Acta*, 131:184–195, 2014.

(148) Dianne K Newman and Roberto Kolter. A role for excreted quinones in extracellular electron transfer. *Nature*, 405(6782):94, 2000.

(149) Minori Uchimiya and Alan T Stone. Reversible redox chemistry of quinones: Impact on biogeochemical cycles. *Chemosphere*, 77(4):451–458, 2009.

(150) Robert C Hider and Xiaole Kong. Chemistry and biology of siderophores. *Natural product reports*, 27(5):637–657, 2010.

(151) Dongwook Kim, Owen W Duckworth, and Timothy J Strathmann. Hydroxamate siderophore-promoted reactions between iron (ii) and nitroaromatic groundwater contaminants. *Geochimica et Cosmochimica Acta*, 73(5):1297–1311, 2009.

(152) Derek R Lovley, Peggy K Widman, Joan C Woodward, and EJ Phillips. Reduction of uranium by cytochrome c3 of desulfovibrio vulgaris. *Applied and Environmental Microbiology*, 59(11):3572–3576, 1993.

(153) Pei-Jie Cai, Xiang Xiao, Yan-Rong He, Wen-Wei Li, Lei Yu, Michael Hon-Wah Lam, and Han-Qing Yu. Involvement of c-type cytochrome cyma in the electron transfer of anaerobic nitrobenzene reduction by shewanella oneidensis mr-1. *Biochemical engineering journal*, 68:227–230, 2012.

(154) Andrea Cherkouk, Gareth TW Law, Athanasios Rizoulis, Katie Law, Joanna C Renshaw, Katherine Morris, Francis R Livens, and Jonathan R Lloyd. Influence of riboflavin on the reduction of radionuclides by shewanella oneidenis mr-1. *Dalton Transactions*, 45(12):5030–5037, 2016.

(155) Di Min, Lei Cheng, Feng Zhang, Xue-Na Huang, Dao-Bo Li, Dong-Feng Liu, Tai-Chu Lau, Yang Mu, and Han-Qing Yu. Enhancing extracellular electron transfer of shewanella oneidensis mr-1 through coupling improved flavin synthesis and metal-reducing conduit for pollutant degradation. *Environmental science & technology*, 51(9):5082–5089, 2017.

(156) Eric E Roden, Andreas Kappler, Iris Bauer, Jie Jiang, Andrea Paul, Reinhard Stoesser, Hiromi Konishi, and Huifang Xu. Extracellular electron transfer through microbial reduction of solid-phase humic substances. *Nature geoscience*, 3(6):417, 2010.

(157) Anke Neumann, Sabine Petit, and Thomas B Hofstetter. Evaluation of redox-active iron sites in smectites using middle and near infrared spectroscopy. *Geochimica et Cosmochimica Acta*, 75(9):2336–2355, 2011.

(158) Vitaly Alexandrov, Anke Neumann, Michelle M Scherer, and Kevin M Rosso. Electron exchange and conduction in nontronite from first-principles. *The Journal of Physical Chemistry C*, 117(5):2032–2040, 2013.

(159) Joel E Kostka, Jun Wu, Kenneth H Nealson, and Joseph W Stucki. The impact of structural fe (iii) reduction by bacteria on the surface chemistry of smectite clay minerals. *Geochimica et Cosmochimica Acta*, 63(22):3705–3713, 1999.

(160) Joel E Kostka, Jun Wu, Kenneth H Nealson, and Joseph W Stucki. Effects of microbial reduction on physical and chemical properties of clay minerals. *Geochim. Cosmochim. Acta*, 63:3705–3713, 1999.

(161) Jennifer C Xu, Joseph W Stucki, Jun Wu, Joel E Kostka, and Gerald K Sims. Fate of atrazine and alachlor in redox-treated ferruginous smectite. *Environmental Toxicology and Chemistry*, 20(12):2717–2724, 2001.

(162) Laura L Sanders. *Manual of field hydrogeology*. Prentice Hall, 1998.

(163) Kangwon Lee, Joel E Kostka, and Joseph W Stucki. Comparisons of structural fe reduction in smectites by bacteria and dithionite: An infrared spectroscopic study. *Clays and Clay Minerals*, 54(2):195–208, 2006.

(164) A Manceau, VA Drits, B Lanson, D Chateigner, J Wu, D Huo, WP Gates, and JW Stucki. Oxidation-reduction mechanism of iron in dioctahedral smectites: Ii. crystal chemistry of reduced garfield nontronite. *American Mineralogist*, 85(1):153–172, 2000.

(165) VA Drits and A Manceau. A model for the mechanism of fe 3+ to fe 2+ reduction in dioctahedral smectites. *Clays and Clay Minerals*, 48(2):185–195, 2000.

(166) Anke Neumann, Tyler L Olson, and Michelle M Scherer. Spectroscopic evidence for fe (ii)–fe (iii) electron transfer at clay mineral edge and basal sites. *Environmental science & technology*, 47(13):6969–6977, 2013.

(167) Drew E Latta, Anke Neumann, WAPJ Premaratne, and Michelle M Scherer. Fe (ii)-fe (iii) electron transfer in a clay mineral with low fe content. *ACS Earth and Space Chemistry*, 2017.

(168) Marion LeRoy Jackson. *Soil chemical analysis: advanced course*. UW-Madison Libraries Parallel Press, 1956.

(169) James E Amonette and J Charles Templeton. Improvements to the quantitative assay of nonrefractory minerals for fe (ii) and total fe using 1, 10-phenanthroline. *Clays and clay minerals*, 46(1):51–62, 1998.

(170) Alfred A Schilt. *Analytical Applications of 1, 10-Phenanthroline and Related Compounds: International Series of Monographs in Analytical Chemistry*. Elsevier, 1969.

(171) DG Rancourt and JY Ping. Voigt-based methods for arbitrary-shape static hyperfine parameter distributions in mössbauer spectroscopy. *Nuclear Instruments and Methods in Physics Research Section B: Beam Interactions with Materials and Atoms*, 58(1):85–97, 1991.

(172) Bingjie Shi, Kai Liu, Lingling Wu, Weiqiang Li, Christina M Smeaton, Brian L Beard, Clark M Johnson, Eric E Roden, and Philippe Van Cappellen. Iron isotope fractionations reveal a finite bioavailable fe pool for structural fe (iii) reduction in nontronite. *Environmental science & technology*, 50(16):8661–8669, 2016.

(173) Joerg Klausen, Serge P Troeber, Stefan B Haderlein, and Rene P Schwarzenbach. Reduction of substituted nitrobenzenes by fe (ii) in aqueous mineral suspensions. *Environmental Science & Technology*, 29(9):2396–2404, 1995.

(174) Dimin Fan, Miranda J Bradley, Adrian W Hinkle, Richard L Johnson, and Paul G Tratnyek. Chemical reactivity probes for assessing abiotic natural attenuation by reducing iron minerals. *Environmental science & technology*, 50(4):1868–1876, 2016.

(175) Peter Komadel, Jana Madejova, and Joseph W Stucki. Reduction and reoxidation of nontronite: Questions of reversibility. *Clays and Clay Minerals*, 43(1):105–110, 1995.

(176) Samuel W Karickhoff and George W Bailey. Optical absorption spectra of clay minerals. *Clays Clay Miner*, 21:59–70, 1973.

(177) GH Faye. The optical absorption spectra of iron in six-coordinate sites in chlorite, biotite, phlogopite and vivianite; some aspects of pleochroism in the sheet silicates. *The Canadian Mineralogist*, 9(3):403–425, 1968.

(178) O Ballet and JMD Coey. Magnetic properties of sheet silicates; 2: 1 layer minerals. *Physics and Chemistry of Minerals*, 8(5):218–229, 1982.

(179) DG Rancourt, IAD Christie, G Lamarche, I Swainson, and S Flandrois. Magnetism of synthetic and natural annite mica: ground state and nature of excitations in an exchange-wise two-dimensional easy-plane ferromagnet with disorder. *Journal of Magnetism and Magnetic Materials*, 138(1-2):31–44, 1994.

(180) E Murad. Mossbauer spectroscopy of clays, soils and their mineral constituents. *Clay Minerals*, 45(4):413–430, 2010.

(181) JG Hering and Werner Stumm. Oxidative and reductive dissolution of minerals. *Reviews in Mineralogy and Geochemistry*, 23(1):427–465, 1990.

(182) Edward J O'loughlin and Yu-Ping Chin. Quantification and characterization of dissolved organic carbon and iron in sedimentary porewater from green bay, wi, usa. *Biogeochemistry*, 71(3):371–386, 2004.

(183) Andreas Fritzsche, Christian Schröder, Arkadiusz K Wieczorek, Matthias Händel, Thomas Ritschel, and Kai U Totsche. Structure and composition of fe–om co-precipitates that form in soil-derived solutions. *Geochimica et Cosmochimica Acta*, 169:167–183, 2015.

(184) Jason D Ritchie and E Michael Perdue. Proton-binding study of standard and reference fulvic acids, humic acids, and natural organic matter. *Geochimica et Cosmochimica Acta*, 67(1):85–96, 2003.

(185) TJ Beveridge and RG Murray. Sites of metal deposition in the cell wall of bacillus subtilis. *Journal of bacteriology*, 141(2):876–887, 1980.

(186) Ignaz J Buerge and Stephan J Hug. Influence of organic ligands on chromium (vi) reduction by iron (ii). *Environmental science & technology*, 32(14):2092–2099, 1998.

(187) Adam L Bussan and Timothy J Strathmann. Influence of organic ligands on the reduction of polyhalogenated alkanes by iron (ii). *Environmental science & technology*, 41(19):6740–6747, 2007.

(188) Iris Bauer and Andreas Kappler. Rates and extent of reduction of fe (iii) compounds and o2 by humic substances. *Environmental science & technology*, 43(13):4902–4908, 2009.

(189) Annette Piepenbrock, Christian Schroỳder, and Andreas Kappler. Electron transfer from humic substances to biogenic and abiogenic fe (iii) oxyhydroxide minerals. *Environmental science & technology*, 48(3):1656–1664, 2014.

(190) Catherine Hirst, Per S Andersson, Samuel Shaw, Ian T Burke, Liselott Kutscher, Melissa J Murphy, Trofim Maximov, Oleg S Pokrovsky, Carl-Magnus Mörth, and Don Porcelli. Characterisation of fe-bearing particles and colloids in the lena river basin, ne russia. *Geochimica et Cosmochimica Acta*, 2017.

(191) John Westall. *MICROQL: I. a chemical equilibrium program in Basic: II. computation of adsorption equilibria in Basic*. EAWAG, 1979.

(192) KJ Powell, LD Pettit, et al. Iupac stability constants database. *Academic Software, Otley*, 1997.

(193) Pan Ming Huang and Martin Schnitzer. Interactions of soil minerals with natural organics and microbes. Technical report, 1986.

(194) Fernando Rosario-Ortiz et al. *Advances in the physicochemical characterization of dissolved organic matter: impact on natural and engineered systems.* Oxford University Press, 2015.

(195) BS Randhawa, R Kaur, and K Sweety. Mössbauer study on thermal decomposition of some hydroxy iron (iii) carboxylates. *Journal of radioanalytical and nuclear chemistry*, 220(2):271–273, 1997.

(196) A Abras and Ester Figueiredo de Oliveira. Synthesis and mössbauer study of iron oxalate coordination polymers of the type fe (c 2 o 4)(l) x (h 2 o) 22- x. *Hyperfine Interactions*, 66(1-4):271–278, 1991.

(197) F Aramu, V Maxia, and C Muntoni. Mössbauer spectroscopy of polymorphous iron oxalate. *Hyperfine Interactions*, 5(1):399–402, 1977.

(198) Maria C D'Antonio, Alejandra Wladimirsky, Daniel Palacios, Liliana Coggiolaa, Ana C González-Baró, Enrique J Baran, and Roberto C Mercader. Spectroscopic investigations of iron (ii) and iron (iii) oxalates. *Journal of the Brazilian Chemical Society*, 20(3):445–450, 2009.

(199) Sergey V Golubev, Andreas Bauer, and Oleg S Pokrovsky. Effect of ph and organic ligands on the kinetics of smectite dissolution at 25 c. *Geochimica et Cosmochimica Acta*, 70(17):4436–4451, 2006.

(200) Thomas B Hofstetter, Anke Neumann, William A Arnold, Akané E Hartenbach, Jakov Bolotin, Christopher J Cramer, and René P Schwarzenbach. Substituent effects on nitrogen isotope fractionation during abiotic reduction of nitroaromatic compounds. *Environmental science & technology*, 42(6):1997–2003, 2008.

(201) Frank M Dunnivant, Rene P Schwarzenbach, and Donald L Macalady. Reduction of substituted nitrobenzenes in aqueous solutions containing natural organic matter. *Environmental Science & Technology*, 26(11):2133–2141, 1992.

(202) Lennart Eberson. Electron-transfer reactions in organic chemistry. In *Advances in physical organic chemistry*, volume 18, pages 79–185. Elsevier, 1982.

(203) George W Luther. The role of one-and two-electron transfer reactions in forming thermodynamically unstable intermediates as barriers in multi-electron redox reactions. *Aquatic Geochemistry*, 16(3):395–420, 2010.

(204) R Guy Riefler and Barth F Smets. Enzymatic reduction of 2, 4, 6-trinitrotoluene and related nitroarenes: kinetics linked to one-electron redox potentials. *Environmental science & technology*, 34(18):3900–3906, 2000.

(205) Ahmet R Mermut and Gerhard Lagaly. Baseline studies of the clay minerals society source clays: layer-charge determination and characteristics of those minerals containing 2: 1 layers. *Clays and Clay Minerals*, 49(5):393–397, 2001.

(206) Timothy J Grundl, Stefan Haderlein, James T Nurmi, and Paul G Tratnyek. Introduction to aquatic redox chemistry. In *ACS Symposium Series*. American Chemical Society, 2011.

(207) Werner Stumm and James J Morgan. *Aquatic chemistry: chemical equilibria and rates in natural waters*, volume 126. John Wiley & Sons, 2012.

(208) Huichun Zhang and Eric J Weber. Elucidating the role of electron shuttles in reductive transformations in anaerobic sediments. *Environmental science & technology*, 43(4):1042–1048, 2009.

(209) Gary P Curtis and Martin Reinhard. Reductive dehalogenation of hexachloroethane, carbon tetrachloride, and bromoform by anthrahydroquinone disulfonate and humic acid. *Environmental Science & Technology*, 28(13):2393–2401, 1994.

(210) Paul G Tratnyek, Michelle M Scherer, Baolin Deng, and Shaodong Hu. Effects of natural organic matter, anthropogenic surfactants, and model quinones on the reduction of contaminants by zero-valent iron. *Water Research*, 35(18):4435–4443, 2001.

(211) Ruey-An Doong and Huai-Chih Chiang. Transformation of carbon tetrachloride by thiol reductants in the presence of quinone compounds. *Environmental science & technology*, 39(19):7460–7468, 2005.

(212) Silvia Orsetti, Christine Laskov, and Stefan B Haderlein. Electron transfer between iron minerals and quinones: estimating the reduction potential of the fe (ii)-goethite surface from aqds speciation. *Environmental science & technology*, 47(24):14161–14168, 2013.

(213) Laura Klüpfel, Annette Piepenbrock, Andreas Kappler, and Michael Sander. Humic substances as fully regenerable electron acceptors in recurrently anoxic environments. *Nature Geoscience*, 7(3):195, 2014.

(214) James T Nurmi and Paul G Tratnyek. Electrochemical properties of natural organic matter (nom), fractions of nom, and model biogeochemical electron shuttles. *Environmental science & technology*, 36(4):617–624, 2002.

(215) Enrico Marsili, Daniel B Baron, Indraneel D Shikhare, Dan Coursolle, Jeffrey A Gralnick, and Daniel R Bond. Shewanella secretes flavins that mediate extracellular electron transfer. *Proceedings of the National Academy of Sciences*, 105(10):3968–3973, 2008.

(216) Kelly P Nevin and Derek R Lovley. Mechanisms for accessing insoluble fe (iii) oxide during dissimilatory fe (iii) reduction by geothrix fermentans. *Applied and environmental microbiology*, 68(5):2294–2299, 2002.

(217) Nicholas J Kotloski and Jeffrey A Gralnick. Flavin electron shuttles dominate extracellular electron transfer by shewanella oneidensis. *MBio*, 4(1):e00553–12, 2013.

(218) Zhi Shi, John M Zachara, Liang Shi, Zheming Wang, Dean A Moore, David W Kennedy, and Jim K Fredrickson. Redox reactions of reduced flavin mononucleotide (fmn), riboflavin (rbf), and anthraquinone-2, 6-disulfonate (aqds) with ferrihydrite and lepidocrocite. *Environmental science & technology*, 46(21):11644–11652, 2012.

(219) Zhi Shi, John M Zachara, Zheming Wang, Liang Shi, and Jim K Fredrickson. Reductive dissolution of goethite and hematite by reduced flavins. *Geochimica et Cosmochimica Acta*, 121:139–154, 2013.

(220) Sungjun Bae and Woojin Lee. Biotransformation of lepidocrocite in the presence of quinones and flavins. *Geochimica et Cosmochimica Acta*, 114:144–155, 2013.

(221) Elizabeth Cottrell, Katherine A Kelley, Antonio Lanzirotti, and Rebecca A Fischer. High-precision determination of iron oxidation state in silicate glasses using xanes. *Chemical Geology*, 268(3-4):167–179, 2009.

(222) A Albert. The metal-binding properties of riboflavin. *The Biochemical Journal*, 47(3):xxvii, 1950.

(223) Evan D Brutinel and Jeffrey A Gralnick. On the role of endogenous electron shuttles in extracellular electron transfer. In *Microbial Metal Respiration*, pages 83–105. Springer, 2013.

(224) Arthur E Martell and Robert M Smith. *Critical stability constants*, volume 1. Springer, 1974.

(225) Jörg Rau, Hans-Joachim Knackmuss, and Andreas Stolz. Effects of different quinoid redox mediators on the anaerobic reduction of azo dyes by bacteria. *Environmental science & technology*, 36(7):1497–1504, 2002.

(226) Tjisse Hiemstra. Formation, stability, and solubility of metal oxide nanoparticles: Surface entropy, enthalpy, and free energy of ferrihydrite. *Geochimica et Cosmochimica Acta*, 158:179–198, 2015.